2003

Renormalization-group Studies of Three Model Systems Far from Equilibrium

Ivan T. Georgiev

RENORMALIZATION-GROUP STUDIES OF THREE MODEL SYSTEMS FAR FROM EQUILIBRIUM

By

Ivan T. Georgiev

M.S. Sofia University, Bulgaria 1997

A THESIS

Submitted in Partial Fulfillment of the

Requirements for the Degree of

Doctor of Philosophy

(in Physics)

The Graduate School

The University of Maine

August, 2003

Advisory Committee:

    Susan R. McKay, Professor of Physics, Advisor

    Kenneth R. Brownstein, Professor of Physics

    Richard A. Morrow, Professor of Physics

    Jayendran C. Rasaiah, Professor of Chemistry

    William N. Unertl, Professor of Physics

External Reader:

    Benjamin Vollmayr-Lee, Assistant Professor of Physics, Bucknell University

RENORMALIZATION-GROUP STUDIES OF THREE MODEL SYSTEMS FAR FROM EQUILIBRIUM

By Ivan T. Georgiev

Thesis Advisor: Dr. Susan R. McKay

An Abstract of the Thesis Presented
in Partial Fulfillment of the Requirements for the
Degree of Doctor of Philosophy
(in Physics)
August, 2003

This thesis describes the development of analytical and computational techniques for systems far from equilibrium and their application to three model systems. Each of the model systems reaches a non-equilibrium steady state and exhibits one or more phase transitions.

We first introduce a new position-space renormalization-group approach and illustrate its application using the one-dimensional fully asymmetric exclusion process. We have constructed a recursion relation for the relevant dynamic parameters for this model and have reproduced all of the important critical features of the model, including the exact positions of the critical point and the first and second order phase boundaries. The method yields an approximate value for the critical exponent ν which is very close to the known value.

The second major part of this thesis combines information theoretic techniques for calculating the entropy and a Monte Carlo renormalization-group approach. We have used this method to study and compare infinitely driven lattice gases. This approach enables us to calculate the critical exponents associated with the correlation length ν and the order parameter β. These results are compared to the values predicted from different field theoretic treatments of the models.

In the final set of calculations, we build position-space renormalization-group recursion relations from the master equations of small clusters. By obtaining the probability distributions for these clusters numerically, we develop a mapping connecting the parameters specifying the dynamics on different length scales. The resulting flow topology in some ways mimics equilibrium features, with sinks for each phase and fixed points associated with each phase boundary. In addition, though, there are added complexities in the flows, suggesting multiple regions within the ordered phase for some values of parameters, and the presence of an extra "source" fixed point within the ordered phase.

Thus, this study illustrates the successful applicability of position-space renormalization-group and information theoretic approaches to driven lattice gases in one and two dimensions. These methods provide new insights into the critical properties and ordering in these systems, and set the stage for further development of these approaches and their application to additional, more realistic models.

DEDICATION

To the memory of my daughter Aleksandra

ACKNOWLEDGEMENTS

I would like to express my gratitude to my thesis advisor Professor Susan McKay. Besides introducing me to the field of the non-equilibrium phenomena, she has always been ready to give me advice, support or just to talk about the problems that I have had in my life during the years as a graduate student. The atmosphere that she was able to make and her constant care for everything has greatly helped and stimulated me and my research.

I also would like to thank the members of my comittee: Dr. Kenneth Brownstein, Dr. Richard Morrow, Dr. Jay Rasaiah and Dr. Bill Unertl for their invaluable comments and suggestions. I am indebted to Dr. Dave Feldman who introduced me to the field of the information theory and its applications in statistical mechanics. I also want to acknowledge the help of Steve Gehrs who managed, against the odds, to keep our computers running all of the time. My research has been partially supported by the National Science Foundation under Grant No. 9720842 and by a University Graduate Research Assistantship in 2000.

I thank my wife, my family and my friends in Bulgaria for their support and care over the years of my study here.

TABLE OF CONTENTS

Chapter

LIST OF TABLES

LIST OF FIGURES

CHAPTER 1

INTRODUCTION

In this work we study the critical properties of three stochastic non-equilibrium lattice gases using position-space renormalization-group methods. The exploration of critical phenomena has always been fascinating to researchers because of its complexity and difficulty. In nature, the number of cases of collective behavior of the constituent elements of a system seem to outnumber the cases in which we observe simple uncorrelated behavior between elements. Pressure, temperature and concentration gradients keep subsystems of living organisms out of equilibrium. The biological realm is full of examples of collective behavior in which the individual "particles" move in concert with each other producing stable patterns in time and space. The same elements of behavior occur in many physical systems close to their critical points.

The nature of the second order phase transition involves huge fluctuations, which are even macroscopically observable, and correlation lengths between the particles spanning the size of the system. It is common for open systems to maintain their highly correlated state for long periods of time, evolving only within a small volume of the parameter space without decaying into an uncorrelated state. The search for solutions that model this behavior has been one of the most active areas in science. In this work we concentrate on models that have steady states which are not close to some equilibrium state, i.e. models far from equilibrium. To explore the critical region of these model systems, we have developed methods which are natural extensions of the well known analytical and computational methods of equilibrium statistical mechanics. The usual Hamiltonian formulation of the equilibrium statistical models allows the definition of appropriate functionals, such as the free energy functional,

by which we define the location of the transition points in the model's parameter space. Analogous approaches can be designed for systems in a general steady state by designing functionals from which the steady state can be obtained. A subtle difference exists, though, between equilibrium and non-equilibrium models: the total independence of the critical properties for equilibrium models from the underlying dynamics. This independence is not the case for systems far from equilibrium, for which the dynamics plays a crucial role in determining their critical properties.

Our work is focused on model systems kept in a steady state far from equilibrium. The models discussed in this thesis undergo first and second order phase transitions and show many typical characteristics of the complex behavior in non-equilibrium phenomena. They are non-Hamiltonian systems for which the dynamics is defined by stochastic rules. One conventional approach is to define a master equation and then try to find its solutions, which is an almost insurmountable task (Oppenheim et al., 1977). In some of the methods that we develop we use the properties of the solutions of the master equation when the system reaches its steady state.

Chapter 2 provides a background discussion of the different methods that will be used for studying the critical properties of the models. We conduct our investigations using the more intuitive position-space renormalization-group approach, working in the phase space spanned by the set of the relevant parameters of the model. In Chapter 3 we show our analytical results for a one-dimensional stochastic model with open boundaries (Krug, 1991; Derrida et al., 1992, 1993). Because the solution in terms of the probability distribution over the possible configurations is known exactly, this simple model is a valuable testing ground for different approaches to systems out of equilibrium, analogous to the two dimensional Ising ferromagnet without a magnetic field for equilibrium processes. This one-dimensional model has a rich phase diagram with first and second order phase transitions. We construct a position-space renormalization-group mapping by using the knowledge of the general form of

the steady state probability distribution and the steady state particle current. The method captures all of the relevant features of the model and an estimate of the correlation length critical exponent is obtained.

We present in Chapter 4 our results for two-state two-dimensional driven lattice gases (Katz et al., 1984). Inspired by the possibility of calculating the entropy density for stationary processes, we develop a Monte Carlo renormalization-group method from which we estimate the correlation length critical exponents. This work involves two basic steps: the first is the calculation of the Shannon entropy for small clusters of sites on the lattice, from which we obtain the entropy density of the lattice; the second step is to use this entropy to find the critical temperature and the correlation length critical exponents by a suitably designed Monte Carlo renormalization procedure. Our main goal is to show how one can apply these methods to study the criticality of the driven lattice models. We also contribute some information related to the long standing controversy of the universality class of different driven lattice models. The main emphasis of this investigation is the information theoretic techniques employed, which prove to be extremely useful when applied here, for the first time, to driven lattice gases.

The last model, considered in Chapter 5 of this thesis, is the two-dimensional three state driven lattice gas (Schmittmann and Zia, 1995). We work with a small closed set of parameters that control the dynamics of the system. Based on the simplicity of the interactions between the particles, we are able to construct a mapping between the parameters (in the renormalization-group sense) of the model from the steady state probability distributions of clusters of sites on the lattice. The results that we report show the flow diagram in different regions of the whole parameter space. The success of the method relies on the accuracy of the approximation of the probability distribution for small clusters obtained via Monte Carlo simulation. We use a multi-spin algorithm which has two advantages: (i) it is extremely fast

compared to a conventional algorithms that need to be run many times with different initial random seeds to yield the same statistics; (ii) by using it, we collect data from 32 different lattices yielding probability distributions for the clusters involved in the calculation that satisfy the requirement of translational invariance. In the last chapter we summarize the results obtained from this work and provide suggestions for future work.

CHAPTER 2

POSITION-SPACE AND MONTE CARLO RENORMALIZATION-GROUP APPROACHES IN STATISTICAL MECHANICS

The renormalization-group formalism developed by Kenneth Wilson is now one of the basic theoretical tools in equilibrium statistical mechanics (Wilson, 1971, 1975). We briefly review in this chapter the basic ideas and methods behind the renormalization-group procedure, which has been developed to explain the critical properties of matter and is going to be useful for our investigation of non-equilibrium models.

2.1 Second order phase transitions and scaling phenomena

Since the year 1869 when Andrews reported to the Royal Society about his observations of carbon dioxide in a tube of glass, there have not been any explanations why, above the temperature of $\approx 31.04°$ C, the transition from liquid to gaseous phase becomes continuous. The observed *critical opalescence* suggests that there are huge macroscopic fluctuations in the local density of the substance. The same applies for the Ising ferromagnet at the critical point, where one observes clusters of aligned spins of all sizes. These features shift the problem to a rather new area of the physics, an area where the fluctuations are dominant and where one cannot start with something that is "well defined" and then consider the fluctuations as a small perturbation.

The conceptual foundation of the renormalization-group approach lies in the idea of *self-similarity* at the critical point. Let's consider the Ising ferromagnet on an infinite lattice. At the critical point (the Curie temperature) there are long wavelength
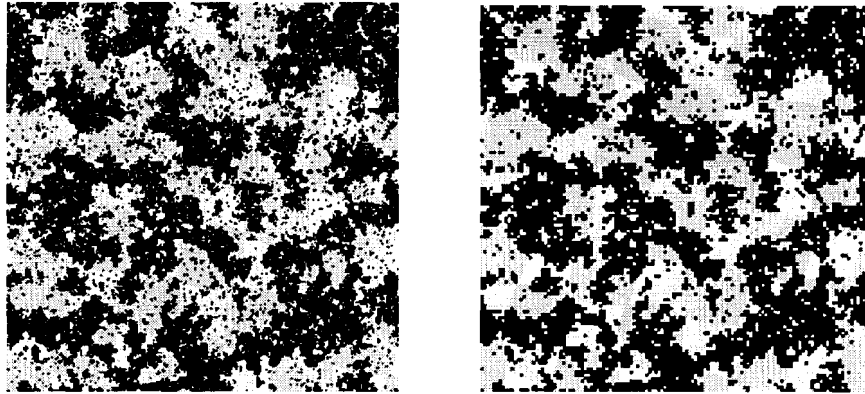
Figure 1: Two-dimensional Ising ferromagnet at the critical point. On the left is shown a 256 × 256 lattice and on the right the coarse-grained 128 × 128 one, where the majority rule has been used for the coarsening. The dark pixels represent down-spins and the light ones up-spins.

fluctuations of the magnetization. Clusters of all kinds of shapes and sizes are present and the whole lattice looks like a self-similar random fractal (see left picture on Fig. 1). One can "zoom-out" and still see the same picture of clusters on the lattice. In the following discussion we will use the two-dimensional Ising ferromagnet as a prototype for our reasoning (for more details see Binney et al. (1992); Creswick et al. (1992)). Each spin on the lattice is addressed by a composite index $\mathbf{i} = (i_x, i_y)$, where i_x and i_y are the coordinates along the two axes. The spin can be up ($\sigma_{\mathbf{i}} = 1$) or down ($\sigma_{\mathbf{i}} = -1$).

Self-similarity of the system provides a natural way to explain the power law behavior of thermodynamic quantities close to the critical point observed experimentally and by simulations. If the correlation function between two spins at sites $\mathbf{i}$ and $\mathbf{j}$, which are separated by distance r, is $G(r) = \langle \sigma_{\mathbf{i}} \sigma_{\mathbf{j}} \rangle$, then two other spins separated by distance λr would have correlation

$$G(\lambda r) = \phi(\lambda, r)\, G(r)\ , \text{where } \lambda \neq 1. \tag{2.1}$$

Here $\phi(\lambda, r)$ is a rescaling function. At the critical point ϕ cannot depend on r. The reason for this is that ϕ and λ are dimensionless while r has a dimension of length. Therefore ϕ can only depend on the ratio of r and some other length ξ. This

quantity ξ cannot be L (the dimension of the lattice) or a (the distance between the sites), because we consider an infinite lattice and the microscopic properties should be irrelevant as well. At the critical point, by the assumption of self-similarity, there is no other characteristic length ξ to be used, therefore ϕ cannot depend on r. One can see that, for the scaling function ϕ in Eq. (2.1), the following equality holds:

$$\phi(\lambda\mu) = \phi(\lambda)\phi(\mu) . \tag{2.2}$$

Assuming that ϕ is differentiable we can get

$$\frac{\mathrm{d}\phi(\lambda\mu)}{\mathrm{d}(\lambda\mu)} \frac{\mathrm{d}(\lambda\mu)}{\mathrm{d}\mu} = \phi(\lambda) \frac{\mathrm{d}\phi(\mu)}{\mathrm{d}\mu} . \tag{2.3}$$

Then, by setting $\mu = 1$ one gets the solution $\phi(\lambda) = \lambda^x$ where the power x is usually written so that:

$$\phi(\lambda) = \lambda^{-(d-2+\eta)} \tag{2.4}$$

where d is the dimension of the space and η is the critical exponent for the correlation function (usually called the anomalous dimension). Therefore by choosing $\lambda = a/r$ and substituting in Eq. (2.1) we get the following expression for the correlation function at the critical point:

$$G(r) \propto r^{-(d-2+\eta)}. \tag{2.5}$$

Close to the critical point there is another characteristic length built naturally into the system, namely the correlation length ξ which is the average size of the correlated fluctuations on the lattice. It depends on the reduced temperature $t = 1 - T/T_c$ where T_c is the critical temperature. Therefore we can write

$$\xi(\lambda t) = \tilde{\varphi}(\lambda, t) \, \xi(t) , \tag{2.6}$$

and, by the same arguments, treating t as the length in the discussion above for the correlation function, one can prove that

$$\xi \propto |t|^{-\nu} . \tag{2.7}$$
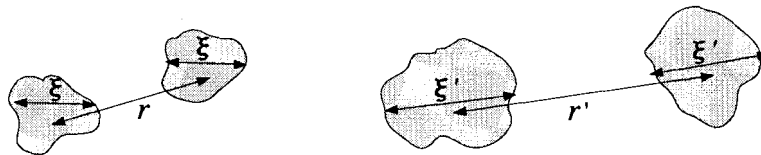
Figure 2: Formation of correlated domains. Regions of correlated fluctuations are shown with typical volume of ξ^d on the left. On the right hand side, the regions are at a temperature a little bit closer to the critical point ($\xi' = \lambda\xi$ for $\lambda > 1$).

We can assume the following form of the correlation function in the vicinity of the critical point:

$$G(r, \xi) = r^{-(d+2-\eta)} \, \tilde{g}\left(\frac{r}{\xi}\right) . \tag{2.8}$$

From it, one can get the power law behavior of the susceptibility χ defined by $\chi = \frac{L^d}{k_B T}\left(\langle m^2 \rangle - \langle m \rangle^2\right)$ where $m = \frac{1}{L^d} \sum_i \sigma_i$ is the order parameter for the model. The susceptibility can be found by integrating the correlation function over the volume of the system

$$\chi \propto \int \mathrm{d}^d r G(r, \xi) \tag{2.9}$$

After a change in the variable $\vec{r} \to \vec{r}/\xi$ one obtains

$$\chi \propto \xi^{2-\eta} \propto |t|^{-\nu(2-\eta)} , \tag{2.10}$$

from which one calculates the critical exponent of the susceptibility $\gamma = \nu(2 - \eta)$.

In order to find the critical exponent β of the order parameter m, we consider the the system at some reduced temperature $t > 0$ (Patashinskii and Pokrovskii, 1979; Dünweg, 1996). Then we can characterize the domains of correlated fluctuations by the correlation length ξ at that temperature (see Fig. 2). If we take two spins σ_i and σ_j in these regions that are separated by a distance $r \gg \xi$ their correlation $\langle \sigma_i \sigma_j \rangle$ will be

$$\langle \sigma_i \sigma_j \rangle \approx \langle m_I m_J \rangle , \text{where } m_I = \xi^{-d} \sum_{i \in I} \sigma_i. \tag{2.11}$$

Here I and J are the indices of the two domains under consideration. If we get closer to the critical point we observe correlated domains with a typical size of $\xi' = \lambda\xi$

($\lambda > 1$) which is the correlation length at that new temperature $t' < t$. If we characterize the fluctuations in terms of the correlation length only, then we should get the same fluctuation picture of domains for the two temperatures. Therefore we move the domains to a distance $r' = \lambda r$ so that the ratio r/ξ remains a constant. The correlation function will rescale as $G \to \lambda^{-(d-2+\eta)}G$ and, for consistency, we should rescale the magnetization in the domains as $m_I \to \lambda^{-(d-2+\eta)/2}m_I$. The total magnetization rescales as the domain magnetization, so we have

$$m(\lambda\xi) = \lambda^{-(d-2+\eta)/2}m(\xi), \tag{2.12}$$

and, after setting $\lambda = a/\xi$, we get

$$m \propto \xi^{-(d-2+\eta)/2} \propto t^{\nu(d-2+\eta)/2}, \tag{2.13}$$

from which one gets $\beta = \nu(d-2+\eta)/2$.

The basic idea of the renormalization-group theory is to reduce iteratively the degrees of freedom of the system, leaving the physics of the model unchanged. This procedure for lattice gases is most conveniently done by the blocking procedure (see Fig. 3).
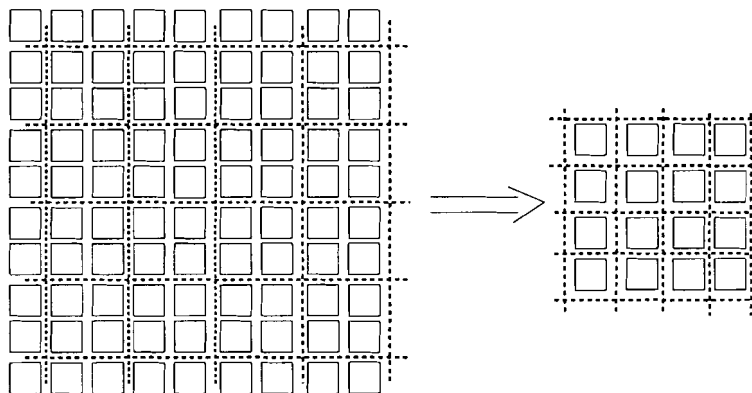
Figure 3: Blocking procedure for lattice models. Blocks of 2×2 spins on the original lattice (left) are mapped to a single spin on the coarse-grained lattice (right) according to some rule.

One divides the original lattice into $b \times b$ blocks, where $b > 1$ is an integer, and maps each block into a single site on the coarse-grained lattice. Mathematically this

can be written as:

$$\sigma_{\mathbf{I}}^{(n+1)} = f(\{\sigma_{\mathbf{i}}^{(n)}\}) \text{ , where } \mathbf{i} \text{ is in the } \mathbf{I}^{th} \text{ block.} \tag{2.14}$$

Here n is the iteration number of the blocking procedure. The original lattice is assumed to be the zeroth iteration. There are many choices for the mapping function f and not all of them provide good results. Obviously for spin models the mapping function f has to generate either -1 or 1 from the spins in the block. For spin systems, the most commonly used are the majority rule and the decimation map (see Fig. 1). For particles choosing a rule is a little bit trickier because one has to keep the number of the particles constant. We propose a modification of the majority rule later on for this purpose.

The probability distribution will follow the recursion relation:

$$P^{(n+1)}(\{\sigma_{\mathbf{I}}^{(n+1)}\}) = \sum_{\mathbf{i}\in\mathbf{I}} P^{(n)}(\{\sigma_{\mathbf{i}}^{(n)}\}) \text{ ,} \tag{2.15}$$

which shows how the weight of the block-spin microscopic configuration at the $(n+1)$ iteration is calculated from the probability distribution of the previous iteration (all time dependences are ruled out by considering only systems in steady state). By using the fact that the steady state probability distribution for systems in equilibrium is related to the Hamiltonian of the model through the usual Boltzmann factor, one can generate an iterative mapping in the space spanned by the parameters of the Hamiltonian. For the Ising model, these parameters are the external magnetic field, the strength of the interaction between nearest-neighbors, the next nearest-neighbors interaction strength, etc. This iterative procedure generates a flow in the parameter space of the system. The attractors (trivial fixed points of this flow) and their basins in the flow diagram correspond to different thermodynamic phases. These regions are divided by separatrices associated with relevant fixed points from which one can

get the critical exponents and determine the universality class of the model. Additional attractors on the critical surface, unstable to points off of the surface, usually correspond to multicritical points.

The topology of the flow in the parameter space generated by the renormalization group yields qualitative information about the critical behavior of the system. Alternatively, one can work in momentum space, in which case techniques from quantum field theory can be used, i.e. perturbative schemes like the ϵ-expansion can be very successful (Wilson and Fisher, 1972; Bellac, 1991). For this study, we have chosen to work directly in position space (Burkhardt and van Leeuwen, 1982; Niemeijer and van Leeuwen, 1973; Burkhardt and van Leeuwen, 1976).

2.2   Properties of general non-equilibrium models

Systems in thermal equilibrium are much harder to find in nature than non-equilibrium systems. However, systems "close" to equilibrium are pretty common and for such systems the so called local equilibrium approximation can be used successfully. In these systems the intensive thermodynamic quantities (such as temperature, pressure, chemical potential, etc.) become inhomogeneous functions in the physical space. In this thesis we do not consider these models. Our research is focused on systems far from equilibrium, which are also common in nature.

The exact solution of equilibrium processes uses two assumptions: the detailed balance condition and the ergodicity condition. The first one simply assumes that the flow from one state a to another state b of the system is equal to the flow from b to a. In other words $w(a \rightarrow b)\ P_a = w(b \rightarrow a)\ P_b$, where w is the transition rate between the states and P is the equilibrium probability distribution. From this condition we can see that the transition probability must be a self adjoint operator on the space of the configurations of the system with an inner product weighted by the equilibrium probability distribution. The ergodicity condition requires that any two

states are connected with nonzero probability and that there are no sub-spaces in the configuration space that are visited cyclically. In an ergodic system, time averages taken during one long run are equivalent to those obtained from shorter runs done on a collection of systems in the ensamble, begun with different initial conditions. For models far from equilibrium, the detailed balance condition is not generally satisfied. As a consequence of this, its steady state is characterized not only by the steady state probability distribution but also by the probability currents in the configuration space that are required to maintain the steady state.

Usually non-equilibrium systems evolve in time from some initial state toward their steady state in a way that depends not only on the interactions between the particles but also on the dynamics of the model. Therefore the usual techniques from equilibrium statistical mechanics cannot be used. Generally one needs to solve the master equation of the model, which is usually much harder than finding, for example, the solution for the partition function of equilibrium models. As in equilibrium models, systems that undergo phase transitions are very interesting to study, showing collective behavior over long distances. In order to observe scale-invariant behavior in equilibrium models, one has to adjust the parameters of the system to their critical values. This is not the case for many systems far from equilibrium that have reached a steady state. They can exhibit scale-invariant states over a broad range of parameters. Thus the power law behavior in many characteristics of the systems (correlations in space or time, power spectra fluctuations, etc.) is abundant in nature, but its explanation remains a difficult and nontrivial task still to be accomplished.

The concept of universality classes can be applied to non-equilibrium systems as well (Hinrichsen, 2000; Ódor, 2002), although the experimental evidence is very preliminary, partially due to the larger diversity in the properties of the system governed by various symmetries in the underlying dynamics. For models far from equilibrium one can only rely on Eq. (2.15) to design constructive renormalization-group schemes

for generating a flow in the parameter space. In the next section we outline a general theory that can be used when trying to calculate the critical exponents of general stochastic models.

2.3   Critical exponents, general theory

Let us formalize the approach for a general stochastic model controlled by a set of parameters $(K_1, K_2, \ldots, K_n)$ which is called the K-space. For equilibrium systems this set is usually the set of all interactions and fields that are present in the Hamiltonian of the model. For a general stochastic model, these are the parameters that enter the microscopic master equation governing the time evolution of the system. Let's denote by $\mathbf{K}' = (\{K_i'\}_{i=1}^n)$ and $\mathbf{K} = (\{K_i\}_{i=1}^n)$ two vectors whose elements are the parameters for the rescaled and the original systems respectively. We assume that $\mathbf{K}'$ is a function of $\mathbf{K}$ via the renormalization-group transformation defined by the blocking procedure, i.e.

$$\mathbf{K}' = \mathbf{F}(\mathbf{K}) . \tag{2.16}$$

Then the critical points are associated with the fixed points of the map defined by Eq. (2.16). Around these points we can linearize the map to obtain

$$K_i' - K_i^* = \sum_j (K_j - K_j^*) \frac{\partial K_i'}{\partial K_j}\bigg|_{K^*} , \tag{2.17}$$

which can be re-written in matrix format as

$$\mathbf{K}' - \mathbf{K}^* = \hat{\mathbf{M}}(\mathbf{K} - \mathbf{K}^*) , \tag{2.18}$$

where the matrix $\hat{\mathbf{M}}$, with elements $\hat{M}_{ij} \equiv (\partial K_i'/\partial K_j)|_{K^*}$, specifies the topology of the fixed point. Usually one aims to determine the matrix $\hat{\mathbf{M}}$ because, from it, critical exponents can be calculated in the following manner. Assume that $\hat{\mathbf{M}}$ can be diagonalized by a transformation $\hat{\mathbf{Q}}$ so that $\hat{\mathbf{Q}}\hat{\mathbf{M}}\hat{\mathbf{Q}}^{-1}$ is a diagonal matrix. Then by transforming the parameters $\mathbf{K}'$ and $\mathbf{K}$ to $\mathbf{x}' = \hat{\mathbf{Q}}(\mathbf{K}' - \mathbf{K}^*)$ and $\mathbf{x} = \hat{\mathbf{Q}}(\mathbf{K} - \mathbf{K}^*)$ we

obtain

$$\mathbf{x'} = \hat{\Lambda}\mathbf{x} \,, \tag{2.19}$$

where the matrix is a diagonal matrix with elements equal the eigenvalues of the matrix $\hat{M}$. Standard notation is used for classifying the new parameters $\mathbf{x}$ according to the value of their λ_i's ($x_i' = \lambda_i x_i$). Those x_i's that grow under the renormalization flow (i.e. $\lambda_i > 1$) are called *relevant variables*. *Irrelevant* variables are those that get smaller ($\lambda < 1$) and *marginally relevant* are those that do not change to linear order ($\lambda = 1$) under the flow generated by the matrix $\hat{M}$.

The correlation length diverges at the critical point. So

$$\xi \propto |x_i|^{-\nu_i} \tag{2.20}$$

defines the critical exponent ν_i. We can see that only the relevant parameters contribute to the divergence in the correlation length, i.e only for them do we obtain the corresponding ν_i to be positive:

$$\nu_i = \frac{\log b}{\log \frac{dx_i'}{dx_i}} = \frac{\log b}{\log \lambda_i} \,. \tag{2.21}$$

The number of relevant parameters is equal to the number of independent critical exponents and varies depending upon the model.

2.4 Monte Carlo renormalization

Another approach for calculating the critical exponents is the Monte Carlo renormalization-group method developed by Swendsen for equilibrium models (Swendsen, 1979, 1982). The basic idea is pretty simple and we review in this section the important steps, using again the Ising ferromagnet as an example (Newman and Barkema, 1999; Landau and Binder, 2000).

One performs a Monte Carlo simulation of the model generating microstates with the correct frequencies, namely proportional to the corresponding Boltzmann factor.

There is a constantly growing number of different algorithms by which this can be achieved, but we will keep this discussion general by not specifying the underlying "generator-of-states". The reduction of the degrees of freedom comes again from the blocking procedure. We divide the original $L \times L$ lattice into blocks of $b \times b$ squares. The distance between the spins on the coarse-grained lattice, measured in new lattice constants, is divided by b, i.e. $r \rightarrow r/b$. All lengths must be rescaled this way. Thus one generates a corresponding microstate on the smaller $L/b \times L/b$ lattice by using some sort of decision formula (Eq. 2.14) which provides with some probability a spin/particle on the coarse-grained lattice from the spins or particles within the block on the original lattice.

The major assumption that we are going to make here is as follows: the only difference between the states generated on the coarse-grained lattice of $L/b \times L/b$ sites and the states generated on a lattice originally with $L/b \times L/b$ sites is the values of the parameters controlling the evolution of the system. For the Ising ferromagnet in the absence of an external field, this is the temperature (or more precisely the ratio $J/k_B T$ which enters in the Hamiltonian of the system). In other words, we assume that the sequence of states on the coarse-grained lattice is generated with frequencies proportional to the correct (Boltzmann) factor but for a different set of parameters (different temperature T' as opposed to T which is the temperature on the original lattice).

It is this assumption that makes the estimation of the error of the results hard. This method has produced excellent results for some equilibrium models and less spectacular ones for others (a notable example of the latter is the Potts model). In this chapter, we provide further investigation and clarification of the method applied to the Ising ferromagnet with nearest neighbor interactions and conserved particle number. As far as we know this approach has not been applied to this model and we

use it here as a test for our investigations on driven diffusive two-dimensional models discussed later in this thesis.

We have performed a Monte Carlo simulation of the two-dimensional Ising model with conserved particle number using the usual Metropolis algorithm for generating a sequence of states on small lattices with dimensions 64 × 128 and 32 × 64. The Hamiltonian of the model is ($J > 0$):

$$H = -4J \sum_{\langle \mathbf{ij} \rangle} n_{\mathbf{i}} n_{\mathbf{j}} \, , \tag{2.22}$$

where each site can be occupied ($n_{\mathbf{i}} = 1$) or vacant ($n_{\mathbf{i}} = 0$) and the usual notation $\langle \mathbf{ij} \rangle$ is used to indicate that the sum is over the nearest neighbors only. For density 0.5 it is well known that this model exhibits a second order phase transition at temperature $T_o \approx 2.2692 J/k_B$ (Onsager's critical temperature). We have simulated the 64 × 128 lattice and have coarse-grained it to a 32 × 64 lattice using a modified version of the majority rule which we have introduced to keep the number of particles exactly equal to half of the sites on the lattice under rescaling.

The rule (which describes the function f in Eq. (2.14)) is as follows:

- From each configuration on the original system we cast the 2 × 2 block-spins into three classes according to the number of particles in each block. One class consists of the set of all blocks that have more particles than holes, i.e. these that contain 3 or 4 particles; another class is the set of blocks that have exactly 2 particles and 2 unoccupied sites; and the last class of blocks is the set containing only blocks that have 1 or 0 particles;

- We fill in our coarse-grained lattice of 32 × 64 sites with holes only, i.e. all $\tilde{n}_I = 0$;

- We choose randomly blocks from the set of blocks having 3 or 4 particles and generate a particle on the corresponding site of the coarse-grained lattice until

the number of particles generated becomes exactly half of the number of the sites on the lattice (in which case we are done generating a state on the small lattice and quit the procedure), or we have exhausted the blocks that are in this set;

- We choose randomly blocks from the second set of blocks that have exactly 2 particles and generate a particle on the lattice until we have reached the state with exactly half of the sites occupied (and quit) or we do not have more blocks on the big lattice that have exactly 2 particles in them;

- We choose blocks from the last set of blocks, having 1 or 0 particles in them, and generate particles until the density of the lattice becomes 0.5 (This case is needed only for very low temperatures, far away from the critical point) and then quit;

For the newly generated state on the coarse-grained lattice, we calculate properties such as the order parameter, the energy, the entropy density, etc. In our example, we determine the entropy density $s'(T)$ of the system (see section 4.3). Then we compare the entropy density of the coarse-grained lattice with the entropy density $s(T)$ of a model that has originally been simulated on a 32 × 64 lattice. The results are shown in Fig. 4.

Our basic assumption is that, close to the critical point, the only difference between the states generated on the coarse-grained 32 × 64 lattice compared to the states obtained from a simulation on a 32 × 64 lattice is that they appear to be generated from a simulation on a 32 × 64 lattice but at different temperature. At the point where the two curves cross each other, the system is scale invariant, signaling the critical point. We would like to mention here that we have tried to reduce the finite size effects by comparing two lattices that have the *same* dimensions and therefore finite size effects should in principle be reduced.
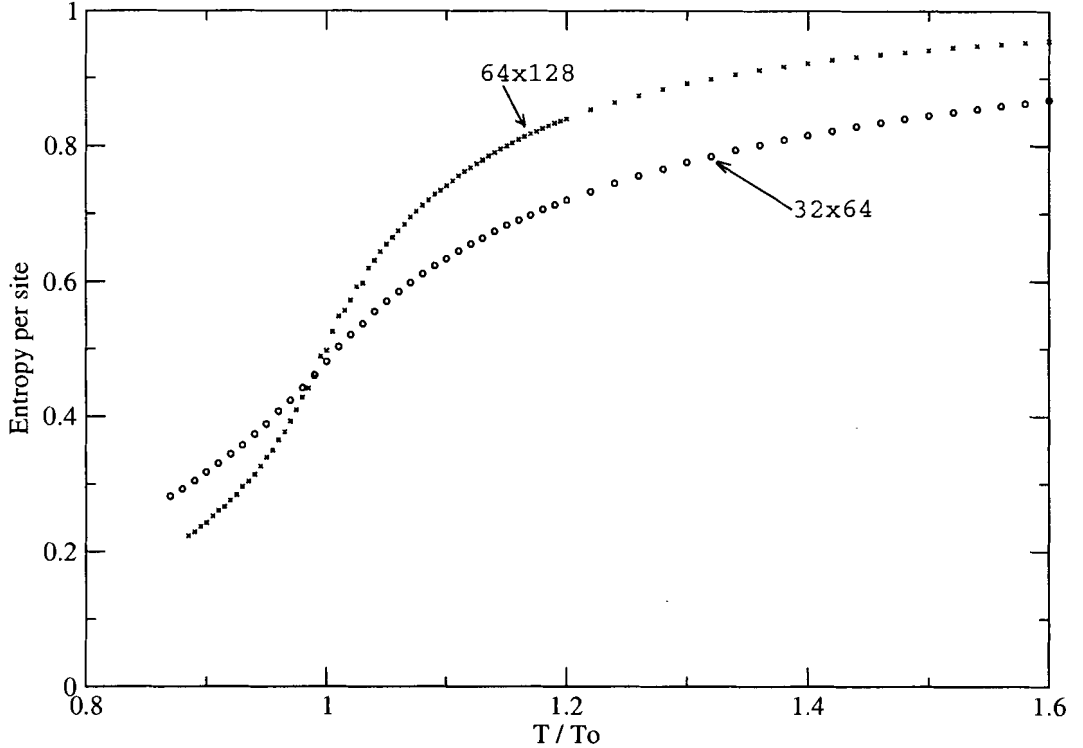
Figure 4: The entropy calculation for the Ising model with conserved number of particles on two lattices: a 32×64 and a 64×128 which has been coarse-grained to a 32×64 lattice. The temperature is in units of Onsager's critical temperature and the entropy density is in bits/site.

Close to the critical point (where the two curves cross each other) we can fit a regression polynomial for the two curves, thus obtaining the functional dependence $s'(T)$ and $s(T)$ for the coarse-grained and the original entropy density respectively (see Fig. 5).

At the critical point the correlation length diverges, therefore the above mentioned rule should produce microstates on the coarse-grained lattice with the same frequencies as the Metropolis algorithm on a system with the same dimension. Precisely speaking this is true only for infinite lattices where we can expect scale-invariance at all length scales. For finite systems we can observe scale-invariance over just few decades but nevertheless it appears to work well enough to determine the critical properties of the model. At the critical point, any observable function of the microstate should have the same value on both lattices, i.e. we should have $s'(T_c) = s(T_c)$ at
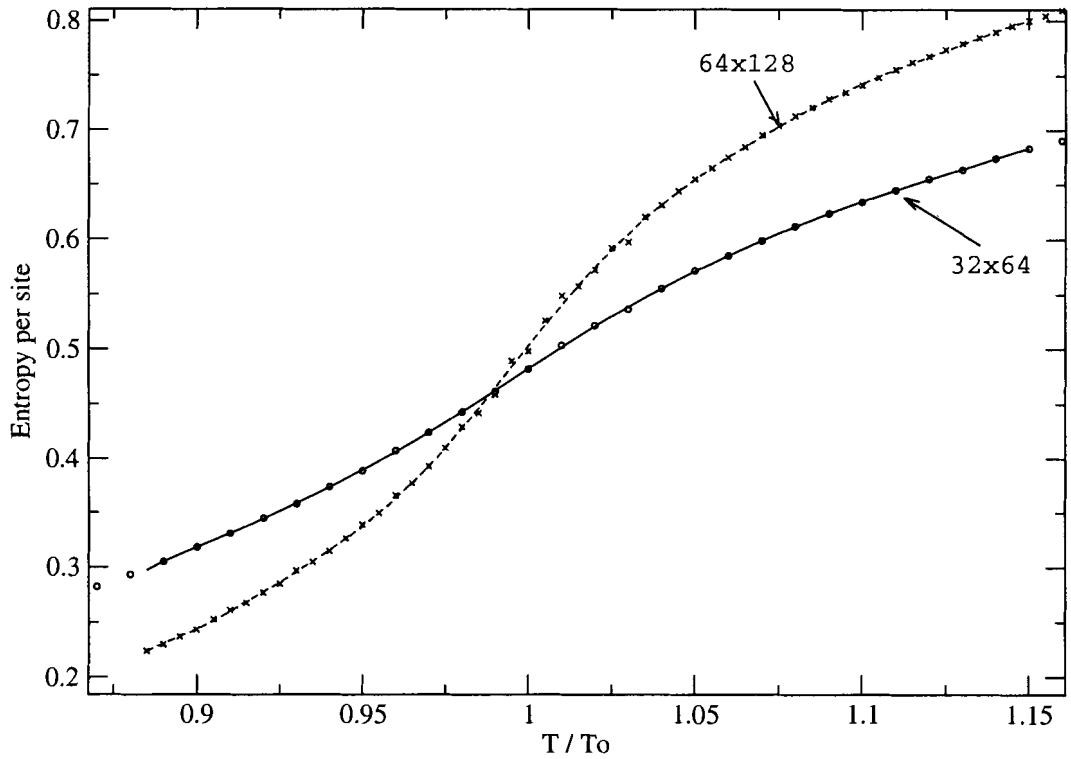
Figure 5: Fitted regression polynomials close to the critical point.

the critical point. Also, mathematically the requirement that the states produced by the blocking procedure look like those generated by a Monte Carlo algorithm but at a different temperature can be written as:

$$s'(T) = s(T') \, , \qquad (2.23)$$

from which we get the mapping $T \to T'$:

$$T' = s^{-1}\big[s'(T)\big] . \qquad (2.24)$$

The above formula is useful for calculating the correlation length critical exponent ν. We know that

$$\xi \propto |t|^{-\nu} \, , \qquad (2.25)$$

where t is the reduced temperature defined by $t = 1 - T/T_c$. For our blocked system we have a similar relation

$$\xi' \propto |t'|^{-\nu} . \qquad (2.26)$$

Dividing Eq. (2.25) by Eq. (2.26) yields

$$\left(\frac{t}{t'}\right)^{-\nu} = \frac{\xi}{\xi'} = b. \tag{2.27}$$

All of these equation are expected to be valid only close to the critical temperature, where we can assume that t and t' are small. In this region, we can expand the functional dependence $T'(T)$ (from Eq. (2.24)) around the fixed point T_c to get

$$T' = T_c + (T - T_c)\left(\frac{\mathrm{d}T'}{\mathrm{d}T}\right)_{T_c}. \tag{2.28}$$

Substituting into Eq. (2.27) we obtain for the critical exponent ν,

$$\nu = \frac{\log b}{\log\left(\frac{\mathrm{d}T'}{\mathrm{d}T}\right)_{T_c}}. \tag{2.29}$$

For our test model, after performing numerical differentiation, we obtain a critical temperature value very close to the exact number: $T \approx 0.989\ T_O$. This calculation gives a correlation length critical exponent $\nu \approx 1.06$ (where the exact value is $\nu = 1.0$). The obvious drawback for the numbers reported is that no error can be estimated, a general characteristic of this method as stated earlier.

The calculation of the order parameter critical exponent β follows similar steps, and one has $m \propto |t|^\beta \propto \xi^{-\beta/\nu}$ and $m' \propto |t'|^\beta \propto \xi'^{-\beta/\nu}$ for the order parameter of the original and the rescaled systems respectively. These equations yield

$$\frac{m'}{m} = b^{\beta/\nu}. \tag{2.30}$$

After using l'Hôpital's rule at the critical temperature (because for infinite lattices both m and m' are zeros above the critical temperature) we finally get

$$\frac{\beta}{\nu} = \frac{\log \frac{\mathrm{d}m'}{\mathrm{d}m}\Big|_{T_c}}{\log b}. \tag{2.31}$$

In the same manner one can obtain the rest of the critical exponents α, γ, etc. There are more accurate Monte Carlo renormalization methods for systems in equilibrium for which the fluctuation dissipation theorem applies, but we are not going to

review them here because the driven diffusive systems, which we are going to study, do not satisfy the fluctuation-dissipation theorem (Schmittmann and Zia, 1995).

CHAPTER 3

THE ONE-DIMENSIONAL ASYMMETRIC EXCLUSION PROCESS

Among non-equilibrium models, a special place is reserved for the asymmetric simple exclusion model. It is a simple stochastic one-dimensional model for an open system. Its steady state probability distribution is known exactly and it exhibits first and second order phase transitions, which is an amazing feature for a one-dimensional system. In this chapter we review the basic properties of the model, give an overview of the methods from which one can obtain the steady state solution, describe our new position-space renormalization-group approach, and show how it can be applied to this model.

3.1   Definition of the model, master equations

Stochastic models are constructed to exhibit the complex behavior of real systems while keeping only their essential properties. These models are usually designed to be simple enough to be tractable while capturing the behavior and complexity of the real process. In lattice models, there are important strong site-to-site fluctuations, which are usually "smoothed-out" when continuous approaches are applied, making realistic solutions hard to find. There are a few lattice models which have known exact solutions, in terms of their probability distribution functions. One such model is the asymmetric simple exclusion process (ASEP) in one dimension, which is one of the simplest models for a driven diffusive system (Krug, 1991; Derrida et al., 1992,
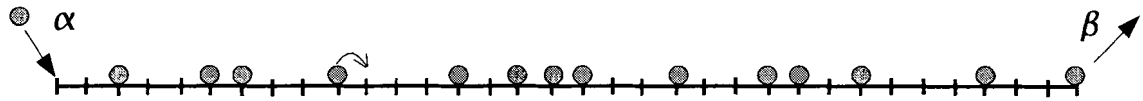
Figure 6: The ASEP model: one-dimensional chain with open boundaries. At each time step, one of the following can happen: a particle enters the chain with probability α from the left boundary provided the leftmost site is empty, a particle leaves the chain from the right with probability β or, in the bulk, a particle hops to its unoccupied neighbor.

1993). The model is a stochastic gas on a one-dimensional chain with N sites and open boundaries (Fig. 6). Each site i can be occupied ($\tau_i = 1$) or empty ($\tau_i = 0$).

A particle can hop to its right neighbor provided that the neighboring site is empty. The simplest interaction is used, hard-core exclusion, which forbids two particles from occupying the same site at any time. The dynamics are sequential: at each time step dt, we choose at random a pair of sites $(i, i+1)$ and, if site i is occupied and site $i+1$ is empty, then the particle at the ith site will jump to the right with probability $p\,dt$:

$$\tau_i(t + dt) = 1, \text{with probability } x_i = \tau_i(t) + [\tau_{i-1}(t)(1 - \tau_i(t)) - \tau_i(t)(1 - \tau_{i+1}(t))]p\,dt$$

$$\tau_i(t + dt) = 0, \text{with probability } 1 - x_i, \text{ where } i \in \{1, ..., N-1\}. \tag{3.1}$$

All of the other sites do not change at this time step. The boundary sites are treated in the following way: when the chosen pair is $(0, 1)$, where site 0 represents the left source of particles, a particle is injected into the chain with probability αdt if the first site of the chain is empty:

$$\tau_1(t + dt) = 1, \text{with probability } x_0 = \tau_1(t) + \alpha[1 - \tau_1(t)]dt$$

$$\tau_1(t + dt) = 0, \text{with probability } 1 - x_0. \tag{3.2}$$

When the chosen pair is $(N, N+1)$, where the $N+1$ site represents the right sink of the chain, the particle at site N, if it is occupied, will flow out of the chain with probability βdt:

$$\tau_N(t + dt) = 1, \text{with probability } x_N = (1 - \beta)\tau_N(t)dt$$

$$\tau_N(t + dt) = 0, \text{with probability } 1 - x_N. \tag{3.3}$$

By opening the boundaries of the one-dimensional chain, we break the translational invariance of the system which is usually encountered when periodic boundary conditions are used. Taking such a step produces so-called boundary induced phenomena. This simple stochastic gas has been used as a model for traffic jams, occurrence of shocks in driven diffusive media and many other applications (Privman, 1997). Applying an external bias in the jump rates of the local dynamical rules drives the system out of reach of the methods suitable for equilibrium systems. The bias is not a small one so perturbative methods suitable for small deviations away from equilibrium are not applicable; thus we are facing a true non-equilibrium one-dimensional problem. The local stochastic rules are specified and we can write the master equation for the system. Also we can simulate the system on a computer mimicking its time evolution but no suitable Monte Carlo procedure exists that samples the different microstates of the system with the *correct* frequencies. There are natural extensions of the model such as allowing possibilities for backward jumps, annihilating and creating particles in the bulk of the chain, allowing particles to flow in (out) from the right (left) end of the chain, etc (Sandow, 1994). This study concentrates on the fully asymmetric exclusion process (FASEP) for which the bulk bias p in Eq. (3.1) equals unity and the only parameters are the two rates α and β and the number of sites in the lattice N. The work described below is also presented in Georgiev and McKay (2003).

To understand this system's properties, we want to calculate the *steady state* probability distribution of all possible microstates. Averaging Eq. (3.1) over the events that may occur in one time step dt and over the histories up to time t, one obtains (Derrida and Evans, 1997):

$$\frac{d}{dt}\langle \tau_i \rangle = \langle \tau_{i-1}(1 - \tau_i) \rangle - \langle \tau_i(1 - \tau_{i+1}) \rangle, \text{ for } i \in \{1, ..., N-1\}$$

$$\frac{d}{dt}\langle \tau_1 \rangle = \alpha\langle 1 - \tau_1 \rangle - \langle \tau_1(1 - \tau_2) \rangle$$

$$\frac{d}{dt}\langle \tau_N \rangle = \langle \tau_{N-1}(1 - \tau_N) \rangle - \beta\langle \tau_N \rangle \tag{3.4}$$

for the one-site probability distributions and:

$$\frac{d}{dt}\langle \tau_i \tau_{i+1} \rangle = \langle \tau_{i-1}(1 - \tau_i)\tau_{i+1} \rangle - \langle \tau_i \tau_{i+1}(1 - \tau_{i+2}) \rangle, \text{ for } i \in \{1, ..., N-1\}. \tag{3.5}$$

for the two-site probability distributions. In the same way, one can obtain any other correlation function $\langle \tau_i \tau_j ... \rangle$. We should emphasize that the above equations are exact and give the time evolution of any correlation function. To solve Eq. (3.4) for the one-site probability function $\langle \tau_i \rangle$ one needs the knowledge of $\langle \tau_i \tau_{i+1} \rangle$ (two-site probability distribution) which in turn requires the knowledge of three-site probability functions and so on, making the problem an N-body problem, i.e. to find one correlation function you need to know all of the other correlation functions.

Since the dynamic rules conserve the number of particles in the system, we can use the continuity equation:

$$\frac{d}{dt}\langle \tau_i \rangle = \langle J_{i-1} \rangle - \langle J_i \rangle. \tag{3.6}$$

where stationary current J_i between sites $(i, i+1)$ equals:

$$\langle J_i \rangle \equiv \langle \tau_i(1 - \tau_{i+1}) \rangle \tag{3.7}$$

The average current is a constant in the steady state and does not depend on the lattice site so we drop the index in our further discussions.

3.2 Mean field approach

One of the most used methods in statistical mechanics is the mean field approximation. In applying this method, one neglects all fluctuations by factoring the

k-point correlation function into a product of k one-site correlation functions, i.e. $\langle \tau_i \tau_j \tau_s \ldots \rangle = \langle \tau_i \rangle \langle \tau_j \rangle \langle \tau_s \rangle \ldots$. If we denote $\langle \tau_i \rangle$ by t_i we obtain the following equations:

$$
\begin{aligned}
t_{i-1} - t_{i-1} t_i &= t_i - t_i t_{i+1} \equiv C \\
t_1 - t_1 t_2 &= \alpha(1 - t_1) \\
\beta t_N &= t_{N-1} - t_N t_{N-1}
\end{aligned}
\tag{3.8}
$$

where C is a constant equal to the current of particles in the chain. It defines a simple mapping between the t_i's:

$$
t_{i+1} = 1 - \frac{C}{t_i}
\tag{3.9}
$$

This recursion has two fixed points for $C < 1/4$:

$$
t_{1,2} = \frac{1}{2} \{ 1 \pm (1 - 4C)^{\frac{1}{2}} \}.
\tag{3.10}
$$

The larger one is a stable fixed point while the smaller one is unstable. For $C = 1/4$, there is only one marginal fixed point and we have no fixed points for $C > 1/4$ (Derrida et al., 1992). All these simple observations suggest that a transition point exists when the steady state current J equals $1/4$. We can think of it as a *boundary induced* transition. It is well known that, for equilibrium systems, the mean field treatment can predict a transition which is destroyed in low dimensions by fluctuations in the system. Therefore other approaches are required to check whether the predicted transition for this one-dimensional non-equilibrium system does indeed occur. In the next two sections we describe some exact methods for solving this model involving operator algebra and discuss the approximate methods that we have developed using scaling approaches and position-space renormalization-group techniques.

3.3 Exact solutions and phase diagram

One of the exact approaches uses a clever trick, namely a mapping between the master equation of the system and the Schrödinger equation in imaginary time. Then the asymmetric exclusion model is re-written in a pseudo-spin language where the evolutionary operator plays the role of the quantum spin Hamiltonian. From there one can use the techniques available for one-dimensional quantum spin chains (Essler and Rittenberg, 1996; Grynberg et al., 1994; Grynberg and Stinchcombe, 1995).

Another approach is the operator algebra method which represents any microstate of the model as a string of operators. In other words our microstate of particles and holes is represented by a string of symbols D (for particles) and E (for holes). The main idea of the method is to seek the steady state probability for a microstate as an expectation value of the corresponding string of operators. For example:

$$\langle 10\dots 11010\dots 00\rangle = \frac{\langle W|DE\dots DDEDE\dots EE|V\rangle}{\langle W|C\dots C|V\rangle} \tag{3.11}$$

Here W and V are vectors, D, E and $C \equiv D+E$ are operators and the brackets on the left-hand side indicate that this is the average value for this particular microstate while the ones on the right-hand side have the standard *bra-ket* meaning in quantum mechanics. It can be shown that, in all cases except the case when $\alpha + \beta = 1$, the operators D and E (and their corresponding matrices) are infinite dimensional. The algebra of the operators is generated by the bulk dynamics and the operators do not usually commute. For the FASEP, if we choose the operators to obey

$$
\begin{aligned}
D|V\rangle &= \frac{1}{\beta}|V\rangle \\
\langle W|E &= \frac{1}{\alpha}\langle W| \\
DE &= D+E \equiv C
\end{aligned}
\tag{3.12}
$$

then the steady state probability for a microstate $(\tau_1, \tau_2, \ldots, \tau_N)$ can be written as (for proof see Derrida and Evans (1997)):

$$P_N(\tau_1, \tau_2, \ldots, \tau_N) = \frac{\langle W| \prod_{i=0}^N (\tau_i D + (1 - \tau_i)E)|V\rangle}{\langle W|C^N|V\rangle}.$$ (3.13)

With this result, it becomes very easy to obtain any correlation function. For example, if one wants to compute the average value for the spin/particle at position i, τ_i, the following expression has to be calculated:

$$\langle \tau_i \rangle = \frac{\langle W|C^{i-1}DC^{N-i}|V\rangle}{\langle W|C^N|V\rangle}.$$ (3.14)

Here N indicates that we consider a finite chain of N sites. The formula for the two-site correlation function between particles at sites i and j $(i < j)$ is:

$$\langle \tau_i \tau_j \rangle = \frac{\langle W|C^{i-1}DC^{j-i-1}DC^{N-j}|V\rangle}{\langle W|C^N|V\rangle}$$ (3.15)

As shown in the next section, to construct our position-space renormalization scheme we need the formula for the steady state current:

$$J = \langle \tau_i(1 - \tau_{i+1}) \rangle = \frac{\langle W|C^{i-1}DEC^{N-i-1}|V\rangle}{\langle W|C^N|V\rangle} = \frac{\langle W|C^{N-1}|V\rangle}{\langle W|C^N|V\rangle}$$ (3.16)

which is of course independent of i as expected in the steady state. Now we consider how to extract the asymptotic behavior for the current in the thermodynamic limit, $N \to \infty$. For large N we find that:

$$\langle W|C^N|V\rangle \propto \begin{cases} N^{-3/2}4^N & \text{, for } \alpha > \frac{1}{2} \text{ and } \beta > \frac{1}{2}, \\ [\alpha(1 - \alpha)]^{-N} & \text{, for } \alpha < \frac{1}{2} \text{ and } \beta > \alpha, \\ [\beta(1 - \beta)]^{-N} & \text{, for } \beta < \frac{1}{2} \text{ and } \alpha > \beta. \end{cases}$$ (3.17)

The case when $\alpha = \beta < 1/2$ is treated specially and one gets $\langle W|C^N|V\rangle \propto N[\alpha(1 - \alpha)]^{-N}$. Using the asymptotic limit and Eq. (3.15) we obtain:

$$J = \begin{cases} \frac{1}{4} & \text{, for } \alpha \geq \frac{1}{2} \text{ and } \beta \geq \frac{1}{2}, \\ \alpha(1 - \alpha) & \text{, for } \alpha < \frac{1}{2} \text{ and } \beta > \alpha, \\ \beta(1 - \beta) & \text{, for } \beta < \frac{1}{2} \text{ and } \alpha > \beta. \end{cases}$$ (3.18)
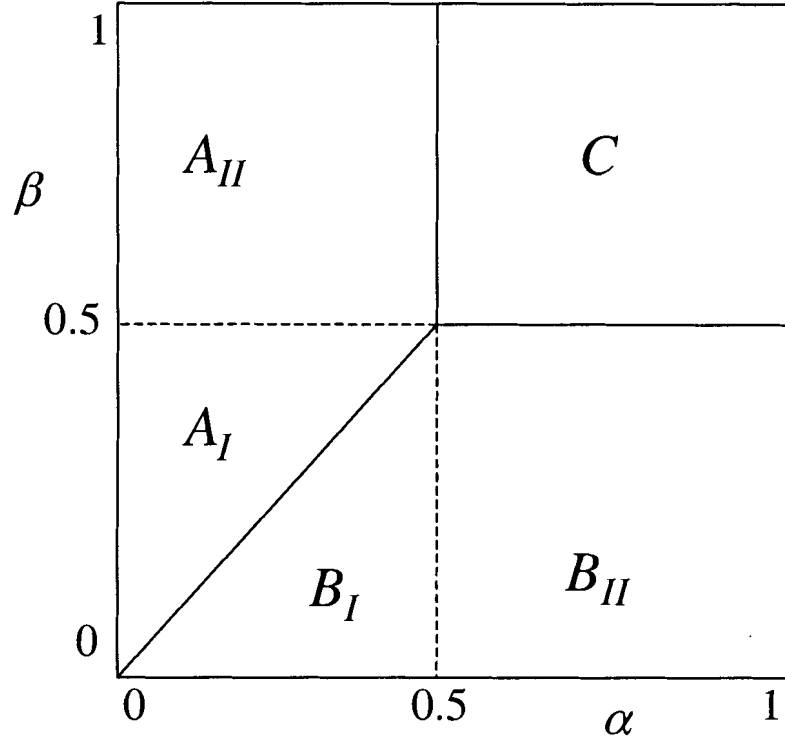
Figure 7: The phase space diagram of the FASEP model (See, for example, Schütz and Domany (1993)). The low density phase A is divided into two phases A_I and A_{II}, and the high density phase B into B_I and B_{II} (see the text). The maximum current phase is labeled C. The bulk densities in the regions A, B, and C are respectively: α, $1 - \beta$, and $1/2$. The lines $\alpha = 0.5$ and $\beta = 0.5$ indicate second order phase transitions. The solid line $\alpha = \beta < 0.5$ is a first order phase transition.

Three different phases are clearly seen from this equation and the phase diagram is summarized in Fig. 7. These values of J can also be derived exactly using a mean field treatment.

Phase A is the low density region. The injection rate α is smaller than the removal rate β so the steady state is established when there is a relatively small population of particles in the bulk. In Phase B, which is the high density region, the opposite takes place, i.e. there are more particles coming into the chain than going out of it and the bulk density is established at a relatively high value. The maximum current phase is the region C. The line $\alpha = \beta < 1/2$ is a first order boundary line, while the lines $\alpha = 1/2$ and $\beta = 1/2$ are the second order phase transition lines. The regions (A_I, A_{II}) and (B_I, B_{II}) are new phases in the low and high density regions that are

not found by mean field considerations. For more details see Schütz and Domany (1993).

In the more general case when one considers the rate of the forward jump in the bulk to be $p < 1$, the phase diagram does not change substantially. As one can easily verify, for this model the phase diagram is the same as in Fig. 7 with the only difference being that, on the axes, we should plot α/p and β/p instead of α and β. In the next section we investigate how a position-space renormalization-group approach can be applied to this model. We chose this model as a test case for our approach since it has such a rich phase diagram for a one-dimensional system.

3.4 Position-space renormalization-group approach

For many models, scaling methods are the only ones from which one can get information about the universality class of the model studied. This situation is even more common in the case of non-equilibrium systems, where no general theoretical framework has yet been established. For this reason, we think it is important to develop scaling approaches for non-equilibrium systems such as the asymmetric exclusion model. The position-space renormalization-group approach combines an inflation of length scale and reduction of the degrees of freedom of the system while maintaining the configuration on a coarser scale. For our model, this transformation requires that the stochastic rates must rescale. In this way, a mapping between the parameters of the original model and the coarse-grained one (see Fig. 8) occurs.

Here we illustrate the general rescaling procedure with a length rescaling factor of three. Using a larger length rescaling factor would be expected to yield more accurate results, but also leads to substantially more involved algebra in the recursion relations. The set $\{\tau_1, \tau_2, ..., \tau_N\}$ maps into the set $\{T_1, T_2, ..., T_{\tilde{N}}\}$, where we have used the majority rule to determine the state (empty or occupied) of the coarse-grained site and $\tilde{N} = N/3$. We assume that the matrix algebra remains the same after the
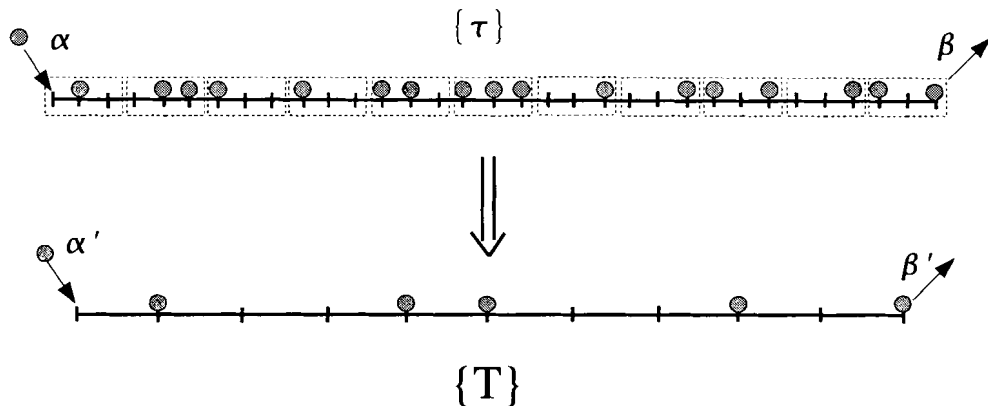
Figure 8: The majority rule for ASEP: from configuration $\{\tau\} = (\tau_1, \tau_2, \ldots, \tau_N)$ we generate a configuration $T = (T_1, T_2, \ldots, T_{N/3})$ by dividing the chain into blocks of length 3 and generating a particle in the coarse-grained chain if there are more particles in the corresponding block than holes. We assume that the state generated by this procedure corresponds to a system with rescaled parameters α' and β'.

blocking procedure prohibiting any expansion of the parameter space. In other words we expect that the blocking procedure generates states that can be considered as an output of dynamics that has different values for the rates only. This assumption produces good results for equilibrium systems that are very close to a critical point and it is natural to expect it to produce good results for our non-equilibrium model close to its critical point(s). The rates α and β evolve under rescaling while the rate for the forward jump $p = 1$ is held constant. It might look strange and arbitrary to keep the bulk forward jump at unity after the rescaling but, since the parameter p establishes only the time scale for the model and actually the ratios α/p and β/p are the only relevant parameters for its steady state, this assumption is valid. From Eq. (3.4) it follows that:

$$
\begin{aligned}
\alpha &= \frac{\langle \tau_1(1 - \tau_2) \rangle}{\langle 1 - \tau_1 \rangle} \\
\beta &= \frac{\langle \tau_{N-1}(1 - \tau_N) \rangle}{\langle \tau_N \rangle}.
\end{aligned}
\tag{3.19}
$$

Therefore, for the rescaled parameters $\tilde{\alpha}$ and $\tilde{\beta}$ of the coarse-grained system we should expect to have:

$$\begin{aligned}
\tilde{\alpha} &= \frac{\langle T_1(1-T_2)\rangle}{\langle 1-T_1\rangle} \\
\tilde{\beta} &= \frac{\langle T_{N-1}(1-T_N)\rangle}{\langle T_N\rangle}.
\end{aligned} \tag{3.20}$$

The one-site and two-site probability distributions in the coarse-grained chain can be expressed in terms of three-site and six-site probability distribution functions of the original chain as follows:

$$\langle 1C^{\tilde{N}-1}\rangle_T = \langle 111C^{N-3}\rangle_\tau + \langle 011C^{N-3}\rangle_\tau + \langle 101C^{N-3}\rangle_\tau + \langle 110C^{N-3}\rangle_\tau$$

$$\langle 10C^{\tilde{N}-2}\rangle_T = \langle 111000C^{N-6}\rangle_\tau + \langle 111001C^{N-6}\rangle_\tau + \langle 111010C^{N-6}\rangle_\tau + ..., \text{ etc.} \tag{3.21}$$

The sub-indices T and τ indicate the system on which the average is calculated. Working out each of these distributions, using the algebra represented by Eq. (3.13), we find that the rescaled values depend on the expression:

$$\frac{\langle W|C^{N-a}|V\rangle}{\langle W|C^N|V\rangle} = \frac{\langle W|C^{N-1}|V\rangle}{\langle W|C^N|V\rangle}\frac{\langle W|C^{N-2}|V\rangle}{\langle W|C^{N-1}|V\rangle} \cdots \frac{\langle W|C^{N-a}|V\rangle}{\langle W|C^{N-a+1}|V\rangle}, \tag{3.22}$$

where a is a natural number. In the thermodynamic limit, each of the ratios on the right-hand side becomes the steady state current J, and this expression can be rewritten as:

$$\lim_{N\to\infty} \frac{\langle W|C^{N-a}|V\rangle}{\langle W|C^N|V\rangle} = J^a . \tag{3.23}$$

After some algebra (see Appendix A), one obtains, from Eq. (3.20) using the operator algebra and Eqs. (3.21, 3.23), the final recursion relations between the parameters on the rescaled and original chains:

$$\begin{aligned}
\tilde{\alpha} &= \frac{3+4J+(6-\frac{3}{\alpha}-\frac{3}{\alpha^2})J^2+(4-\frac{1}{\alpha}+\frac{3}{\alpha^2}+\frac{3}{\alpha^3})J^3+(\frac{4}{\alpha^2}+\frac{3}{\alpha^3})J^4}{1+\frac{1}{\alpha}+\frac{1}{\alpha^2}+\frac{J}{\alpha^2}} \\
\tilde{\beta} &= \frac{3+4J+(6-\frac{3}{\beta}-\frac{3}{\beta^2})J^2+(4-\frac{1}{\beta}+\frac{3}{\beta^2}+\frac{3}{\beta^3})J^3+(\frac{4}{\beta^2}+\frac{3}{\beta^3})J^4}{1+\frac{1}{\beta}+\frac{1}{\beta^2}+\frac{J}{\beta^2}} .
\end{aligned} \tag{3.24}$$

These relations yield the flow diagram shown in Fig. 9.
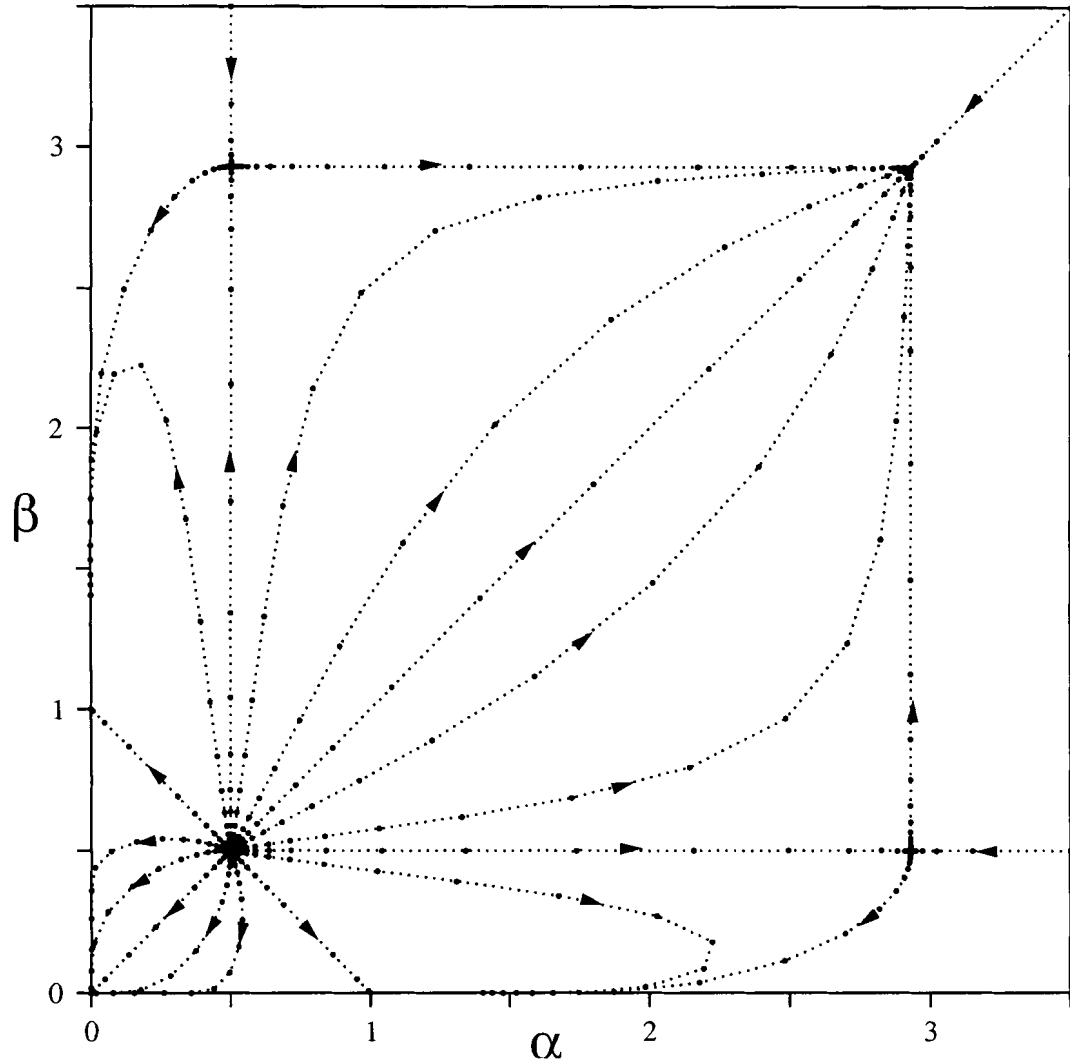
Figure 9: Flow diagram for the fully asymmetric exclusion model. Points start from the vicinity of the repulsive fixed point $\alpha_c = \beta_c = 0.5$. There are fixed points at: $(0,0)$, $(0,1)$, $(1,0)$, $(0.5, 2.929)$, $(2.929, 0.5)$ and $(2.929, 2.929)$. The flow diagram captures exactly all of the major features of the model: the first and second order lines and the fixed point at $(0.5, 0.5)$.

From Eq. 3.24 the flow diagram displayed in Fig. 9 is generated as follows. First we select initial values of α and β. These values determine the current J, which has different values in the $\alpha - \beta$ plane as specified by Eq. 3.18. Plugging the values of α, β, and J into Eq. 3.24 yields the rescaled values $\tilde{\alpha}$ and $\tilde{\beta}$. The rescaled current is obtained again from Eq. 3.11, using the rescaled values of α and β. This process is done iteratively to generate the full flow diagram.

The flow diagram shown in Fig. 9 captures the exact critical point and phase boundaries separating the high and low current and high and low density regions. Attractive fixed points occur at $\alpha = \beta = 0.0$, the zero current fixed point, and at $\alpha = \beta \approx 2.929$, which attracts all points within the maximum current phase. The maximum current phase (C in Fig. 7) is separated from the high and low density phases by second order phase boundaries, corresponding in the flow diagram to the two separatrices, each originating at the $\alpha = \beta = 0.5$ fixed point, with one attracted to the fixed point $(0.5, 2.929)$ and the other attracted to $(2.929, 0.5)$. If one increases the length rescaling factor, these fixed points and the attractor for the maximum current phase should move toward their correct locations, i.e. the value 2.929 should approach infinity.

An interesting closed subspace of the flow diagram is the line connecting $(0, 1)$ and $(1, 0)$, all contained within the low current region. This line, $\alpha + \beta = 1$, has always been treated separately because its steady state solution becomes trivial. One can choose one dimensional matrices (scalars) $D = \beta^{-1}$ and $E = \alpha^{-1}$ to solve the problem. The flow diagram clearly captures this feature, with this line occurring as a closed subspace.

The basins of attraction corresponding to the high and low density regions are separated by a first-order boundary, evidenced in the flow diagram by the line from the unstable critical fixed point to the attractive fixed point at $\alpha = \beta = 0.0$. Thus, the flow diagram reproduces all of the phase boundaries and the critical point. A

similar flow diagram was obtained by Stinchcombe and Hanney by coarse graining the operators D and E and using them to calculate the system properties (Stinchcombe and Hanney, 2002). Our results combined with their treatments indicate that a reliable qualitative picture, and sometimes exact quantitative agreement, can be obtained with these position-space rescaling approaches using small length rescaling factors.

We see that the critical point $\alpha_c = \beta_c = 1/2$ is a repulsive one as expected. The linearized recursion relations around this fixed point can be written as:

$$\begin{bmatrix} \delta\tilde{\alpha} \\ \delta\tilde{\beta} \end{bmatrix} = \begin{bmatrix} \dfrac{\partial\tilde{\alpha}}{\partial\alpha} & \dfrac{\partial\tilde{\alpha}}{\partial\beta} \\ \dfrac{\partial\tilde{\beta}}{\partial\alpha} & \dfrac{\partial\tilde{\beta}}{\partial\beta} \end{bmatrix}_{\substack{\alpha=1/2 \\ \beta=1/2}} \begin{bmatrix} \delta\alpha \\ \delta\beta \end{bmatrix}, \text{where } \delta\tilde{\alpha} = \tilde{\alpha} - 1/2,\, \delta\tilde{\beta} = \tilde{\beta} - 1/2. \quad (3.25)$$

The above matrix has two eigenvalues λ_1 and λ_2 from which we can calculate the critical exponent of the correlation length. From the ratio of the distances between consecutive points in the renormalization-group flow (see Fig. 10), we obtain the numerical values for these eigenvalues

$$\lambda_1 = \lambda_2 = 1.5. \quad (3.26)$$

Thus the eigenvalue matrix is proportional to the identity matrix with a proportionality coefficient of 3/2. The correlation length ξ diverges as $\xi \sim (\delta w)^{-\nu}$ (w in our case is either α or β), where the critical exponent $\nu = \ln b / \ln \lambda$ equals:

$$\nu = \frac{\ln(3)}{\ln(3/2)} \approx 2.710. \quad (3.27)$$

From the exact solution (Schütz and Domany, 1993), a length scale ξ_σ can be defined:

$$\xi_\sigma = -\frac{1}{\ln[4\sigma(1-\sigma)]}, \quad (3.28)$$

where σ can be either α or β and the length scale $\xi^{-1} \equiv \xi_\alpha^{-1} - \xi_\beta^{-1}$ governs the decay of the density profile. When σ tends to $1/2$, this length scale diverges as:

$$\xi_\sigma \propto [\sigma - 1/2]^{-2}, \quad (3.29)$$
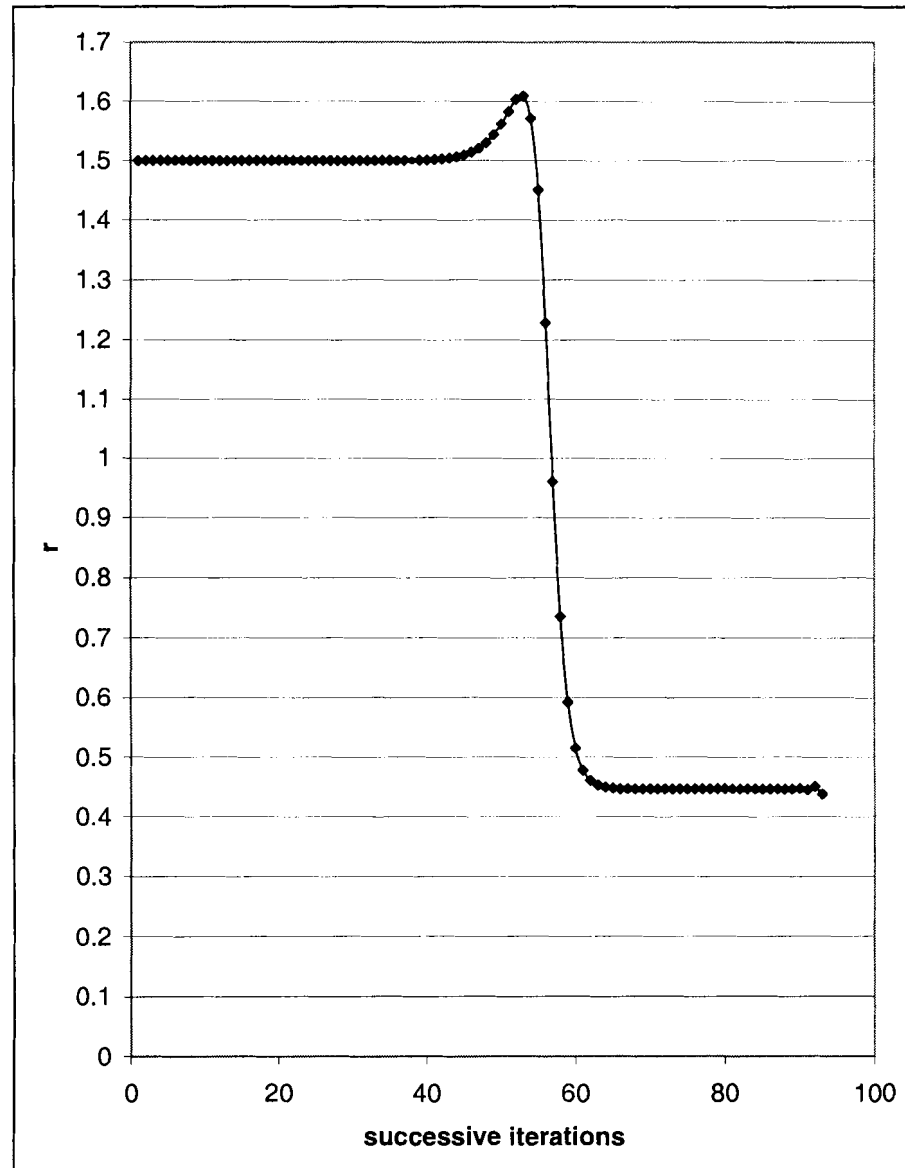
Figure 10: Numerical calculation of the eigenvalues of the renormalization matrix for the FASEP model.The ratio r of the length between successive points, which provides the eigenvalues of the matrix. The ratio of 1.5 occurs in the critical region. The other ratio occurs near the attractor located at $(2.929, 2.929)$.

which gives the critical exponent $\nu = 2.00$, so our result is in good agreement with the exact value.

The same procedure can be applied to the more general system with probability $p\,dt$ for a jump to an empty site on the right. In this case Eqs. (3.4) become:

$$
\begin{aligned}
\frac{d}{dt}\langle \tau_i \rangle &= p\langle \tau_{i-1}(1 - \tau_i) \rangle - p\langle \tau_i(1 - \tau_{i+1}) \rangle \\
\frac{d}{dt}\langle \tau_1 \rangle &= \alpha\langle 1 - \tau_1 \rangle - p\langle \tau_1(1 - \tau_2) \rangle \\
\frac{d}{dt}\langle \tau_N \rangle &= p\langle \tau_{N-1}(1 - \tau_N) \rangle - \beta\langle \tau_N \rangle \,.
\end{aligned}
\tag{3.30}
$$

In terms of new variables $\hat{\alpha} = \alpha/p$ and $\hat{\beta} = \beta/p$, the steady state Eqs. (3.28) become identical to the equations for the system with $p\,dt = 1$. The critical point moves to $\alpha_c = \beta_c = p/2$, in agreement with results obtained using other methods (Sandow, 1994), and the critical exponent stays the same.

An interesting related question is whether the linearized recursion matrix Eq. (3.25) remains proportional to the identity matrix when larger rescaling factors are used (see Fig. 11). This conjecture can easily be proven. The general recursion relations between $(\tilde{\alpha}, \tilde{\beta})$ and (α, β), because of the particle-hole symmetry, would be of the form:

$$
\begin{aligned}
\tilde{\alpha} &= f[\alpha, J(\alpha, \beta)] \\
\tilde{\beta} &= f[\beta, J(\alpha, \beta)].
\end{aligned}
\tag{3.31}
$$

The function $f(u, J)$ would be different for different scaling parameters (here u can be either α or β). It is easy to check that the matrix would become:

$$
\left[
\begin{array}{cc}
\dfrac{\partial \tilde{\alpha}}{\partial \alpha} & \dfrac{\partial \tilde{\alpha}}{\partial \beta} \\
\dfrac{\partial \tilde{\beta}}{\partial \alpha} & \dfrac{\partial \tilde{\beta}}{\partial \beta}
\end{array}
\right]_{\substack{\alpha=1/2 \\ \beta=1/2}}
=
\left[
\begin{array}{cc}
\frac{\partial f}{\partial u} + \frac{\partial f}{\partial J}\frac{\partial J}{\partial \alpha} & \frac{\partial f}{\partial J}\frac{\partial J}{\partial \beta} \\
\frac{\partial f}{\partial J}\frac{\partial J}{\partial \alpha} & \frac{\partial f}{\partial u} + \frac{\partial f}{\partial J}\frac{\partial J}{\partial \beta}
\end{array}
\right]_{\alpha=\beta=1/2}
=
\left[\frac{\partial f}{\partial u}\right]_{\alpha=\beta=1/2}
\left[
\begin{array}{cc}
1 & 0 \\
0 & 1
\end{array}
\right],
\tag{3.32}
$$

Figure 11: Flow diagram in the vicinity of the critical point for the FASEP model. Dots indicate the flow occurring at successive iterations away from the unstable fixed point.

where Eqs. (3.18) are used to calculate the necessary derivatives in the different regions. Therefore the matrix remains proportional to the identity matrix with proportionality coefficient $(\partial f/\partial u)$ evaluated at the critical point. The renormalization-group flow does not distinguish between the high density regions A_I and A_{II} (or between the low density regions B_I and B_{II}) reported in Schütz and Domany (1993). These areas differ only in the way in which the bulk density is approached coming from the boundary site, and thus have identical macroscopic properties in the thermodynamic limit.

We have also tested another approach for constructing the recursion equations, one that imposes the requirement that the current remains invariant under the rescaling, i.e. $\tilde{J} = J$. Applying this approach to the system with $p\,dt \neq 1$, again with a length

rescaling factor of three, we obtain:

$$\tilde{\alpha} = \alpha \frac{\langle 1 - \tau_1 \rangle}{\langle 1 - T_1 \rangle}, \quad \tilde{p} = \alpha \frac{\langle 1 - \tau_1 \rangle}{\langle T_1(1 - T_2) \rangle}, \quad \tilde{\beta} = \beta \frac{\langle 1 - \tau_N \rangle}{\langle T_N \rangle}, \tag{3.33}$$

and, with the matrix algebra changed to $pDE = D + E$, the recursion equations become:

$$
\begin{aligned}
\tilde{\alpha} &= \frac{1}{(\frac{1}{p^2} + \frac{1}{\alpha p} + \frac{1}{\alpha^2})J + \frac{1}{\alpha^2 p}J^2} \\
\tilde{\beta} &= \frac{1}{(\frac{1}{p^2} + \frac{1}{\beta p} + \frac{1}{\beta^2})J + \frac{1}{\beta^2 p}J^2} \\
\tilde{p} &= \frac{1}{\frac{3}{p^2}J + \frac{4}{p^3}J^2 + (\frac{6}{p^4} + \frac{3}{\alpha p^3} + \frac{3}{\alpha^2 p^2})J^3 + (\frac{4}{p^5} - \frac{1}{\alpha p^4} + \frac{3}{\alpha^2 p^3} + \frac{3}{\alpha^3 p^2})J^4 + (\frac{4}{\alpha^2 p^4} + \frac{3}{\alpha^3 p^3})J^5}
\end{aligned}
\tag{3.34}
$$

This approach yields the same value for the critical exponent $\nu = 2.710$. Here the parameters that change during the rescaling are α, β and p. The general case of the Fock representation of the quadratic algebra involves twelve parameters that control the flow of the gas in the bulk of the chain. (Essler and Rittenberg, 1996) The general steady state solution for this case is not known yet. As in the equilibrium case, in order to obtain more accurate calculations, we would have to include in the system after rescaling new dynamical rules, to add more allowed transitions between states. In other words, the rescaled dynamics, with appropriate generality, should include possibilities for the following transitions:

$$
\begin{aligned}
\text{Diffusion to the right:} & \quad 1 + 0 \to 0 + 1, \quad (\text{ rate } \Gamma_{01}^{10}) \\
\text{Coagulation at the right:} & \quad 1 + 1 \to 0 + 1, \quad (\text{ rate } \Gamma_{01}^{11}) \\
\text{Decoagulation at the right:} & \quad 1 + 0 \to 1 + 1, \quad (\text{ rate } \Gamma_{11}^{10}) \\
\text{Birth at the right:} & \quad 0 + 0 \to 0 + 1, \quad (\text{ rate } \Gamma_{01}^{00}) \\
\text{Death at the right:} & \quad 1 + 0 \to 0 + 0, \quad (\text{ rate } \Gamma_{00}^{10})
\end{aligned}
\tag{3.35}
$$

where $1(0)$ means we have a particle(hole) at some particular site. Allowing the possibility of proliferation in parameter space would improve the value for the critical exponent ν but is not a straight-forward task.

There have been recent papers on position-space renormalization for reaction-diffusion systems that successfully studied these models (Hooyberghs and Vanderzande, 2000; Hooyberghs et al., 2001). These studies take advantage of the fact mentioned above that these models can be related to the ground state of a suitably defined quantum Hamiltonian and then employ methods available for quantum spin systems. Another study investigates mainly the asymmetric exclusion model, as we did, by developing a position-space renormalization procedure involving the density and the current in the chain and calculating the dynamical critical exponent of the model (Stinchcombe and Hanney, 2002).

The results that we have presented in this section illustrate the applicability of scaling and renormalization schemes to systems out of equilibrium. The method that we have developed uses the knowledge of the form of the steady state probability distribution of microstates, the operator algebra of the model and the behavior of the current in the different regions of the phase diagram. A similar method can be applied to the exclusion model when one considers possibilities of forward and backward jumps. The extension to this model is not trivial though, and one faces more computational efforts working with the corresponding algebra of the operators. Another obvious improvement would be the use of a larger rescaling factor as mentioned above. The computational task grows exponentially but it is a straight-forward and mechanical application, and the use of a clever computer program that computes terms as shown in Appendix A would greatly reduce the overall effort.

To apply this approach to models for which the current and probability distribution of microstates are not known, one could use the mean field results for these quantities as an approximation. Thus, the method illustrated here provides a general position-space renormalization-group approach for a variety of model systems.

CHAPTER 4

TWO-DIMENSIONAL DRIVEN DIFFUSIVE LATTICE GASES: A MONTE CARLO RENORMALIZATION-GROUP STUDY USING INFORMATION THEORETIC TECHNIQUES

In this chapter we consider a two-dimensional lattice gas which has been used extensively in the past decade for modeling driven diffusive systems. We develop a Monte Carlo renormalization-group approach by calculating, from computer simulations, the measure entropy of the model. In order to do this, we apply some information theoretic approaches, which prove to be very useful when one wants to calculate the entropy of a process with a translationally invariant (in space) stationary probability distribution.

4.1 Properties of driven lattice gases

Two-dimensional lattice models have proven to be a valuable testing ground for new ideas, and their study can lead to a better understanding of the general theory of steady states in systems far from equilibrium. In equilibrium models, one has the usual Boltzmann factor, which specifies the weight of any configuration on the lattice. It seems natural to extend the Boltzmann factors, in a sense that will become clear a little bit later, to be able to make a model that simulates a process out of equilibrium and which continuously maps into an equilibrium model when the non-equilibrium forces vanish.

Driven lattice gas (DLG) models were first introduced in a paper of Katz and co-workers (Katz et al., 1984) and they are probably the most straight-forward extension of the equilibrium Ising model with conserved number of particles. The non-equilibrium features arise due to the inclusion of an external driving field that biases the jumps of the particle along one direction. Here we briefly review their basic properties (for more details see Schmittmann and Zia (1995)). Consider a system of particles on a simple hyper-cubic lattice $\mathbf{Z}^d$ in d dimensions with hard-core exclusion interactions (no more than one particle per site at any moment). The particles are subject to a driving field $\mathbf{E}$ along one of the directions (which will be denoted the $\|$-direction) and are confined in a hyper-box $\mathbf{B} \subset \mathbf{Z}^d$ with periodic boundary conditions. Each particle interacts with its nearest neighbors only, and the whole lattice is thermally activated by a heat reservoir at inverse temperature $\beta = 1/k_B T$. The external field produces net current in the system and the Ohmic power produced by the field relaxes through the heat bath. The topology of the model makes it unlikely for exact physical realization and one can think of it as a generic mathematical model for a system far from equilibrium. It has been used to model fast ionic conductors in a strong electric field and has been surprisingly successful in capturing many of their features (Marro and Dickman, 1999).

The microstate of the system is a set of all possible configurations $\sigma = \{\sigma_i : i \in \mathbf{B}\}$, where σ_i is the occupation number for site i in the lattice:

$$\sigma_i = \begin{cases} 1 & \text{if } i \in \mathbf{B} \text{ is occupied,} \\ 0 & \text{if } i \in \mathbf{B} \text{ is empty.} \end{cases} \tag{4.1}$$

The dynamics is stochastic and is given by the exchange rates $W_E(\sigma' \to \sigma)$ between two configurations σ' and σ that differ at most by a one particle jump into one of its unoccupied nearest neighbor sites. Then, the time evolution of the probability

distribution $P(\sigma; t)$ is given by the master equation:

$$\frac{dP(\sigma; t)}{dt} = \sum_{\sigma'} \left\{ W_E(\sigma' \to \sigma) P(\sigma'; t) - W_E(\sigma \to \sigma') P(\sigma; t) \right\}, \qquad (4.2)$$

where the sum is over configurations that differ by at most one single particle move. The Hamiltonian of the model is

$$H[\sigma] = -4J \sum_{\langle ij \rangle} \sigma_i \sigma_j, \qquad (4.3)$$

where $J > 0$ is the strength of the nearest neighbor interaction (the multiplier of 4 comes from the mapping between the particle σ_i and the spin $s_i = 2\sigma_i - 1$ representations). The $\langle ij \rangle$ notation indicates a sum of the nearest neighbor interactions as usual. By switching the driving field off ($\mathbf{E} = 0$) one recovers the standard Ising ferromagnet with dynamics that conserves the number of particles. For this equilibrium case we have

$$W_{E=0}(\sigma' \to \sigma) = W_{E=0}(\sigma \to \sigma') e^{-\beta \{H[\sigma] - H[\sigma']\}}, \qquad (4.4)$$

which is the usual detailed balance condition that implies the stationarity and reversibility of the Gibbs measure $P_{eq}(\sigma) \propto e^{-\beta H[\sigma]}$, where β is the inverse temperature.

The most important assumption for the DLG relates to *local detailed balance* :

$$W_E(\sigma' \to \sigma) = W_E(\sigma \to \sigma') e^{-\beta \{H[\sigma] - H[\sigma']\}} e^{-\beta \epsilon_{\sigma',\sigma} E}, \qquad (4.5)$$

which includes a term proportional to the work done by the driving field, where in the above equation

$$\epsilon_{\sigma',\sigma} = \begin{cases} 1 & \text{if } \sigma' \text{ and } \sigma \text{ differ by a move of a particle along the } E \text{ direction ,} \\ -1 & \text{if } \sigma' \text{ and } \sigma \text{ differ by a move of a particle against the } E \text{ direction ,} \\ 0 & \text{if } \sigma' \text{ and } \sigma \text{ differ by a move of a particle in the } \perp \text{ subspace .} \end{cases}$$

$$(4.6)$$

With one more assumption (mathematically this is the assumption of large deviations (Ellis, 1985)), one can prove that the model in the thermodynamic limit has

a stationary measure for all densities, a fact that is straightforward to establish for finite $\mathbf{B} \in \mathbf{Z}^d$. Also the stationary distribution must reflect the symmetries of the dynamics that are inherent in the rate coefficients $W(\sigma' \to \sigma)$. For example, the stationary distribution of the ensemble has to be invariant under spatial translation (modulo $\mathbf{B}$). This invariance of the steady state distribution is an important fact that we are going to use for the calculation of the measure entropy of the model.

4.2 Phase transitions of driven lattice gases

From now on, we will concentrate on the two-dimensional DLG, a rectangle with dimensions $(L_{\parallel}, L_{\perp})$. When there is no field and the density is $\rho = 0.5$, the model exhibits a second order phase transition at temperature $T_O \approx 2.2692 J/k_B T$ (the Onsager value). DLG models have been studied with various types of driving fields, namely:

- the infinite driving limit (IDLG) with $\mathbf{E} = \infty$;

- the finite driving case (FDLG);

- the random field model in the infinite case (RIDLG);

- the oscillatory model in the infinite case (OIDLG).

In the last two models, the driving field takes values $\mathbf{E} = \pm\infty$ randomly or with some period in time respectively but uniform in space . The first two models produce a net current along the driving field while the last two generate anisotropy in the lattice but no overall current. Our investigation will consider only two of these models, the IDLG and RIDLG models.

For the order parameter we use:

$$\psi \equiv \frac{1}{2L_{\parallel}} \sin\left(\frac{\pi}{L_{\perp}}\right) \Big| \sum_{\vec{r}} s(\vec{r}) \exp^{i\vec{k}.\vec{r}} \Big|, \qquad (4.7)$$
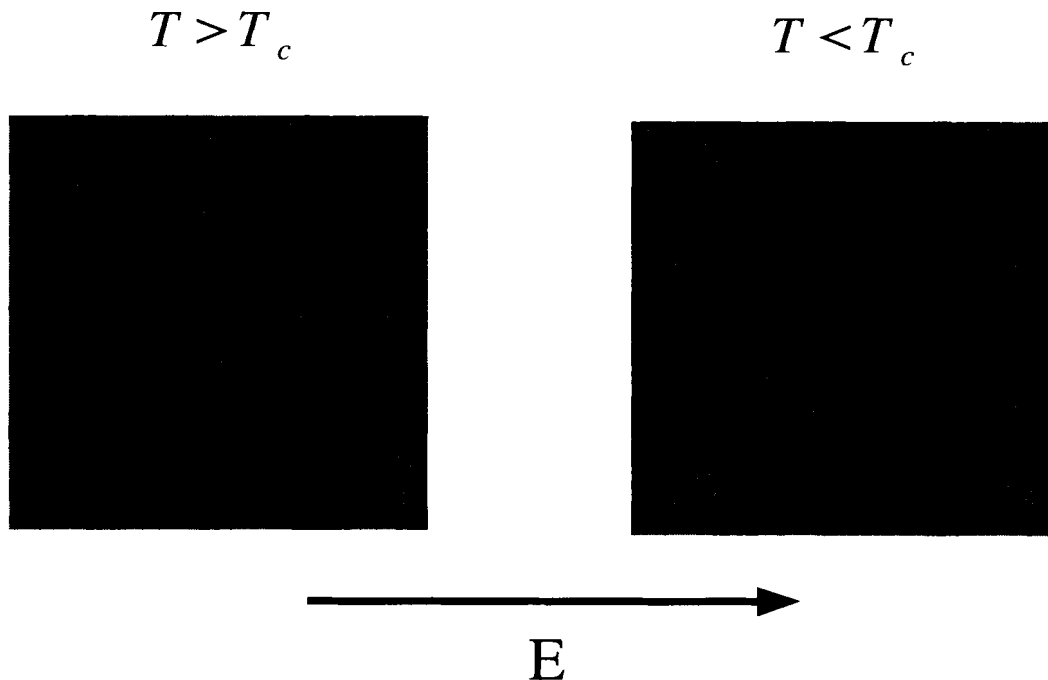
Figure 12: Typical configurations for different phases of DLG: disordered (left) and ordered (right). The driving field is along the horizontal axis. The dark pixels are empty sites and the light ones are particles and T_c is the critical temperature which is $\approx 1.41 T_O$ for the IDLG model.

where $\vec{k} = (0, 2\pi/L_\perp)$ and $s(\vec{r}) = 1 - 2\sigma(\vec{r})$. Monte Carlo simulations show that these models undergo a second order phase transition (for $\rho = 0.5$) at a temperature higher than T_O. The ordered phase consists of a single strip along the $\|$-direction (see Fig. 12). From simulations, it has been observed (Schmittmann and Zia, 1995) that the critical temperature depends strongly on the applied field at low and intermediate field magnitudes. For large driving fields, the value of the critical temperature saturates and does not change much when one increases the magnitude of the external driven field $\mathbf{E}$ further. Field theoretic investigations based on the symmetries and conservation laws predict for the critical exponents in two dimensions the values shown in Table. 1 (Leung and Cardy, 1986; Janssen and Schmittmann, 1986; Schmittmann and Zia, 1991; Præstgaard et al., 2000).

As we can see, these values are quite different from the exponents of the Ising ferromagnet and put these models into a different universality class. Another feature

Table 1: Field-theoretical values for the critical exponents.

IDLG :	$\beta = 1/2$	$\gamma = 1$	$\nu_\| = 3/2$	$\nu_\perp = 1/2$
RIDLG :	$\beta \approx 0.33$	$\gamma \approx 1.17$	$\nu_\| \approx 1.22$	$\nu_\perp \approx 0.63$

of the DLG models is the power law decay of the two-site correlation function at all finite temperatures (Garrido et al., 1990). As discussed earlier, this feature is in contrast with the usual case for equilibrium models, where generally the correlations decay exponentially at temperatures different from the critical temperature and exhibit power law decay only at the critical point. This phenomenon is most likely due to the dynamics which conserves particle numbers, the non-equilibrium steady state, and the spatial anisotropy associated with the dynamics.

There have been recent reports claiming that the two models IDLG and RIDLG are in the same universality class (Garrido et al., 2000; Archahbar et al., 2001; Albano and Saracco, 2002). These reports have produced some discussion about the different field theories for these models (Schmittmann et al., 2000). Our research was inspired by this controversy on the subject, which led us to look at how one can calculate the critical exponents by other methods, namely Monte Carlo renormalization. To apply the Monte Carlo renormalization-group approach, one needs to calculate some observable (a function of the microstate) and to design a mapping between the parameters on the coarse-grained and original systems. Natural choices would be the order parameter and the internal energy of the system. While the former has a well established meaning for both models the latter, we think, is inappropriate for these models since there is a constant external flux of energy that keeps the particles moving. That is why we decided to look for some other well defined function of the microstates and we selected the entropy density of the lattice.

4.3 Information theoretic approach

There are different ways to quantify the ordering of the output of a process. Imagine that we have a process described by a state which can be coded into a finite binary string with length L:

$$\underbrace{001010100010101010100001111010101001001}_{L}$$

For example, the state can be a one-dimensional chain of spins where 1(0) means spin up(down) ; or some *"yes-no"* experiment for events, like "sunny-cloudy" at particular time of the day during a one-year period of time, etc. There are 2^L different binary words that can be generated by the process, but in some systems only some of them might be considered as *accessible* because, for some processes some strings might not occur at all, i.e. they are *forbidden* by the dynamics of the process (which translates into zero probability of occurrence). By recording the frequency of each string's occurrence we can approximate their probability distribution, i.e. the microstate probability distribution. The Shannon entropy of a process X is defined by :

$$H(X) = -\sum_{i=1}^{2^L} p_i \log_2 p_i, \tag{4.8}$$

where p_i is the probability for the ith microstate to occur (the numbering of the different microstate is not important and we usually use the lexicographical ordering). The units of $H(X)$ are bits and we will continue to use the same units even in the cases of lattice gases (in these situations we will assume that the Boltzmann constant $k_B = 1$). The entropy $H(X)$ measures the *uncertainty* associated with the outcome of X. It contains all of the intuitive notions of uncertainty. $H(X)$ has its maximum value of 1 when all of the outputs are equally likely to occur (the most uncertain process, i.e. the totally random case), and becomes zero when only one output occurs, i.e. the deterministic case. As we can see from this definition, in order to calculate the entropy of a process we need to know the *macrostate* of the system.

Here we will call a macrostate of a process the probability distribution over its set of allowed microstates. In order to make our models closer to real systems, we need to make their sizes larger and larger, approaching infinite size or the thermodynamic limit. Therefore, the above formula is not very useful for computations because the number of the microstates grows exponentially with the size of the system and it would require enormous computational power to sample the space of the possible microstates. Also, the Shannon entropy is an extensive quantity, i.e. it approaches infinity in the thermodynamic limit.

For these reasons it is more convenient to consider the entropy density which serves as a good indicator of the complexity of binary sequences that are generated by a stationary stochastic process (Lindgren, 1988; Zhvonkin and Levin, 1970). The entropy density or the *measure entropy* h_μ of a process X is:

$$h_\mu \equiv \lim_{\dim(X) \to \infty} \frac{H(X)}{\dim(X)}, \tag{4.9}$$

where $\dim(X)$ is just the number of microstates which the process X can possibly generate (in our one-dimensional example it equals 2^L).

Another useful quantity in our treatment is the *conditional entropy*. If we have a stochastic process X that generates states in some set $\mathbb{X}$ and another process Y whose outcome is in the set $\mathbb{Y}$, the conditional entropy $H(X|Y)$ of the process X given the outcome of process Y is defined by :

$$H(X|Y) \equiv - \sum_{x \in \mathbb{X}, y \in \mathbb{Y}} p(x,y) \log_2 p(x|y), \tag{4.10}$$

where $p(x, y)$ is the joint probability that the process X generates an output $x \in \mathbb{X}$ *and* the process Y has an output $y \in \mathbb{Y}$. The conditional probability of X given Y is denoted by $p(x|y) \equiv p(x,y)/p(y)$. The conditional entropy tells us how uncertain the output of X is, given the output of Y.

For a stochastic variable X with outcome in set $\mathbb{X}$, which has been observed at different times $(t_1, t_2, \ldots, t_{N-1})$ to have values $(x_1, x_2, \ldots, x_{N-1})$, the conditional

entropy of the output of the process X at time t_N is:

$$H(x_N|x_{N-1}, x_{N-2}, \ldots, x_1) = - \sum_{(x_1, \ldots, x_N) \in \mathbb{X}^N} p(x_1, \ldots, x_N) \log_2 \frac{p(x_1, \ldots, x_{N-1}, x_N)}{p(x_1, \ldots, x_{N-1})}.$$

$$(4.11)$$

In this notation, the measure entropy (or the *entropy rate*) is just:

$$h_\mu = \lim_{N \to \infty} \frac{H(x_N, \ldots, x_1)}{N} .$$

$$(4.12)$$

Another quantity related to the measure entropy is :

$$\tilde{h}_\mu = \lim_{N \to \infty} H(x_N|x_{N-1}, \ldots, x_1),$$

$$(4.13)$$

defined whenever the limit exists. The two quantities h_μ and $\tilde{h}_\mu$ are two different notions of the entropy rate of a process. The first one is the entropy per symbol, while the second one gives the entropy of the last output of the process given the past outcomes. It is quite a remarkable fact that these two limits exist and are equal for *stationary stochastic processes* (Cover and Thomas, 1991)

$$h_\mu \equiv \lim_{N \to \infty} \frac{H(x_N, \ldots, x_1)}{N} = \lim_{N \to \infty} H(x_N|x_{N-1}, \ldots, x_1) \equiv \tilde{h}_\mu. \qquad (4.14)$$

Let us use the notation $H(L) \equiv H(x_L, \ldots, x_1)$. Fig. 13 shows the typical behavior of $H(L)$ vs. L (for more examples, see Crutchfield and Feldman (2003)). The sub-extensive part of $H(L)$ is called the *excess entropy* of the random variable and is defined by:

$$H(L) = \mathbf{E} + h_\mu L .$$

$$(4.15)$$

The excess entropy proves to be a very useful quantity for measuring the complexity of a process. For a recent review see Feldman and Crutchfield (2002). It is not necessary for the excess entropy to be finite and usually it is not at the phase transition points.

Now we turn to the application of these quantities to stochastic lattice systems. The premise for validity of Eq. (4.14) is that we have a stationary stochastic process.
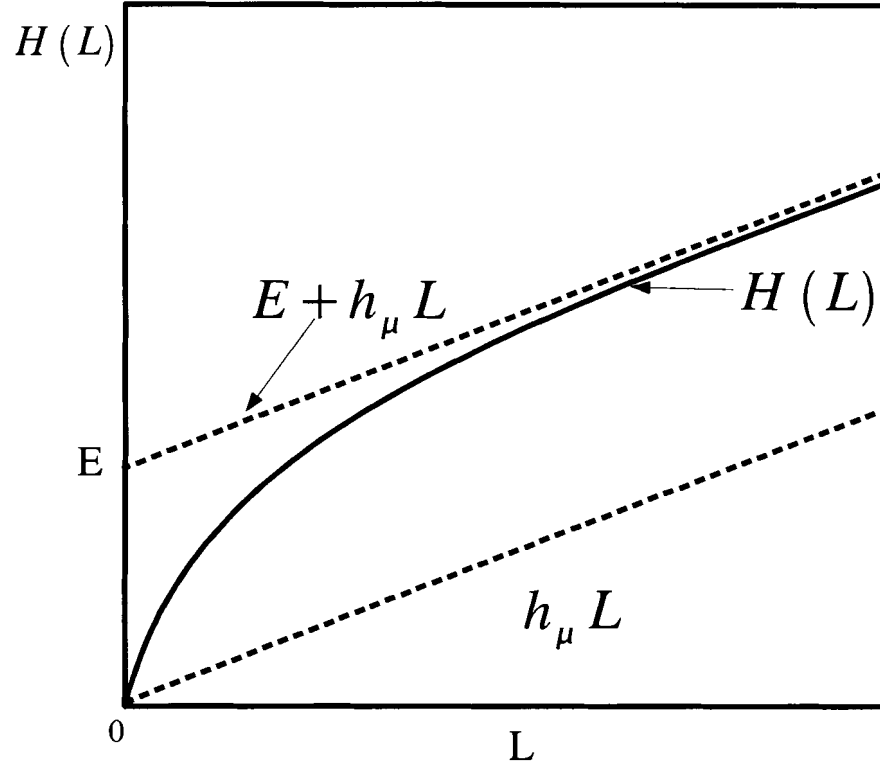
Figure 13: Typical graph for $H(L)$ vs. L. The lower dashed line is the asymptote of $H(L)$ when $L \to \infty$. The intercept E of the upper dashed line is called the *excess entropy*. (from Crutchfield and Feldman (2003))

In other words, the probability distribution for N consecutive outputs of a stochastic process X, $p(x_N, \ldots, x_1)$, must satisfy:

$$p(x_N, \ldots, x_1) = p(x_{N+i}, \ldots, x_{1+i}), \text{for any integer } i, \qquad (4.16)$$

which usually is called the *time translational invariance* (TTI). Generally, in the past development of this approach, one is talking about temporally sequenced events, so the indexes are the outputs of X at times $t_N > t_{N-1} > \ldots > t_1$. Alternatively, we can think of the indexes as spatial coordinates of the sites, in a one-dimensional infinite spin chain for example, and then the condition for stationarity is equivalent to a condition of *spatial translational invariance* (STI) of the steady state probability distribution of a cluster (geometrical collection of sites on the lattice) with N sites. This condition for invariance of the probability distribution for an ensemble of systems is true for all lattice models with translationally invariant interactions between the

particles or dynamics in the more general case. We use this notation

$$H\left[\,\boxed{\overset{\leftarrow\; L\; \rightarrow}{\square\square\square\square\square\square\square}}\,\right] \tag{4.17}$$

to indicate the Shannon entropy of a cluster of N consecutive sites on a finite one-dimensional lattice with periodic boundary conditions. It is not necessary to specify the indices because we have assumed that the system has reached a steady state, characterized by a translationally invariant measure. With this assumption, Eq. (4.14) can be translated into the following equivalent picture:

$$h_\mu = \lim_{L\to\infty} \frac{H\left[\,\boxed{\overset{\leftarrow\; L\; \rightarrow}{\square\square\square\square\square\square\square}}\,\right]}{L} = \lim_{L\to\infty}\left[H\left[\,\boxed{\overset{\leftarrow\; L\; \rightarrow}{\square\square\square\square\square\square\square}}\,\right] - H\left[\,\boxed{\overset{\leftarrow\; L-1\; \rightarrow}{\square\square\square\square\square\square\square}}\,\right]\right] = \tilde{h}_\mu \tag{4.18}$$

Here we use the fact that the conditional entropy of a site on the lattice, given the sites on the right(or left) of it, can be written as:

$$H\left[\,\boxtimes\,\big|\,\boxed{\overset{\leftarrow\; L-1\; \rightarrow}{\square\square\square\square\square\square\square}}\,\right] = H\left[\,\boxed{\overset{\leftarrow\; L\; \rightarrow}{\square\square\square\square\square\square\square}}\,\right] - H\left[\,\boxed{\overset{\leftarrow\; L-1\; \rightarrow}{\square\square\square\square\square\square\square}}\,\right], \tag{4.19}$$

where the crossed box indicates the site on which we are conditioning.

The next step is to develop a corresponding approach to calculate the measure entropy of two-dimensional lattices. Again, if the dynamics are such that the steady state probability distribution is translationally invariant (modulo the dimensions of the lattice), then the entropy for a d-dimensional system is given in terms of the entropy of a $(d-1)$-dimensional system (Goldstein et al., 1990). For the case of nearest neighbor and next nearest neighbor interactions only, the shapes shown in Fig. 14 can be used to estimate the measure entropy (Schlijper and Smit, 1989; Schlijper, 1985; Feldman and Crutchfield, 2002).

For nearest neighbor interactions, the Lth approximation for the measure entropy $h_\mu(L)$ is obtained by calculating the difference between the Shannon entropy $H(L)$ for the upper cluster shown on Fig. 14 that has $L = 2m + 1$ sites (two wings of m sites and the crossed site on which we condition) and the Shannon entropy $H(L-1)$

Figure 14: Two-dimensional shapes for estimating the measure entropy. The upper one is for a lattice gas with nearest neighbor interactions, and the bottom one is for a lattice with next nearest neighbor interactions.

of a cluster made of the two wings only. Graphically this can be shown as:

$$h_\mu(L) = H\left[\begin{array}{c}\end{array}\right] - H\left[\begin{array}{c}\end{array}\right]. \tag{4.20}$$

Therefore, in the limit as $m \to \infty$, one would reach the exact value for the measure entropy. It should be noted here that, for any L, we have $h_\mu \leqq h_\mu(L)$, i.e. we are approximating the exact value from above.

For lattice gases with next nearest neighbor interactions one has to include one more layer of lattice sites as shown in the bottom shape of Fig. 14. Again, by conditioning on the crossed shape, one can obtain an approximation of the entropy density for the model. The general rule is that one needs to include as many layers of sites in one of the directions (in the examples discussed above this is the vertical direction) as the length of the interaction range between the particles.

Here we try to provide an intuitive picture of why we should expect that the conditional entropy for the upper shape on Fig. 14 gives the exact entropy density for a stochastic lattice gas with nearest-neighbor interactions (see Fig. 15). The crossed site on the picture interacts only with its nearest neighbors. The shape includes its left and bottom neighbors. Because of the assumed symmetries of the interactions, the steady state probability distributions will be translationally invariant, so the impact of the rightmost and the uppermost neighbors on the state of the target (crossed)
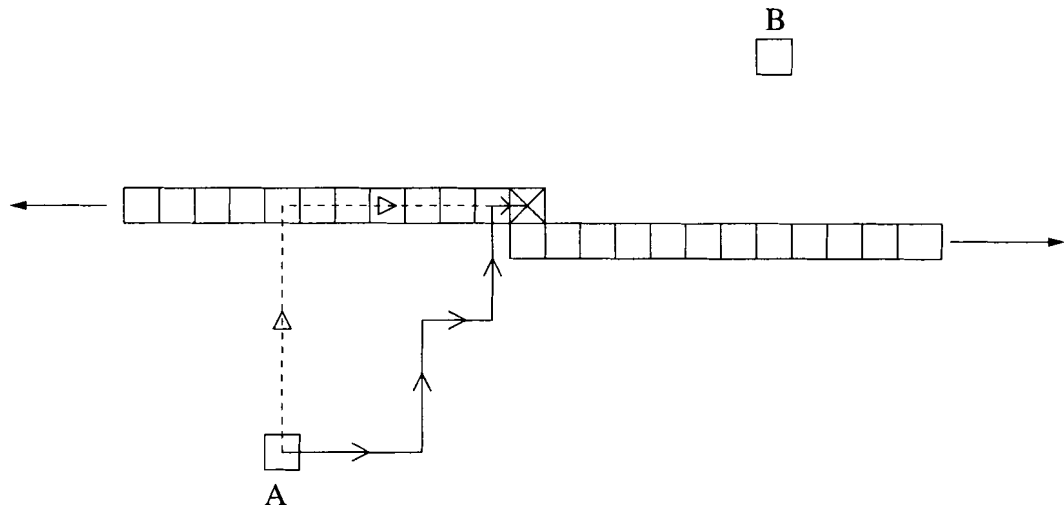
Figure 15: Illustration of intuitive reasoning for calculating the measure entropy. The conditioning on the crossed site gives the exact value for the measure entropy when the wings of the shape become infinite. (See text for discussion.)

spin will be the same as the impact of the ones already included in the shape. If we take a spin located at site A on the picture, we see that it can propagate its state to the target spin (the crossed one) by many different paths, two of which are pictured. We see that at some point all of these paths cross the shape, which extends to infinity in both directions. Therefore the influence of the spin at site A will be captured by some spin in the shape. The influence of a spin located at site B on the lattice will be the same as from a spin which is the symmetrical from the crossed site and therefore will not generate *new* information on the targeted spin. (An added discussion of this point is given in Appendix B).

An important piece of the derivation is that the shape has to be constructed with infinite wings. Although there are recent papers of algorithms about how one can tackle computations with shapes containing millions of sites (see Allegrini et al. (2002)), we will concentrate on small finite shapes with up to twenty sites. For equilibrium models, this method of estimating the entropy density gives remarkable results (Schlijper and Smit, 1989; Mierovitch, 1984, 1999; Kenneway et al., 2003). In these studies, the length of the shape used has been $10 - 15$ sites, yet the approximation
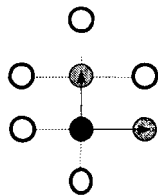
Figure 16: The interaction cluster for DLG. At each time step, we pick randomly a site (the dark one) and a direction, up or across, which defines either the horizontal bond or the vertical one. Then we try to exchange the occupation numbers on the two sites of the bond according to the rules described in the text.

of the thermodynamic entropy differs from the true value by less than a fraction of a percent at the critical temperature, where one would expect that the finite length of the shape would make the method incapable of capturing the macroscopic fluctuations in the system. Based upon these excellent results for equilibrium models, we start our investigation of the criticality of driven diffusive systems.

4.4 Monte Carlo renormalization for the driven lattice gas

We use the Metropolis algorithm to generate a sequence of microstates starting from a random initial configuration on the lattice. The system equilibrates into a steady state after typically $1 - 5 \times 10^5$ Monte Carlo steps per site (MCS). This initial equilibration time depends upon the size and temperature of the system. Since we have dynamics that conserves the number of particles we basically have diffusion occuring which is very slow and takes many MCS for the system to reach the steady state. The number of total MCS that we have used at each temperature varies from 2×10^6 to 10^7 and data is taken every $10 - 25$ steps. At each time step, we pick randomly one bond on the lattice, horizontal or vertical, as shown in Fig. 16. We consider an exchange of the occupation numbers (given that they are different) between the sites on the bond based on the factor (see Eq. (4.5)):

$$\beta[\Delta H + \epsilon E(t)] \, , \tag{4.21}$$

where β is the inverse temperature, ΔH is the change of the energy between microstates if the jump occurs, $E(t)$ is the value of the driving field at time t (it is a constant in time and space for IDLG model and random in time but constant in space for RIDLG model), and ϵ is:

$$\epsilon = (-1, 0, +1) \text{ for jumps (along, perpendicular, against) the direction of } E. \quad (4.22)$$

The models that we have studied here are the IDLG and the RDLG, which both have a driving field of infinite magnitude and therefore the jumps in the horizontal direction are independent of the occupation numbers of the other nearest neighbors of the horizontal bond. For example, if the driving field is from the left to the right, then a particle on the left site of the horizontal bond will jump to an unoccupied right site of the bond regardless of the nearest neighbors with which it interacts according to Eq. (4.4). For jumps in the transverse direction (the vertical bond on Fig. 16), the usual Ising ferromagnetic change in the energy takes place.

The rate functions in Eq. (4.5) are chosen to be the standard Metropolis rates $w(x) = \min\{1, \exp(-x)\}$, where x is the factor from Eq. (4.21). Every $10-30$ MCS data is collected and the relevant observables of the system are calculated based upon the current microstate of the system. We have used a very fast multi-spin coding algorithm (described in Appendix C) that speeds up the collection of data by a factor of sixteen compared to a conventional algorithm.

To calculate the entropy density we have used shapes (see Fig. 14) with 13 or 15 sites in our simulations. Shapes with a total length of 17 sites have been used for checking the convergence of the measure entropy with the length of the shape. At each time step, when we make a snapshot of the configuration on the lattice, we put the target site of the shape (the crossed one on Fig. 14) on every lattice site as shown on Fig. 17. Thus, we collect $L_{\parallel} \times L_{\perp}$ binary words from the current state on the lattice. If we use a shape with length L then the maximum number of binary words that can be coded with this shape is 2^L. By collecting the histogram of all of these
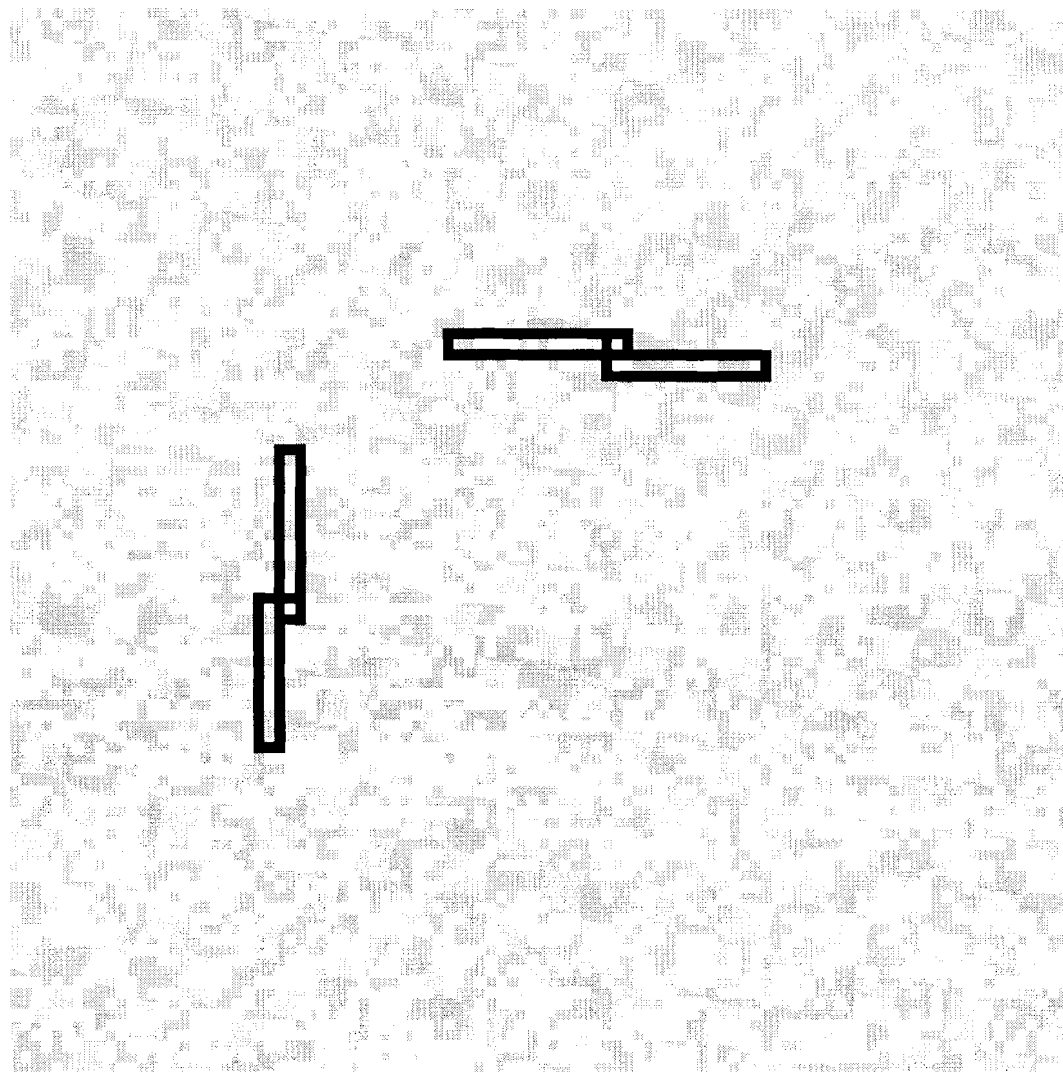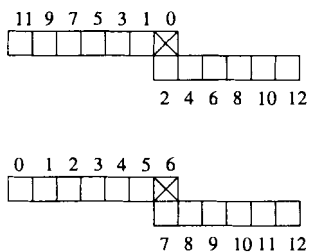
Figure 17: Horizontal and vertical shapes on a lattice. We move the horizontal/vertical shape (shown in black) at every lattice site and collect the histogram of the binary words appearing with the shape.

binary words we approximate their probability distribution from which we calculate the Shannon entropy using Eq. (4.20).

The order of the binary words is taken to be in the lexicographical order, i.e. $00\ldots00$ is the first word, $00\ldots01$ is the second word , etc. Different coding schemes can be used to map the state of a cluster into a binary word. All of them are equivalent in terms of obtaining the entropy. Therefore, we have used the most efficient ones to minimize the computation time. We have used two mappings for the shape into a binary word of length L shown on the following picture

```
11  9  7  5  3  1  0
 _____
|  |  |  |  |  | X|
 ‾‾‾‾‾‾‾‾‾‾‾‾‾| | | | | | |
              ‾‾‾‾‾‾‾‾‾‾‾‾‾
              2  4  6  8 10 12


 0  1  2  3  4  5  6
 _____
|  |  |  |  |  | X|
 ‾‾‾‾‾‾‾‾‾‾‾‾‾| | | | | | |
              ‾‾‾‾‾‾‾‾‾‾‾‾‾
              7  8  9 10 11 12
```

Here the target site (the crossed block) on the upper shape represents the lowest order bit in the word (the right most bit) and the other bits follow the numbers of the sites on the picture. This coding method is particularly efficient for calculating the excess entropy and studying the convergence of $h_\mu(L)$ (see Eq. 4.20). The method shown on the bottom shape has been used for calculating the entropy using Eq. (4.20).

Fig. 18 shows a typical probability distribution of the binary words generated from a shape with 13 sites for the IDLG model at a temperature above the critical temperature. From this spectrum, we calculate $H(L) = -\sum_{i=1}^{2^L} p_i \log_2 p_i$ and $H(L - 1) = -\sum_{i=1}^{2^{L-1}} p_i \log_2 p_i$ for the binary words generated from the shapes used in Eq. (4.20). Fig. 19 shows the convergence of $h_\mu(L)$ with the length of the shape. At high temperatures one can obtain an excellent approximation for the entropy, even with shapes of only $5-6$ sites. For the perpendicular shape, this observation remains true even for temperatures approaching the critical temperature from above. We see considerable decrease in the convergence rate of the entropy estimated by the
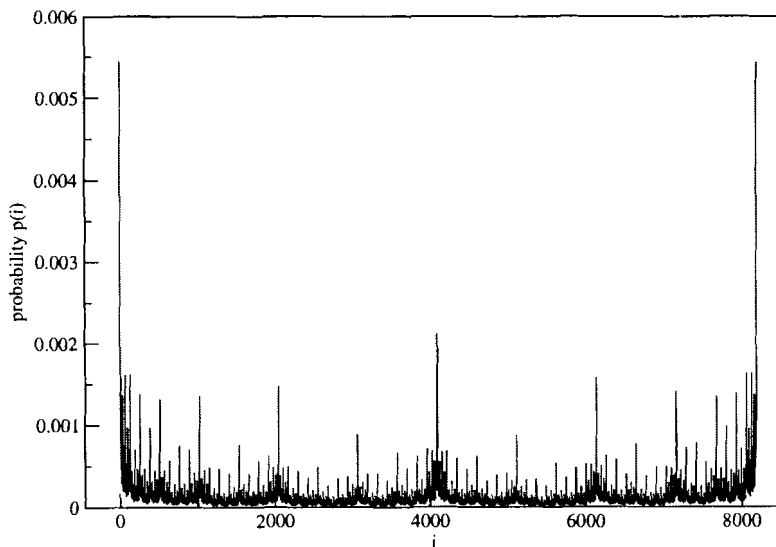
Figure 18: Example of the histogram of binary words. The shape used has a length of 13 sites ($i \in \{0, \ldots, 2^{13} - 1\}$) and the model is the IDLG simulated at temperature $T = 1.5\, T_o$.
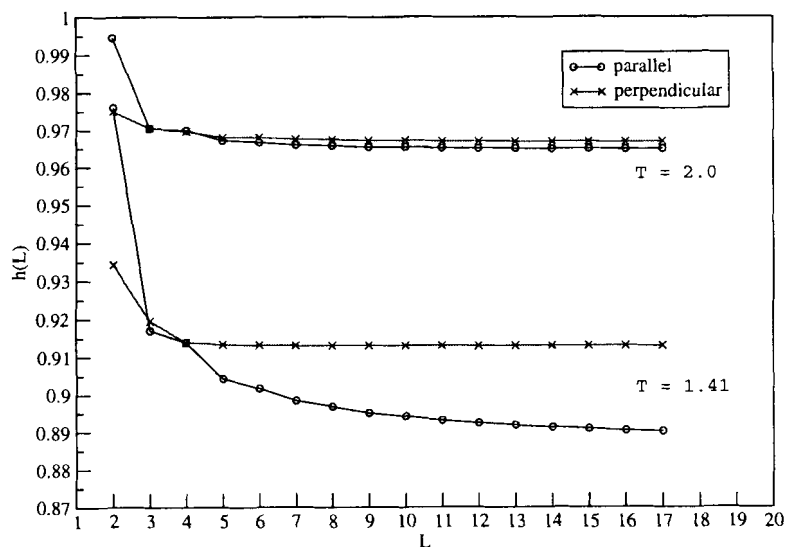

Figure 19: The convergence of $h_\mu(L)$ for shapes oriented parallel and perpendicular to the field for high ($T = 2.0$) and close to the critical point ($T = 1.41$) temperatures (the temperature is in units of the Onsager's temperature).

shapes in the parallel direction. Considering large shapes is extremely difficult with the our algorithms because it would require approximately 4GB of RAM for a shape with a length of 21 sites. As mentioned earlier, new algorithms involving adapting dictionaries could be applied in order to study longer shapes (Allegrini et al., 2002).

The difference between the values for $\lim_{L\to\infty} h_\mu(L)$ along the two directions is a result of the strong anisotropy in the system. It is not hard to understand that difference quantitatively. Indeed, the quantity that we calculate is the conditional entropy of the target site given the state of its neighbors. In the parallel case we condition on the evidence of spins in the shape along the driving field, while for the perpendicular shape we build our knowledge for the target spin given the evidence of the state of the sites in the shape perpendicular to the field. Given the strong anisotropy of the model we would expect those two conditional entropies to be different even for infinite shapes and finite temperatures.

Fig. 20 shows the advantage of using the multi-spin algorithm. By using this algorithm, we simulate 32 lattices simultaneously, using the 32-bit architecture of our computers, at the same temperature and build the histograms for the different shapes from the snapshot configurations on these 32 lattices. Apart from the obvious difference in the speed of algorithms the results obtained by using one or the other algorithm agree for any temperature. From the same graph one can gain information about the statistical error in the estimation of the entropy density. The different runs are obtained from different random initial configurations on the lattices starting with different random seeds. Thus, we treat the end results from the different runs as statistically independent and use the usual statistical methods to estimate the error of the entropy density. However, as mentioned in Chapter 2, this error in determining the entropy density can hardly be used to estimate the errors in the critical exponents obtained by the Monte Carlo renormalization. In all of the graphs that follow, the error bars for the entropy estimate are smaller than the plotting symbols used.
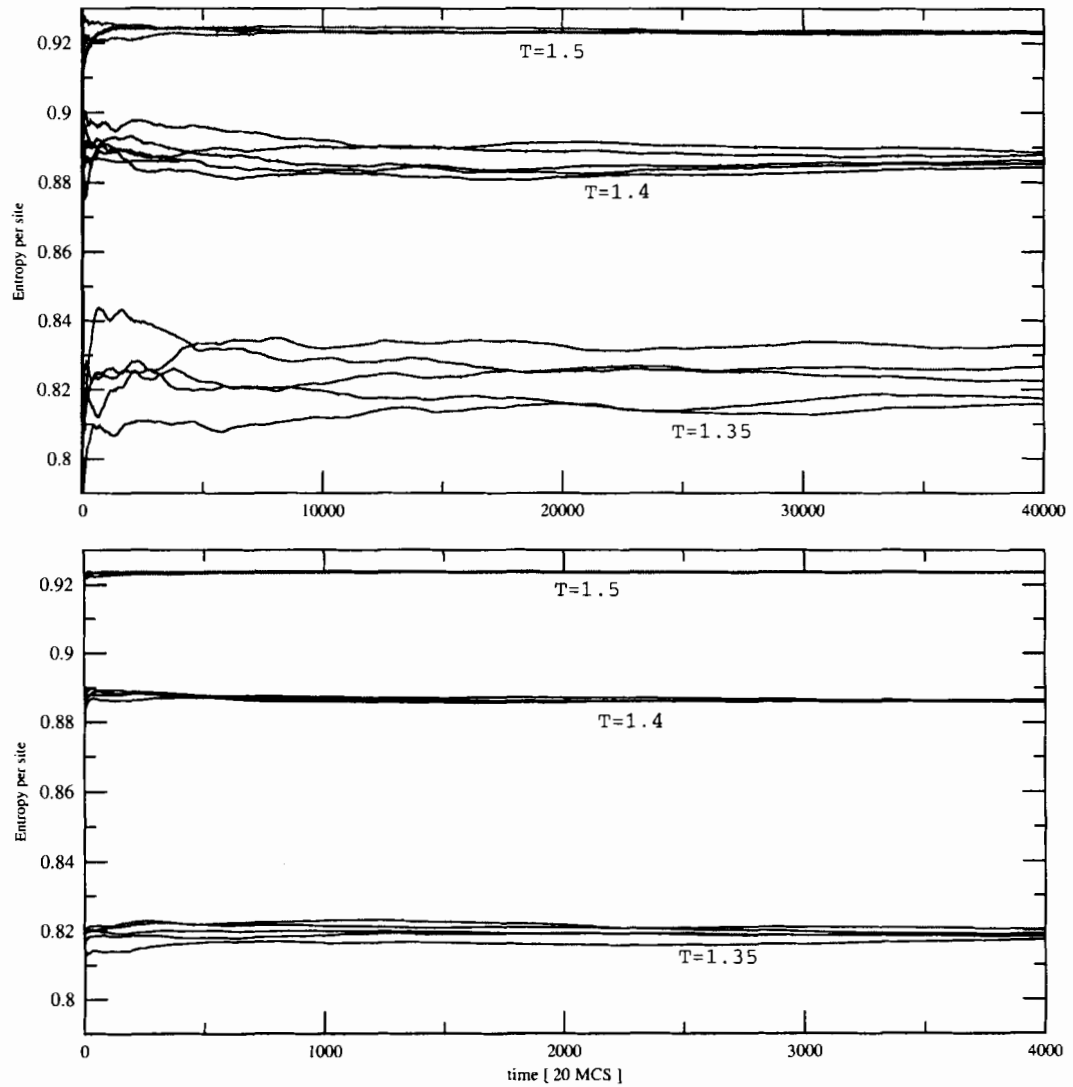
Figure 20: Comparison between the usual Metropolis algorithm (above) and multi-spin algorithm (below). As seen from the time coordinate by using the multi-spin coding one can get the same statistics for from 10 to 16 times less MCS. The three sets of lines on both figures correspond to runs at the same temperature for the two algorithms with different initial random seeds.
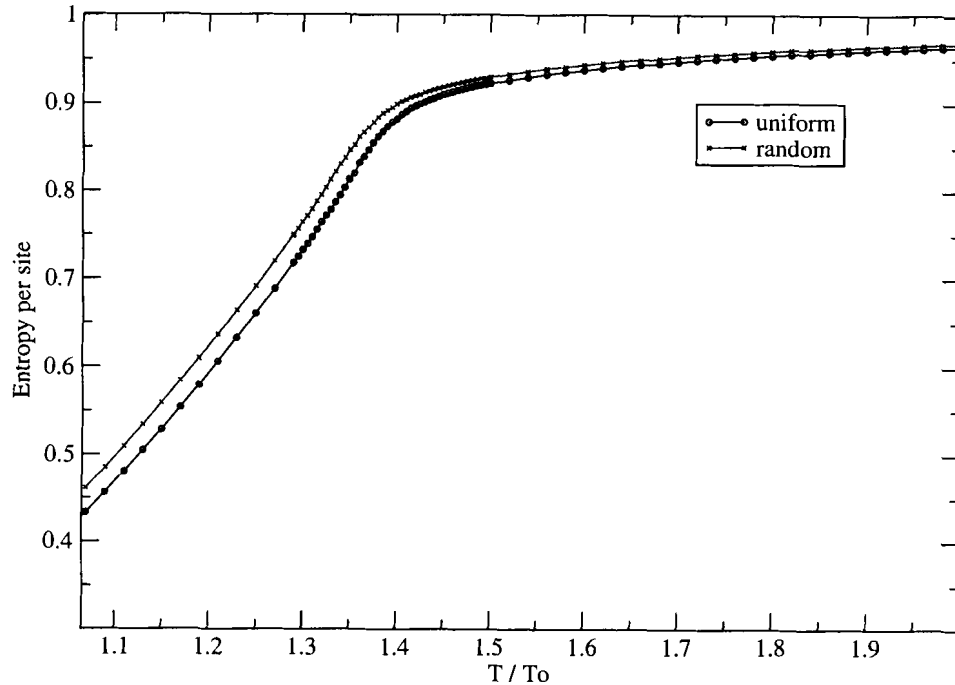
Figure 21: The entropy for the uniformly and randomly driven models. The simulations were done on a 128 × 128 lattice with a shape comprised of 15 sites oriented parallel to the driving field.

The two models, uniformly and randomly driven gases, have almost the same order parameter, internal energy and structure factor for all temperatures. This is a surprising fact because, theoretically, it has been argued that these models should be in different universality classes and thus have different critical exponents (see Eq. (1)). It is naturally to expect that the two models are in different universality classes because they have different symmetries. The steady state of the uniformly driven model is invariant under any two of the following transformations:

$$s \rightarrow -s, \quad E \rightarrow -E, \quad r_\| \rightarrow -r_\| \,, \tag{4.23}$$

implying a symmetry under $s \rightarrow -s$, and $r_{\parallel} \rightarrow -r_{\parallel}$, while the steady state for the randomly driven model is symmetrical under

$$s \rightarrow -s, \quad \text{or} \quad r_{\parallel} \rightarrow -r_{\parallel} \, . \tag{4.24}$$

Fig. 21 shows a comparison of the entropy density calculated by using shapes with a total of 15 sites oriented along the driving field on a 128×128 lattice. Unlike other macroscopic properties discussed above, the entropy density is different for the two models, which strengthens our expectations that this quantity is appropriate for exploring the criticality of the models by Monte Carlo renormalization.

It should be noted here that if we take the derivative of the entropy density with respect to the temperature numerically and multiply this quantity by the temperature (this is the specific heat capacitance for equilibrium systems) the maximum for this quantity is located at a lower temperature than the temperature obtained by Monte Carlo renormalization. This maximum has strong dependence on the size of the lattice studied. The dependence of the entropy density on the size of the lattice is shown on Fig. 22. As expected, on larger lattices the curve become steeper closer to the critical point.

Fig. 23 shows a typical graph of the behavior of the entropy density on the original and coarse-grained lattices, from which we obtain the correlation length critical exponent. Regression polynomials (from a fourth to a tenth power) have been used close to the crossing point of the two data sets to draw a smooth line (not shown on the figure). The point where these polynomials cross we report as the critical temperature. The same procedure has been followed for a set of simulations done with the shape oriented perpendicular to the driving field. A comparison of the entropy on the original and the coarse-grained lattice for shapes along and perpendicular to the field is shown on Fig. 24.

The results for $\nu_{\parallel}$ and $\nu_{\perp}$ are shown in Table 2 and Table 3 respectively. In the last column we show the ratio of the slopes of the entropy curves at the critical
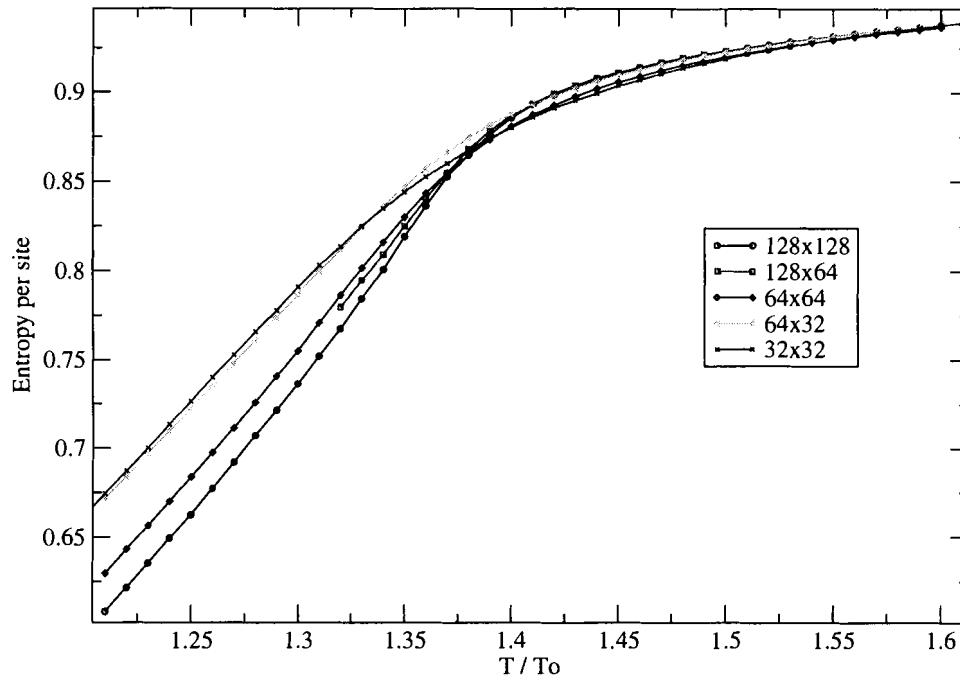
Figure 22: The entropy density calculated on different lattices for the uniformly driven model with the shape parallel to the driving field.

point (see Eq. (2.29)). In all simulations the rescaling factor b is 2. For calculating the correlation length critical exponents we have used the natural assumption for a strongly anisotropic system that we have two distinct correlation lengths diverging with different critical exponents :

$$\xi_{||} \propto |t|^{-\nu_{||}} \quad \text{and} \quad \xi_{\perp} \propto |t|^{-\nu_{\perp}} . \tag{4.25}$$

Then, by the same reasoning as for the derivation the Eq. (2.29), and the geometrical fact that $\xi'_{||}(t') = \xi_{||}(t)/b$ and $\xi'_{\perp}(t') = \xi_{\perp}(t)/b$, we obtain

$$\nu_{||} = \frac{\log b}{\log \left(\frac{dT'_{||}}{dT_{||}} \right)_{T_c}} \quad \text{and} \quad \nu_{\perp} = \frac{\log b}{\log \left(\frac{dT'_{\perp}}{dT_{\perp}} \right)_{T_c}} , \tag{4.26}$$

where the indexes $||$ or $\perp$ indicate which pair of curves to be considered (see Fig. 24).
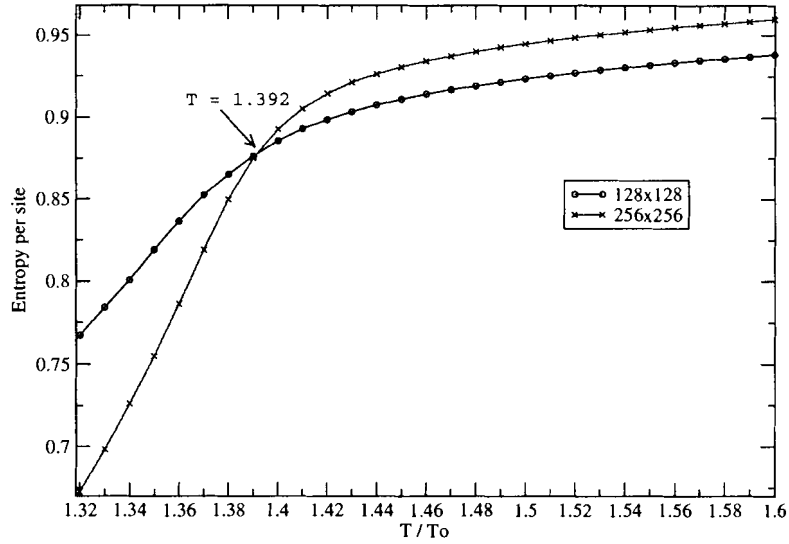
Figure 23: The entropy density for the original 128 × 128 lattice and the coarse-grained 256 × 256 lattice using 2 × 2 rescaling blocks. Results are for the IDLG using a shape with 15 sites oriented parallel to the driving field.
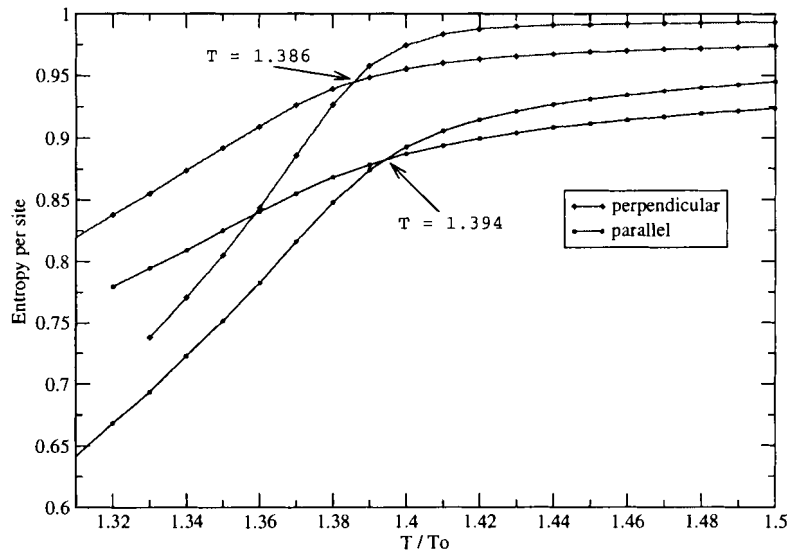
Figure 24: The entropy for parallel and perpendicular shapes. Comparison between the entropy of the original and the coarse-grained system on a 128 × 64 lattice for shapes parallel and perpendicular to the driving field for the IDLG model, with a shape comprised of 15 sites.

Table 2: The results for $\nu_\parallel$ for different lattices.

model	$L_\parallel \times L_\perp$	$T_c\,[T_o]$	$\nu_\parallel$	slope ratio
uniformly driven	64×32	1.397	0.81	1.431/0.608
	64×64	1.396	0.91	1.564/0.7324
	128×64	1.394	0.84	1.958/0.860
	128×128	1.392	0.95	2.026/0.979
randomly driven	64×64	1.392	1.02	1.232/0.625
	128×64	1.390	0.96	1.301/0.631
	128×128	1.392	0.99	1.362/0.674

From the results we see that the fixed point obtained for shapes perpendicular to the field is less than the one calculated from shapes along the field. This difference is most probably due to the fact that when the shape is aligned perpendicular to the field for $T \lesssim T_c$ it will be perpendicular to the interface between the low and high density regions. The size of the shape is comparable to the size of $L_\perp$, from 11% up to 46% of $L_\perp$ for the lattices and shapes that we have used. Shapes that frequently are positioned accros the interface introduce additional randomness when calculating the histograms for the perpendicular case, which in turn shifts the transition temperature to a lower value. This effect is present in the parallel case as well, but the $\parallel$-shape extends over just 2 sites in the perpendicular direction, which makes the impact of the interface negligible.

Table 3: The results for $\nu_\perp$ for different lattices.

model	$L_\parallel \times L_\perp$	$T_c\,[T_o]$	$\nu_\perp$	slope ratio
	64×32	1.380	0.56	1.990/0.582
uniformly driven	64×64	1.380	0.63	2.456/0.817
	128×64	1.385	0.56	3.086/0.895
	64×32	1.376	0.58	2.111/0.642
randomly driven				
	128×64	1.381	0.50	3.348/0.827

4.5 Analysis of the results for $\nu_\parallel$ and $\nu_\perp$

Compared to the theoretical values (Table 1), the values for $\nu_\parallel$ that we report here differ substantially. This discrepancy is not too surprising though, because there is currently no consensus regarding which is the correct mesoscopic equation to describe most effectively the criticality of the DLG (Santos and Garrido, 1998; Garrido and Marro, 2000; Archahbar et al., 2001; Schmittmann et al., 2000). Within the limits of applicability of the Monte Carlo renormalization method for DLG, our results match most closely the early results (see Zhang et al. (1988)) obtained from a direct estimation of the correlation length. In these studies, the two-site correlation function along the principle direction on the lattice $C_\parallel(r) = \langle \sigma_x \sigma_{x+r} \rangle$ is written as

$$C_\parallel(r) \propto \left[1 + \left(\frac{r}{\xi_\parallel} \right)^2 \right]^{-1}, \tag{4.27}$$

which serves as a phenomenological definition for the correlation length $\xi_\parallel$. From these assumptions it has been concluded that $\nu_\parallel \approx 0.7 \pm 0.3$. No reliable data for $\nu_\perp$ has been found, due to the negative correlation in the transverse direction. Based upon the $\nu_\parallel = 0.7$ value and a square lattice finite size analysis, an excellent collapse

on a single curve has been obtained for the order parameter of IDLG model (Marro et al., 1996). It has been argued further that at the critical point only one relevant correlation length, and therefore one correlation length critical exponent, plays an essential role. As mentioned above, recently new continuum theory for the IDLG has been proposed essentially casting the IDLG and RIDLG models into the same universality class.

The method that we have used to calculate the entropy density is general and applicable to any lattice gas with translationally invariant dynamics. The general applicability of Monte Carlo renormalization in the form that we use it here is a more subtle issue and merits further study, particularly for anisotropic systems. Our combined approach has the advantage of measuring the correlation length exponents in a direct way, and also the results from it have a much smaller dependence on the size of the system under consideration. The values for $\nu_{\|}$ that we report in Table 2 for the IDLG and RIDLG do not differ by much, although we believe hat the small difference is not due to statistical errors.

We have determined separately a $\nu_{\|}$ and $\nu_{\perp}$, calculated from the same shape with parallel and perpendicular orientaion. It is not clear to what extent the interface between the phases affects the data for the perpendicular shape. Further insight can be gained by considering different shapes for calculating the conditional entropy. We used the angle-like shape "G" shown in Appendix B in a simulation on a small 64×32 lattice for the two, IDLG and RIDLG, models. The shape has a total of 15 sites - 9 along the $\|$-direction and 6 in the $\perp$-direction. Thus it is designed to probe correlations in both directions simultaneously.

As shown on Fig. 25 the difference in the conditional entropy for the two models changes. In this case, the conditioning in the directions to the right and below the targeted site makes the RIDLG more ordered (less entropy) than the IDLG. The
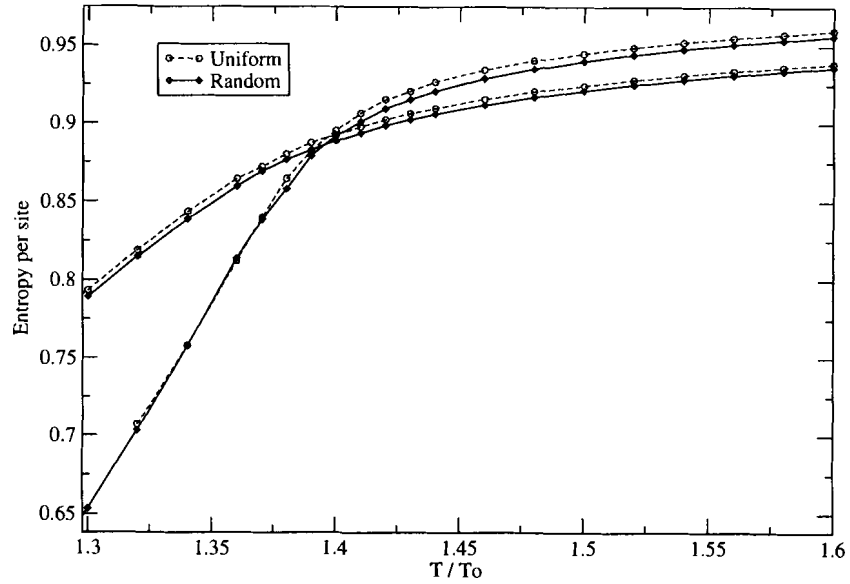
Figure 25: Results from shape "G" on a 64 × 32 lattice. The dotted lines are for the original and coarse-grained lattice on the IDLG and the solid lines are for the RIDLG.

results for the critical temperature and critical exponent ν are

model	T_c/T_o	ν	slopes ratio
IDLG	1.395	0.78	1.425/0.588
RIDLG	1.396	0.79	1.325/0.554

$$(4.28)$$

thus making the two models almost indistinguishable. It is also worth mentioning here that the entropy curves for this angled shape are very close to the ones obtained from the shape used previously in the parallel direction, rather than somewhere in the middle between the entropy from the parallel and perpendicular shapes. This result suggests that either (1) the system has one relevant correlation length exponent $\nu \approx 0.8$ or (2) the parallel orientation of the shape "H" (see Appendix B) samples an average of $\nu_{\parallel}$ and $\nu_{\perp}$, which is also ≈ 0.8.

For completeness we have calculated the excess entropy (see Eqn. (4.15)) from the shape "H" (see Appendix B) with a total of 11-sites on a small 64 × 32 lattice for the two models (see Fig. 26). As mentioned above, the excess entropy is essentially
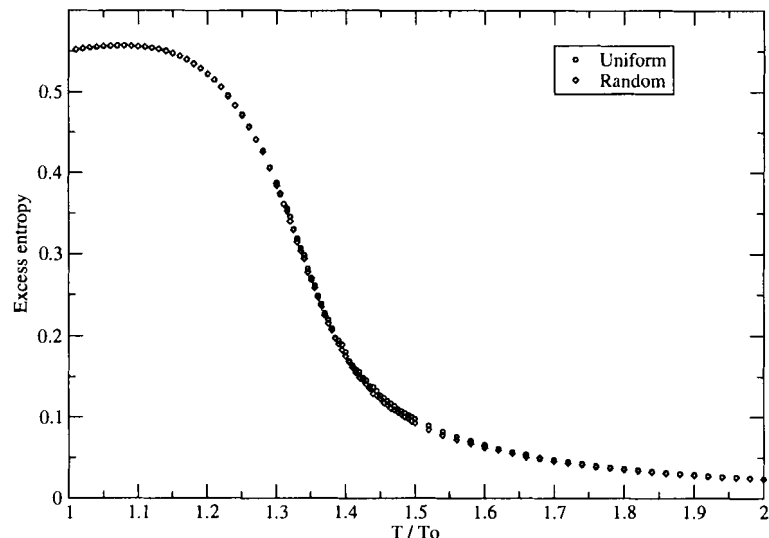
Figure 26: The excess entropy on a 64 × 32 lattice for the two models. Shapes with 11 sites have been used oriented along the parallel direction.

the sub-extensive part of the entropy of a system, a quantity usually neglected in thermodynamics. It is one way to define and quantify the *complexity* of a system. The results show no significant difference in complexity between the two models, although more data from larger lattices and longer shapes is needed to prove or disprove this conclusion. We believe that small differences can be found, as suggested already in Fig. 26 in the critical region.

4.6 Critical exponent β for the IDLG model

For calculating the order parameter of the IDLG model, we need to take into account the strong anisotropy of the system and modify Eq. (2.31) accordingly. These modifications can be done in the following manner. We assume that there are two relevant lengths and consequently we assume two different correlation length exponents $\nu_{\|} \neq \nu_{\perp}$. Standard finite size scaling analysis suggests for the order parameter the following homogeneous function (Privman, 1990):

$$\psi\left(\frac{1}{L_\perp}, \frac{1}{L_\|}, t\right) = b^{-\beta/\nu_\perp}\psi\left(b\,\frac{1}{L_\perp}, b^{\nu_\|/\nu_\perp}\,\frac{1}{L_\|}, b^{1/\nu_\perp}t\right). \qquad (4.29)$$

Thus, Eq. (2.31) modifies to

$$\frac{\beta}{\nu_{\parallel}} = \frac{\log \frac{dm'}{dm}\big|_{T_c}}{\log b^{\nu_{\parallel}/\nu_{\perp}}} \quad \text{or} \quad \frac{\beta}{\nu_{\perp}} = \frac{\log \frac{dm'}{dm}\big|_{T_c}}{\log b} \ . \tag{4.30}$$

Fig. 27 shows the results from the Monte Carlo simulations for the order parameter (see Eq. (4.7)). Typically, runs from 10^7 to 3×10^7 MCS have been performed and data is taken every 10 MCS. The initial configuration of the lattice is random and the temperature is reduced in steps of 0.01 (0.005 close to the critical point). The top graph in Fig. 27 shows the order parameters for isotropic rescaling using 2×2 blocks. One simulation uses a 128×64 lattice and a 256×128 lattice that is rescaled down to 128×64. The point where the two curves cross yields the critical temperature. On the bottom graph, the result of the simulations using anisotropic rescaling of 8×2 (a 512×64 lattice rescaled to a 64×32 one) and 4×2 (a 256×64 mapped to 64×32) blocks. Table 4 summarizes the results. The critical temperature is very close to

Table 4: The results for the ratio $\beta/\nu_{\parallel}$ for the IDLG model.

rescaling	$L_{\parallel} \times L_{\perp}$	$T_c\ [T_o]$	$\beta/\nu_{\parallel}$	slope ratio
2×2	256×128	1.398	0.93	(-6.643)/(-3.474)
4×2	256×64	1.405	0.83	(-5.796)/(-1.845)
8×2	512×64	1.408	0.71	(-7.646)/(-1.737)

the one obtained from the entropy analysis. If we assume that $\nu_{\parallel} \approx 0.8$ then for the three rescalings we obtain:

$$\nu_{\parallel}/\nu_{\perp} = 1 \quad : \quad \beta \approx 0.74$$

$$\nu_{\parallel}/\nu_{\perp} = 2 \quad : \quad \beta \approx 0.66$$

$$\nu_{\parallel}/\nu_{\perp} = 3 \quad : \quad \beta \approx 0.57$$

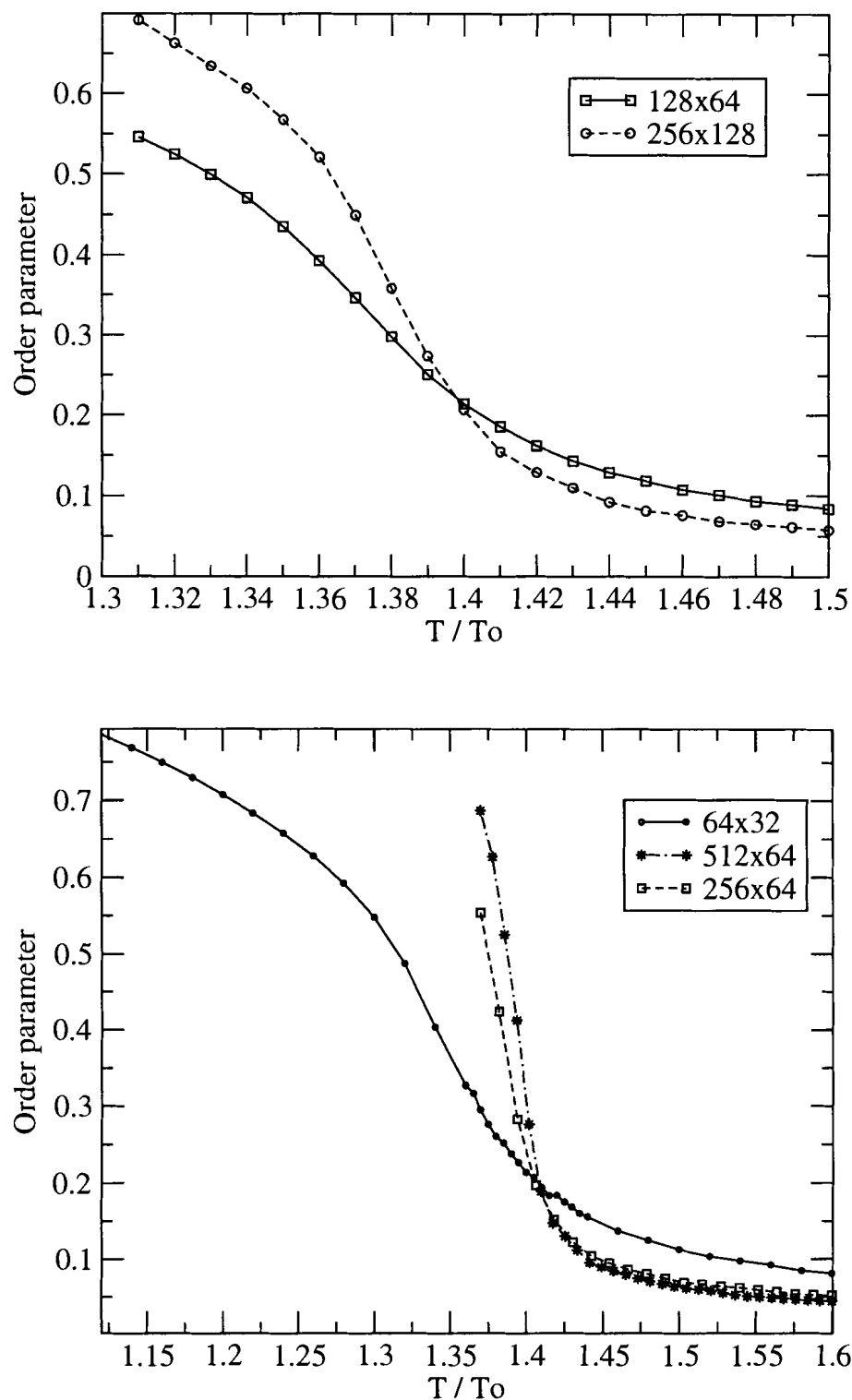Figure 27: The order parameter of the IDLG model vs. the temperature on different lattices. The top graph shows the case of isotropic 2×2 rescaling on a 256×128 lattice. On the bottom graph two anisotropic rescalings, 4×2 and 8×2, are shown.

The conclusion from these results is that, if one assumes an anisotropic rescaling as in Eq. (4.29), the numbers that we obtain are a little too high with the exception of the last result, which is close to the field theoretic prediction of $\beta = 1/2$. Thus, alternative anisotropic rescaling functions need to be explored in order to understand better this issue and more data from larger lattices would also be useful.

4.7 Summary and general remarks

In this chapter we have developed a general method using a Monte Carlo renormalization-group and entropy density analysis that is applicable to any stochastic model that has a translationally invariant measure. We find the critical temperatures for the IDLG and RIDLG are in excellent agreement with other studies of these models that use the more "traditional" finite size scaling approach. From the entropies of the model we have estimated their correlation length critical exponents. The values we obtain agree best with the early estimation obtained from the direct observation of the correlation length from simulations for different temperatures (Zhang et al., 1988). The method that we have developed is computational and high accuracy of the data is important for obtaining good results.

From our data we can conclude that the IDLG and RIDLG models do not differ much, if at all, at the critical point. Their critical exponents are so close to each other that the suggestion that they are in the same universality class is very plausible. While our results are not the final word on the universality classes of these models, they contribute some understanding to the complex picture of the criticality for DLG models. Planned future work includes the development of algorithms that are able to study larger shapes, so that more quantitative answers can be given. More qualitative understanding of the role that the interface between the phases plays at the critical region is needed and we believe that the entropy estimation and comparison from the different shapes will be very useful in understanding criticality and comparing the

ordering in these models. Application of these different shapes to other anisotropic systems about which more is known will also provide additional insights.

CHAPTER 5

THE THREE-STATE DRIVEN LATTICE GAS: A POSITION-SPACE RENORMALIZATION-GROUP STUDY BASED UPON THE MICROSCOPIC MASTER EQUATION

In this chapter we study a simple two-dimensional driven diffusive lattice gas without interactions between the particles. We present a scheme for a general position-space renormalization-group approach based upon the possibility of a closed form representation of the parameters of the system in terms of the steady state probability distribution of small clusters.

5.1   Definition of the model and its properties

The model is a two-dimensional lattice gas with two species (positively and negatively charged particles) that are driven by an external field along one of the axes of the lattice (the horizontal axis in Fig. 28) and vacancies. This model is a natural extension of the two-state model, studied in the previous chapter, formed by introducing an additional species with the opposite charge driven in opposite direction by the external field (Schmittmann and Zia, 1995; Korniss et al., 1997; Korniss, 1997). We consider a periodic $L_x \times L_y$ lattice each site of which can be empty or occupied by one of the two kinds of particles. The numbers of positive and negative particles are the same, so the total charge of the system is zero. The only interaction is the hard-core volume
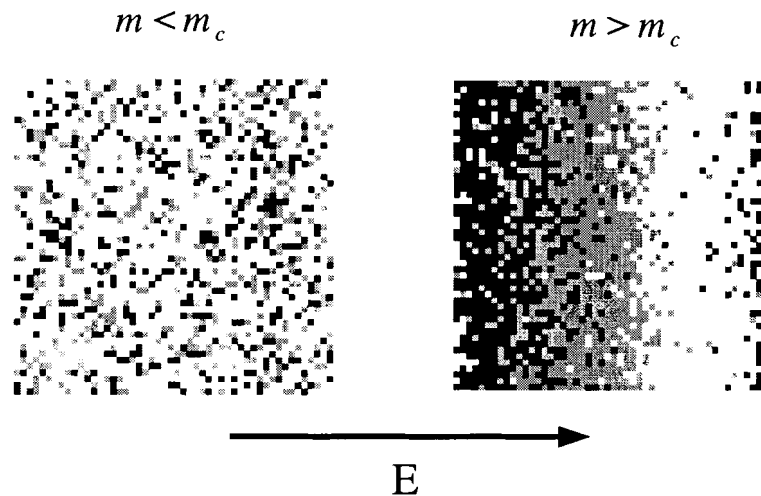
Figure 28: Typical configurations for the 3-state model: disordered (left) and ordered (right) phases. The driving field is along the horizontal axis as shown by the arrow. The black pixels are the positive particles and the gray ones are the negative ones.

exclusion. We can define occupation numbers at each site $\mathbf{r} = (x, y)$ on the lattice by

$$
n_{\mathbf{r}}^{+} = \begin{cases} 1 & \text{if the site is occupied by a positive particle} \\ 0 & \text{otherwise} \end{cases}
$$

$$
n_{\mathbf{r}}^{-} = \begin{cases} 1 & \text{if the site is occupied by a negative particle} \\ 0 & \text{otherwise} \end{cases} \tag{5.1}
$$

The dynamics are stochastic and governed by three parameters: the magnitude of the driving field $\mathbf{E}$, the rate at which a particle jumps into a nearest neighbor unoccupied site in the direction perpendicular to the field δ, and the parameter controlling the rate of exchange for the two kinds of particles γ. Without the bias produced by the field, the model yields simple diffusion of two non-interacting species on a lattice, a model that has no phase transitions. When the driving field is present, the jumps are biased, with the positive (negative) particles favoring jumps in the direction of (opposite to) the field. This simple model produces a rich phase diagram with both first and second order phase transitions. Typical ordered and disordered configurations are shown in Fig. 28.

At each step we choose a bond, either parallel or perpendicular to the field (in our simulations the parallel direction is along the horizontal axis). If the bond has a particle and a hole (particle-hole exchange) in the sites the probability for a jump of the particle is given by:

$$w_{ph} = \begin{cases} \min\{1, \exp(\eta E)\} & \text{for a jump in the } \parallel\text{-direction,} \\ \delta & \text{for a jump in the } \perp\text{-direction,} \end{cases} \quad (5.2)$$

where $\eta = 1$ if a positive particle jumps along the field or negative one jumps against the field, and $\eta = -1$ if a positive particle jumps against the field or a negative one along the field. If the bond has particles of both kinds (particle-particle exchange) in its sites, the rate is:

$$w_{pp} = \begin{cases} \gamma \min\{1, \exp(2\,\eta\,E)\} & \text{for a jump in the } \parallel\text{-direction,} \\ \gamma\,\delta & \text{for a jump in the } \perp\text{-direction,} \end{cases} \quad (5.3)$$

where $\eta = 1$ if the positive and the negative particles switch positions in the favorable direction, and $\eta = -1$ if the exchange of the two particles happens in the unfavorable direction. The factor of 2 in the exponent comes from the fact that two oppositely charged particles exchange their positions.

The "blocking" parameter γ is very important for the ordering shown on Fig. 28. Usually we will limit our considerations to the case when $\delta = 1$, so the jumps of a particle into an unoccupied site in the transverse direction always occur. The order parameter is defined through the quantities:

$$\begin{aligned} \phi_\mathbf{r} &= 1 - (n_\mathbf{r}^+ + n_\mathbf{r}^-) \\ \psi_\mathbf{r} &= (n_\mathbf{r}^+ - n_\mathbf{r}^-) , \end{aligned} \quad (5.4)$$

and their Fourier transforms

$$\begin{aligned} \phi_\mathbf{k} &\equiv \frac{1}{L_\parallel L_\perp} \sum_\mathbf{r} \phi_\mathbf{r}\, e^{-i\mathbf{k}\cdot\mathbf{r}} \\ \psi_\mathbf{k} &\equiv \frac{1}{L_\parallel L_\perp} \sum_\mathbf{r} \psi_\mathbf{r}\, e^{-i\mathbf{k}\cdot\mathbf{r}} , \end{aligned} \quad (5.5)$$
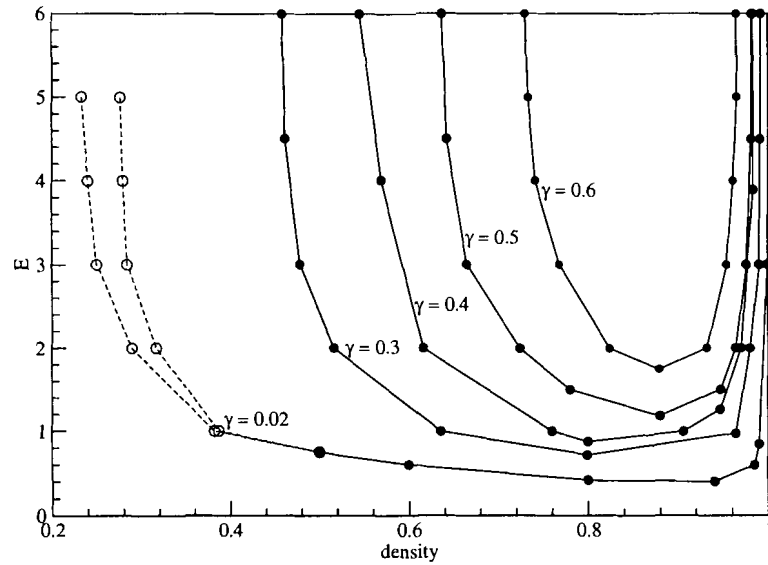
Figure 29: The phase diagram for the model. Simulations were performed on a 40×40 lattice. The dashed lines indicate a first order phase transition and the solid line is a second order phase transition. Inside of each "U" we observe the ordered phase and outside is the disordered region.

where $\mathbf{k} = (k_{||}, k_\perp)$. Thus, these order parameters are amplitudes of the longest wavelength longitudinal Fourier component, i.e.

$$\Phi \equiv |\phi_{(\frac{2\pi}{L_{||}},0)}|$$

$$\Psi \equiv |\psi_{(\frac{2\pi}{L_{||}},0)}| . \tag{5.6}$$

The phase diagram of the model is shown in Fig. 29 where data for different values of the parameter γ are shown.

For low γ and low densities we observe a first order phase transition. If we keep, for example, the value of the driving field fixed and change the density of the system by adding only two particles (one from the two kinds) we observe an abrupt change in the order parameter (see Fig. 30). We can also find the typical hysteresis for a first order phase transitions by conducting simulations when the density is increased first and then, after the change into the ordered phase, decreased. For high values of γ only a second order phase transition occurs. Fig. 31 shows the typical behavior of the order parameter Φ as a function of the density, with the driving field and the
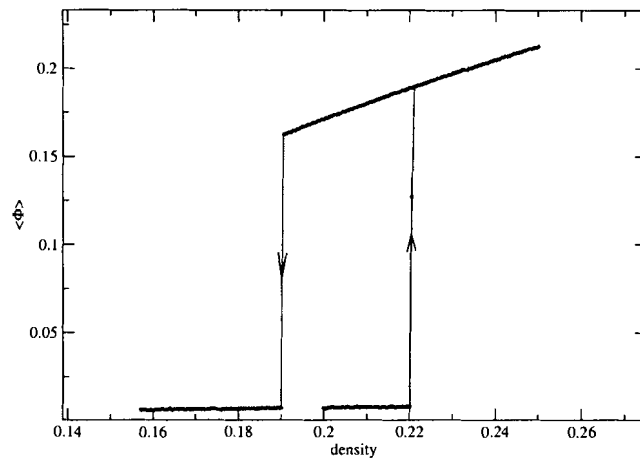
Figure 30: The order parameter Φ for $\gamma = 0.02$ and $E = 2.0$ on a 60×60 lattice. The change of the order parameter is sharp indicating the occurrence of a first order phase transition.
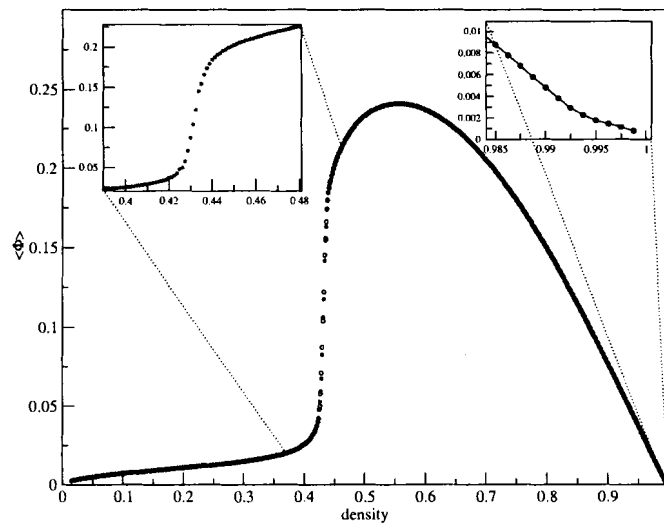

Figure 31: The order parameter Φ for $\gamma = 0.02$ and $E = 0.5$ on a 60×60 lattice. The change of the order parameter is gradual indicating the occurrence of the two second order phase transitions. The insets show the data close to the transition points.
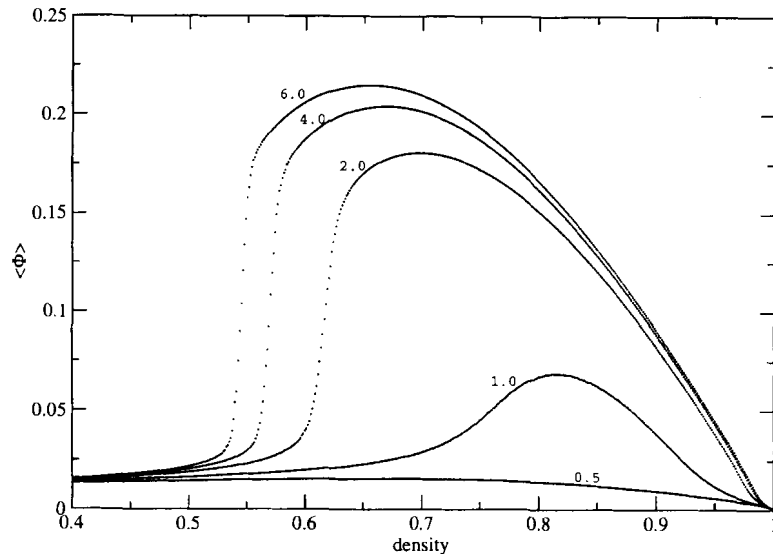
Figure 32: The order parameter Φ for $\gamma = 0.4$ and different fields on a 40×40 lattice.

parameter γ fixed. Hysteresis does not occur in this case and the curves obtained by increasing the density and by decreasing the density coincide within the error bars.

In our Monte Carlo simulations, we have again used a fast multi-spin algorithm that allows us to simulate 32 lattices simultaneously (see Appendix). We have worked on small lattices with sizes from 40×40 up to 80×80 and the results that we present for the phase diagram are thus only qualitatively correct. The locations of the phase boundaries exhibit substantial shifts as the lattice sizes are increased.

5.2 Master equations for small clusters

The master equation for the time evolution of the probability distribution $P(\vec{\sigma}; t)$ where $\vec{\sigma} = \{n_{\mathbf{r}}\}_{\mathbf{r}=(x,y)}$, is

$$\frac{dP(\vec{\sigma}; t)}{dt} = \sum_{\vec{\sigma}'} \left\{ W(\vec{\sigma}' \to \vec{\sigma}) P(\vec{\sigma}'; t) - W(\vec{\sigma} \to \vec{\sigma}') P(\vec{\sigma}; t) \right\}, \qquad (5.7)$$

The rates W for a transition between two configurations are given by Eqs. (5.2) and (5.3). In that form they are suitable for computer simulation; below we will retain

their general form for the development of our renormalization-group treatement. The particle-hole and particle-particle exchange rates are:

$$
w_{ph} = \begin{cases} \varphi(\eta\,E) & \text{for jump in the } \|\text{-direction,} \\[2mm] \delta & \text{for jump in the } \perp\text{-direction,} \end{cases}
$$

$$
w_{pp} = \begin{cases} \gamma\,\varphi(2\,\eta\,E) & \text{for jump in the } \|\text{-direction,} \\[2mm] \gamma\,\delta & \text{for jump in the } \perp\text{-direction.} \end{cases} \tag{5.8}
$$

The meaning of η ($\eta = \pm 1$) is the same as before and $\varphi(x)$ is an analytical function describing the bias produced by the driving field. Standard choices for $\varphi(x)$ are

$$
\begin{array}{lll}
\text{Metropolis} & \varphi(x) = \min\{1,\,\exp(-x)\} \\[2mm]
\text{Kawasaki} & \varphi(x) = \frac{2}{1+\exp(x)} & \tag{5.9} \\[2mm]
\text{Van Beijeren-Schulman} & \varphi(x) = \exp(-x/2)
\end{array}
$$

where $x = \pm E$. The dynamics therefore depends on this set of quantities:

$$
\{\ \delta,\ \varphi(-E),\ \varphi(+E),\ \gamma\varphi(-2E),\ \gamma\varphi(+2E),\ \gamma\delta\ \}\,. \tag{5.10}
$$

The largest term in the set determines the time scale of the dynamics. Since we are interested in the steady state properties of the model we usually consider it to be unity in the Monte Carlo simulations. Our main idea is to express the above set in terms of stationary probability distributions of small clusters.

Let $A \subset \mathbf{Z}^2$ be a small compact cluster on a two-dimensional lattice. The state of this cluster will be denoted by $\vec{\sigma}^{(A)} = \{n_r\}_{r \in A}$. The steady state probability distribution for this cluster is given by

$$
P_A(\vec{\sigma}^{(A)}) \equiv \sum_{\vec{\sigma} - \vec{\sigma}^{(A)}} P(\vec{\sigma})\,, \tag{5.11}
$$

where the notation $\vec{\sigma} - \vec{\sigma}^{(A)}$ indicates the summation over all of the sites of the lattice that do not belong to the cluster. For spatially invariant rates, as in our case, we
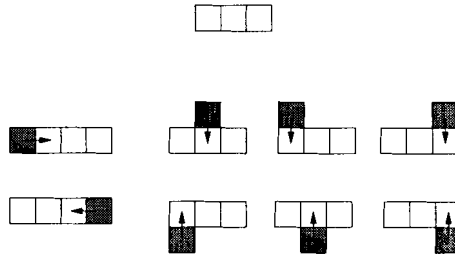
Figure 33: An example of cluster A, the triplet along the horizontal direction on the top. Its A_c-clusters are show below.

should expect the steady state measure to be translationally invariant (in space) as well. Therefore we will have

$$P_A(\vec{\sigma}^{(A)}) = P_{A'}(\vec{\sigma}^{(A')}) \,, \tag{5.12}$$

for two clusters A and A' of the same shape that are in different locations. The time dependent master equation for the probability distribution $P_A(\vec{\sigma}^{(A)} ; t)$ can be found after "integrating" Eq. (5.7) over the degrees of freedom not included in the cluster:

$$\frac{\mathrm{d}P_A(\vec{\sigma}^{(A)}; t)}{\mathrm{d}t} = \sum_{\vec{\sigma} - \vec{\sigma}^{(A)}} \sum_{\vec{\sigma}'} \left\{ W(\vec{\sigma}' \to \vec{\sigma}) P(\vec{\sigma}'; t) - W(\vec{\sigma} \to \vec{\sigma}') P(\vec{\sigma}; t) \right\}. \tag{5.13}$$

It is not hard to see that the sum on the right hand side reduces to a sum of terms, where each one is in the form $w\ P(\vec{\sigma}^{(A_c)})$. Here w is one of the rates and the cluster A_c is either the same cluster A or one made of A plus one nearest neighbor (see Fig. 33). This simple form is possible because the particles do not interact, except the excluded volume interaction. Fig. 33 shows the clusters A_c that contribute to the one time step evolution of the probability distribution of cluster A (in this example just a triplet of sites in the $\|$-direction). The arrows indicate the possible change affecting P_A.

We have chosen the simplest nontrivial cluster for further investigation, i.e. a pair of neighboring sites along the $\|$-direction. To simplify the notation, we use a notational convention for the different probability distributions as shown on Fig. 34. Since we can have three states on each site of a cluster with a total of N sites, we have
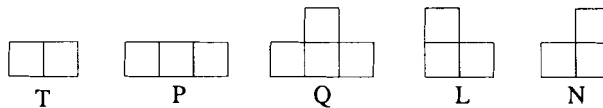
Figure 34: Notational convention for the probability distributions of different clusters.

3^N different states available for the cluster to sample. We denote a positive particle as 1, a negative particle as 2 and a hole as 0. The state of the cluster is coded into a trinary word ordered lexicographically. The highest bit in the word corresponds to the site above or below the pair, if present, and the rest of the bits in the word are ordered from left to right along the cluster. For example:

$$\langle +- \rangle \quad \rightarrow \quad \langle 12 \rangle \rightarrow 1 \times 3^1 + 2 \times 3^0 = 5 \rightarrow T_5$$

$$\left\langle 0 \overset{+}{-} + \right\rangle \quad \rightarrow \quad \left\langle 0\overset{1}{2}1 \right\rangle \rightarrow 1 \times 3^3 + 0 \times 3^2 + 2 \times 3^1 + 1 \times 3^0 = 34 \rightarrow Q_{34} \ ,$$

where the brackets denote the time average for the state of the cluster. The master equations for probability distributions of pairs $\vec{T} = \{T_0, T_1, \ldots, T_8\}$ can be written in this symbolic form:

$$\frac{\mathrm{d}\vec{T}}{\mathrm{d}t} = \widehat{W_1} \cdot \vec{T} + \widehat{W_2} \cdot \vec{P} + \widehat{W_3} \cdot (\vec{L} + \vec{\tilde{L}}) + \widehat{W_4} \cdot (\vec{N} + \vec{\tilde{N}}) \ , \tag{5.14}$$

where $\widehat{W_1}$ is a (9×9) dimensional transition matrix; $\widehat{W_i}$ for $i = (2,3,4,)$ are (81×9) matrices; $\vec{P}$, $\vec{L}$, and $\vec{N}$ are 81-component vectors. The symbols with a tilde in the equation are for the clusters symmetrical to the ones shown on Fig. 34 with respect to the horizontal axis. Appendix D shows Eq. (5.14) written in components.

As expected, the time evolution of a two-site cluster involves a hierarchy of three-site clusters, whose states need to be known in order to solve the master equation for the two-site cluster. Our goal here is not to solve these equation, but to use them in order to express the parameters of the dynamics (E, γ, δ) as functions of the steady state probability distributions of the clusters presented in Eq. (5.14).

5.3 Expression for the dynamical parameters

According to Eq. (5.10) we can define our parameter space μ to be the set

$$\mu = \{E,\ \gamma,\ \delta\}\,, \tag{5.15}$$

and for the function φ we choose the Metropolis rate (see Eq. (5.9)). We simplify our dynamics further by assuming that the particle-hole exchange rate δ is 1. Thus, we continue our investigation in a two-dimensional parameter space $\mu = \{E,\ \gamma\}$.

We can write the master equations for the T-cluster as

$$\frac{\mathrm{d}T_i}{\mathrm{d}t} = \sum_{j=0}^{8} (W_1)_{ij}\, T_j + \sum_{j=0}^{80} \left\{ (W_2)_{ij}\, P_j + (W_3)_{ij}\, [L_j + \tilde{L}_j] + (W_4)_{ij}\, [N_j + \tilde{N}_j] \right\}\,, \tag{5.16}$$

for any $i \in \{0,1,\ldots,8\}$. Here the components of the W's are from the set (see Appendix D):

$$\{\ 1,\ 0,\ \gamma,\ \exp(-E),\ \gamma \exp(-2E)\ \} \tag{5.17}$$

Therefore, for any of the nine master equations for the components of the T-cluster we have:

$$\frac{\mathrm{d}}{\mathrm{d}t}T_i = F_i(\gamma,\ E\ ;\ \vec{T},\ \vec{P},\ \vec{L},\ \vec{\tilde{L}},\ \vec{N},\ \vec{\tilde{N}})\,, \tag{5.18}$$

where by F_i we have denoted the right-hand side of Eq. (5.16). When the system reaches its steady state, the left-hand side of the above equation is zero. Consequently, we get a system of 9 equations for two (γ and E) unknowns

$$F_i(\gamma,\ E\ ;\ \vec{T},\ \vec{P},\ \vec{L},\ \vec{\tilde{L}},\ \vec{N},\ \vec{\tilde{N}}) = 0\,, \text{for } i = 0,\ldots,8. \tag{5.19}$$

We can always choose two (independent) equations and try to find an expression for γ and E, but in this way the numerical errors are substantial and this approach does not work well over the whole parameter space. The reason is that, in the different regions of the phase space, some clusters will have small probability of occurrence, and thus more computational time will be needed to get reliable statistics for them. We don't know *a priori* where in the phase space we will move in the next iteration,

so it is very difficult to choose a pair of equations that will give good results for our unknowns γ and E over the whole parameter space.

In order to determine the dynamical parameters from Eqs. (5.19) we have transformed the problem into an optimization task. Namely, we try to find the minimum of

$$F(\gamma , E) = \sum_{i=0}^{8} [\, F_i(\gamma, \, E \, ; \, \vec{T}, \, \vec{P}, \, \vec{L}, \, \vec{\tilde{L}}, \, \vec{N}, \, \vec{\tilde{N}}) \,]^2 \, . \tag{5.20}$$

We have $F(\gamma, \, E) \geq 0$ for any γ and E with equality for those parameters satisfying Eqs. (5.19).

Fig. 35 shows the accuracy of the minimization method for the important regions of the phase space. Runs on a 40×40 lattice have been performed for different values of γ, E and the particle density. The first 5×10^5 MCS are discarded and are usually enough for this lattice to reach its steady state. Then, for the next 5×10^5 MCS the histograms for the different components for the clusters T, P, L, $\tilde{L}$, N, and $\tilde{N}$ are collected every 100 MCS. From the histograms we approximate the probability distribution for the different clusters and use these numbers to minimize the function in Eq. (5.20) for γ and E. Typically, the average of 10-20 independent runs is compared to the values used to simulate the lattice. We obtain very good results in the whole phase space and in most of the cases the error is less than a percent with the worst case of about 2%. Obviously, one can improve the results by considering more independent runs and taking their average.

As we can see from the plots in Fig. 35, this minimization method has one more good feature, i.e. the results from it are self-correcting. This means that we can obtain the minimum at some point such that, say γ, is far away from the real value but then the value for E is going to be also far away from its real value in such a way that we will stay in the same phase. It is clearly visible on the plots that the points tend to order on a line rather than scatter randomly around the true value.
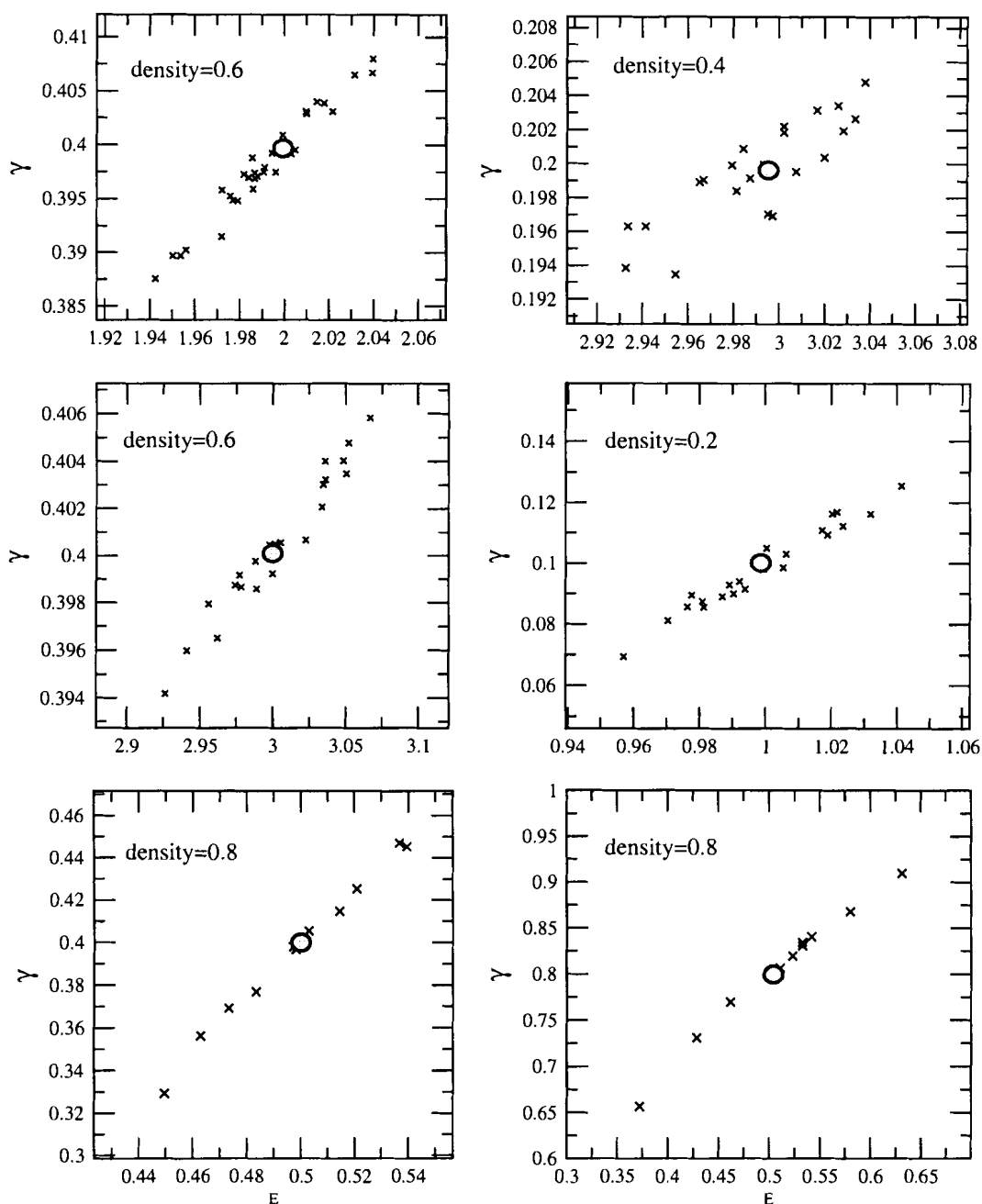
Figure 35: Obtaining values for γ and E from the minimization procedure discussed in the text. The circles are the exact values and the ×'s are the values obtained from the minimization method from 10-20 independent runs. On the bottom graphs are shown the worst cases, but even for them the average of 10 independent runs is only a maximum of $\sim 2\%$ off from the exact values. The simulation is done on a 40×40 lattice, each run is 10^6 MC steps, the first half discarded and data is taken every 100 MCS.

The way we designed the function $F(\gamma, E)$ in Eq. (5.20) makes it a paraboloid around its minimum, so we can use some very efficient optimization algorithms, such as the Powell's TOLMIN method, which solves linearly constrained optimization problems (Powell, 1989). The constraints for the optimization task are $0 \leqq E \leqq \infty$ and $0 \leqq \gamma \leqq 1.0$. We have assumed that $E = 40.0$ approximates the case $E = \infty$ sufficiently because, for the time of our simulation, an event with probability of $\exp(-40.0) \approx 10^{-18}$ will never occur, so the backwards jumps, for example will never happen, reflecting infinite field behavior.

The "worst" region for this method is the area close to the completely random case, i.e $\gamma = 1.0$ and $E = 0.0$. In this case, as one can easily verify from Eqs. (D.1), the coefficients in function $F(\gamma, E)$ of Eq. (5.20) theoretically are approaching zero, so the method would yield enormous errors. Therefore we limit our simulations to other regions of the parameter space.

5.4 Flow diagrams for the model

In this section we present the main results obtained using this Monte Carlo renormalization-group approach. We have followed the same steps as in Chapter 4 to design a mapping between the parameters $\mu = \{\gamma, E\} \rightarrow \mu' = \{\gamma', E'\}$ of the original and the coarse grained lattices, done with a rescaling factor b of 2. Initially we simulated a lattice of 80×80 sites at fixed density and μ. The first 5×10^5 MCS were discarded and in the next 5×10^5 steps at every 100 MCS we took the current configuration on the lattice and remapped this configuration into a configuration on a 40×40 lattice using a blocking procedure similar to the one in Section 2.4. Because we now have three states per site (vacancy, positive particle and negative particle) we modified the procedure as follows: (i) we divide the original lattice into 2×2 blocks and classify each block into a class depending upon the states of the sites in the block; (ii) we start generating particles on an initially empty 40×40 lattice by choosing randomly blocks

from the class with the largest number of the same kind of particle until we generate as many particles of this type as needed to maintain the same density, or exhaust this class and continue on the next one according of the number of that particle. At the end we have a microscopic state on the coarse-grained lattice that has the same density of the particles as on the original lattice and which "looks similar" to the state on the original lattice.

We are going to make the same general assumption about the configurations generated on the smaller lattice, namely that they appear as if they were generated from a Monte Carlo simulation that is running with a different set of values of the parameters μ'. We prohibit any expansion of the parameter space, and assume that the particle-hole rate in the $\perp$-direction $w_{ph} = 1$ on the coarse-grained lattice.

Next, we collect the histograms for the appropriate shapes mentioned above and approximate their probability distributions. From Eq. (5.20) we find those γ' and E' that minimize the function. This procedure is done 10 times and the average of the values yields the next point of the trajectory, $\mu' = (\gamma', E')$. To continue further, the original values of the parameters on the larger, (80×80), lattice are replaced with the ones just found. The next 5×10^5 MCS are usually needed for the system to reach a new steady state and the remapping occurs again. The step in which we continue the simulation on the bigger lattice with the parameters obtained from the minimization procedure on the coarse-grained lattice certainly introduces errors due to finite size effects. We discuss this issue later in this chapter.

Fig. 36 shows the results for the flow in the subspace of density=0.4. In Fig. 40, two iterations of the flow are shown closer with the 10 independent runs needed to obtain their positions more accurately. On the graphs, the arrows indicate the direction of the flow and the $\times$'s are the different estimations of the parameters from 10 independent runs.
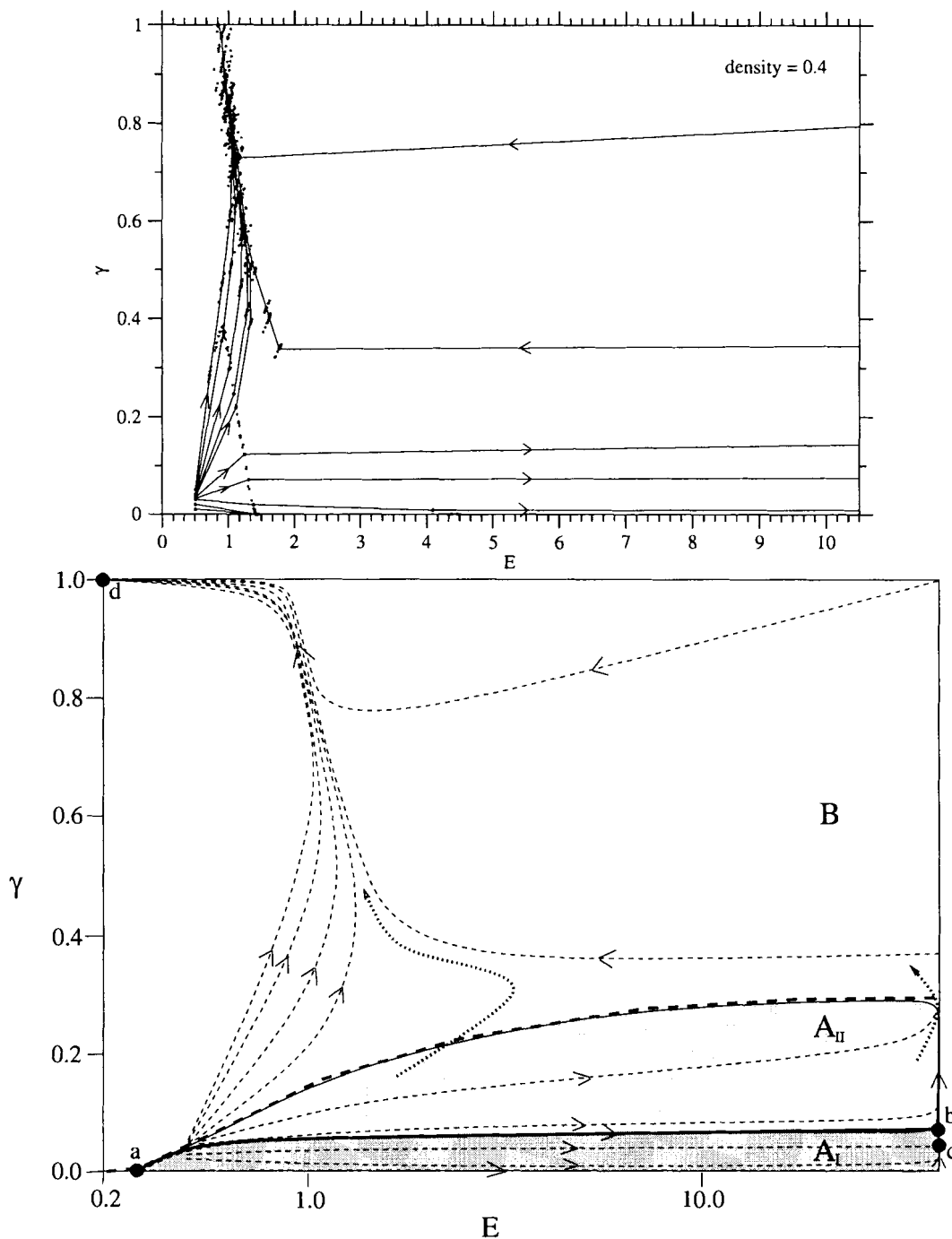
Figure 36: Flow diagram for density=0.4. The top graph shows the data for the flow from the renormalization-group procedure with a density of 0.4 . On the bottom graph is the continuous schematic flow in this subspace. The arrows indicate the direction of the flow and the filled circles are the fixed points. The phases A_I and A_{II} are the ordered phases and B is the disordered phase.
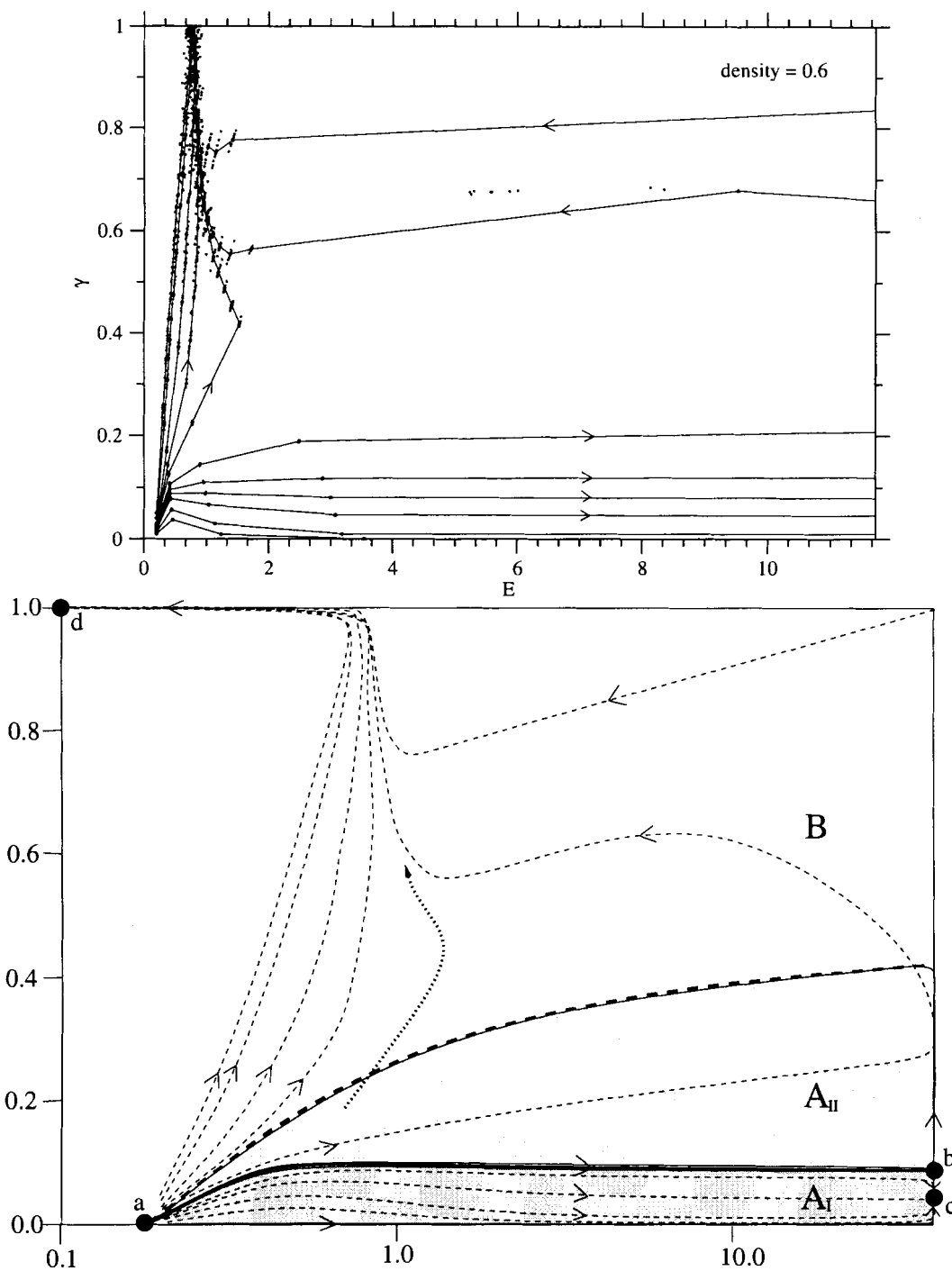
Figure 37: Flow diagram for density=0.6. The top graph shows the data for the flow from the renormalization-group procedure with a density of 0.6. On the bottom graph is the continuous schematic flow in this subspace. The arrows indicate the direction of the flow and the filled circles are the fixed points. The phases A_I and A_{II} are the ordered phases and B is the disordered phase.
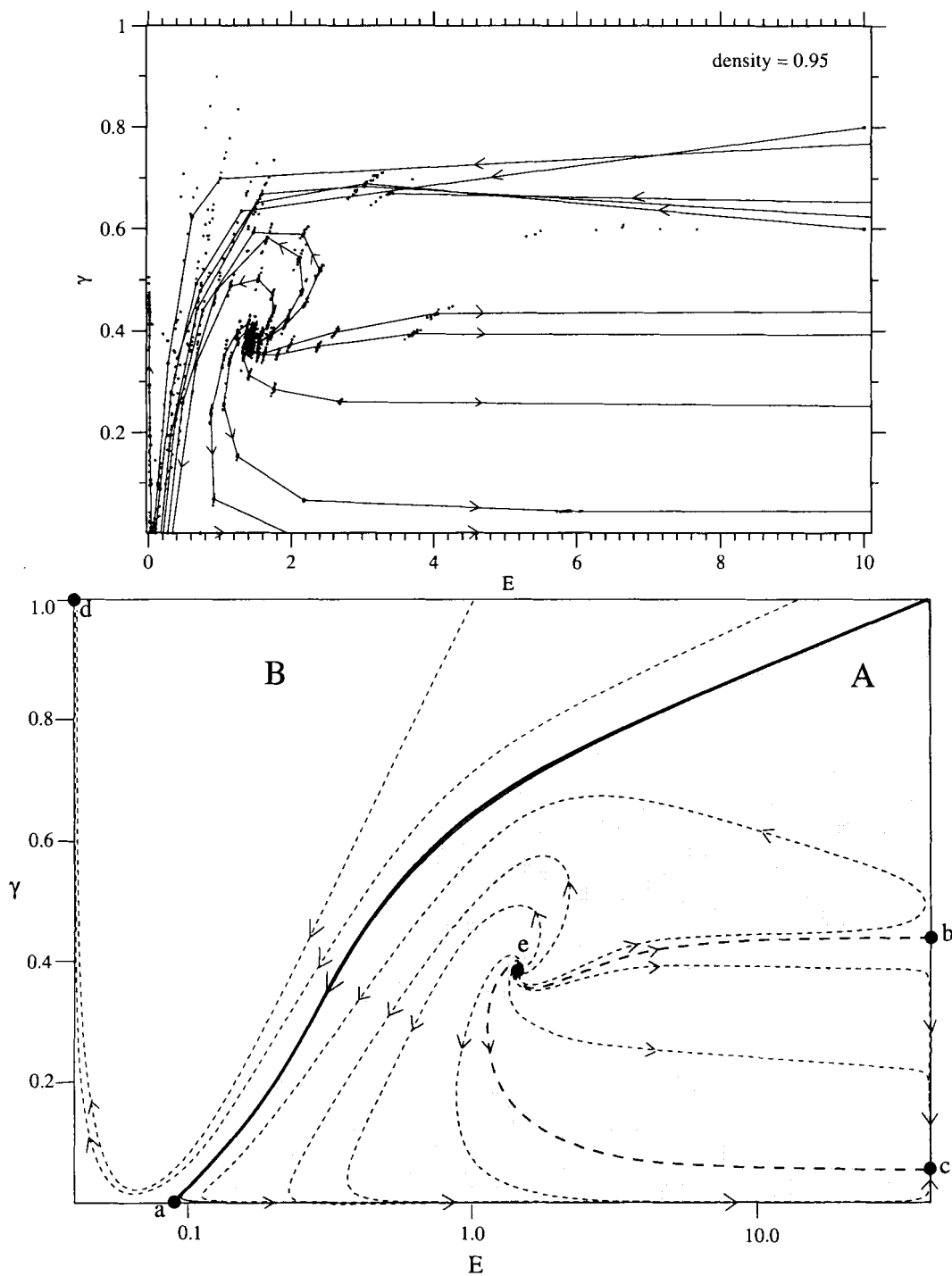
Figure 38: Flow diagram for density=0.95. B is the disordered phase and A is the ordered one, separated by a phase boundary denoted by the bold line.

Figure 39: Flow diagram for density=0.98. B is the disordered phase and A is the ordered one, separated by a phase boundary denoted by the bold line.
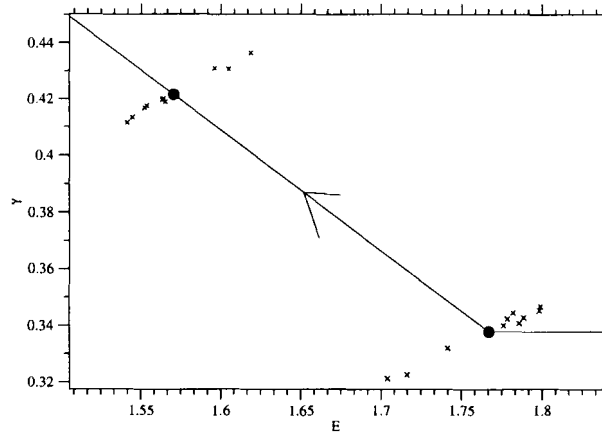
Figure 40: An example of the flow for two iterations.

On the schematic graph in Fig. 36 we have labeled the different phases by A_I and A_{II} for the ordered region and B for the disordered phase. The thin dashed lines are the flow lines and the filled circles are the fixed points of the mapping. The thick dashed line separates the two phas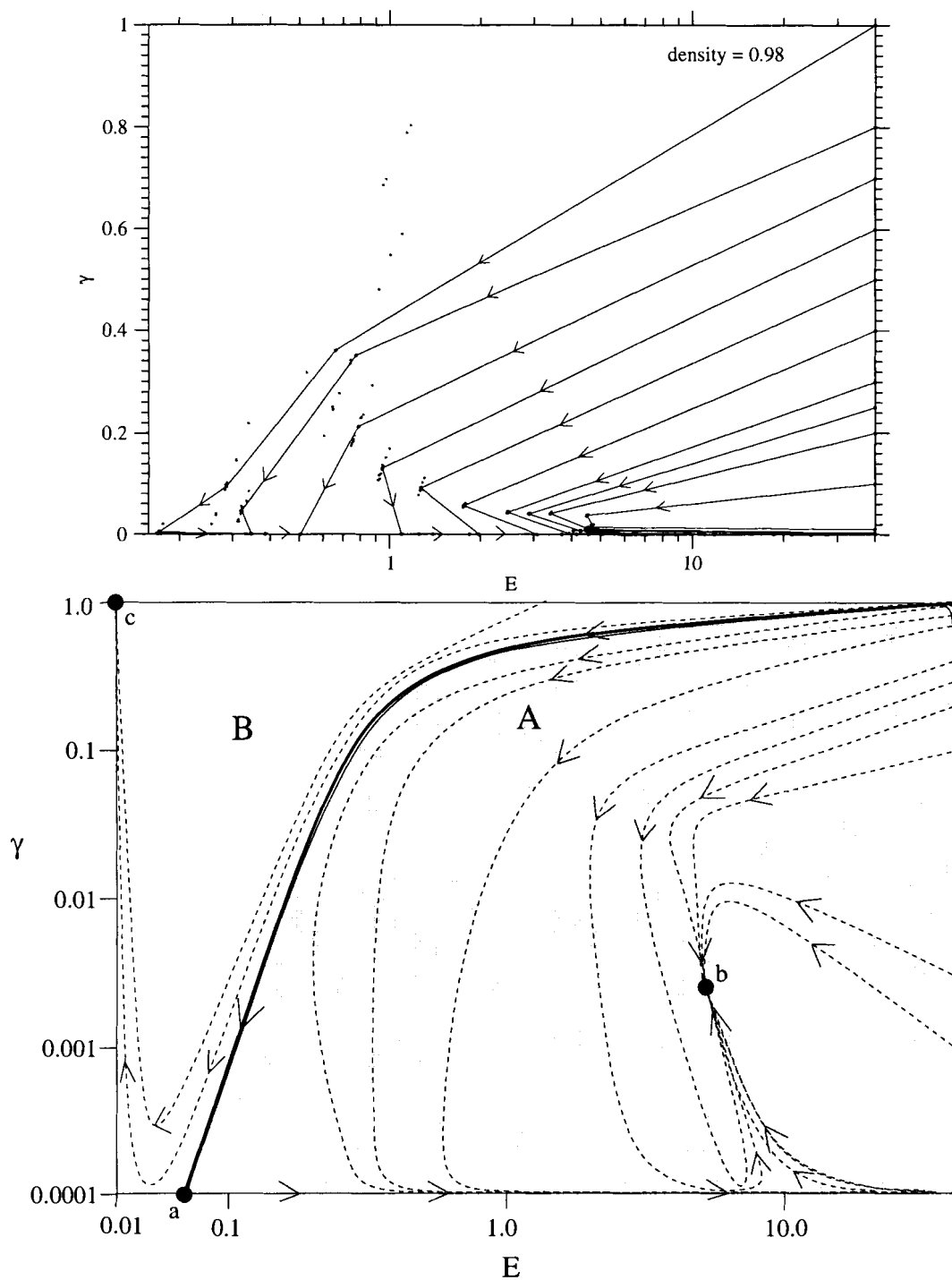es. If we start in the disordered phase the consecutive iterations will remain in this phase and will converge to the fixed point $d = (0.0, 1.0)$, the sink for the disordered phase. The fixed point $a = (0.37, 0.0)$ indicates that on the segment for $\gamma = 0$ and $E < 0.37$ we have only the disordered phase.

The flow in the ordered phase behaves a bit unexpectedly. The regions A_I and A_{II} are separated by a boundary indicated by the bold line on the graph and ending at $E = \infty$ with a fixed point $b = (\infty, 0.07)$. The flow lines in the region A_I do not leave this region and the sink for this phase is $c = (\infty, 0.04)$. The point $(\infty, 0.0)$ is an isolated fixed point. The flow in the second region A_{II} has the property that it "escapes" the ordered phase by jumping into the disordered phase as shown by the two short long-dotted lines ending with arrows. If we start in this region from some relatively small field then the flow will eventually make a jump into the disordered phase for some finite field. If we start with a large value of E the flow will reach the $E = \infty$ boundary and will make few iterations straight up until it enters into the disordered phase and continues from there towards the fixed point d.

The flow diagram in the subspace of density=0.6 is shown on Fig. 37 and it is similar to the flow in the cross section of density=0.4 . The labels and meaning of the symbols on the graph are the same. The fixed points now are at:

$$a = (0.18,\ 0.0), \quad b = (\infty,\ 0.08), \quad c = (\infty,\ 0.043) \text{ and } d = (0.0,\ 1.0)\ .$$

Both flow diagrams for densities 0.4 and 0.6 are on the left-hand side of the "U"'s on the phase diagram in Fig. 29. Possible explanations for the "escaping" flows from the ordered phase A_{II}, ordered in decreasing plausibility according to us, could be these:

(i) The region A_{II} is actually a new distinct phase which, from the order parameter, should be classified as the ordered phase. Though this phase is indistinguishable from phase A_I by the order parameter, it could have some other unique feature(s). The method we apply shows that phases A_I and A_{II} are distinct phases by the flow and the phases A_{II} and B are distinct by the order parameter. This viewpoint suggests that the phase A_{II} is a less stable ordered phase;

(ii) Only the region A_I is the true ordered phase for the infinite lattice. The bold line on the graphs which ends at the fixed points a and b is the phase boundary between the ordered and the disordered phase;

(iii) The "escaping" flow from the ordered phase A_{II} that we observe is due to finite size effects. The width of the "U" shapes on the general phase diagram (see Fig. 29) tends to become bigger on bigger lattices, i.e. the left boundaries would move toward lower density and the right ones toward fully filled lattice. Thus, points for γ and E that lead to disordered phase on the (80×80) lattice will lead to ordered phase on the smaller lattice;

The flow diagrams change dramatically for high densities as shown in Fig. 38 for the density at 0.95. The bold line separates the ordered phase A from the disordered B. The sinks for the ordered and the disordered phases are the points c and d

respectively. The coordinates for the fixed points are:

$$a = (0.09,\ 0.0),\ b = (\infty,\ 0.44),\ c = (\infty,\ 0.042),\ d = (0.0,\ 1.0) \text{ and } e = (1.44,\ 0.39)\ .$$

The region around the fixed point e has an unusual spiral topology. The line $e - b$ separates the flow in the ordered phase and appears to be a closed subspace of the flow, analogous to the $\alpha + \beta = 1$ line for the FASEP. Fig. 39 shows the flow for the density of 0.98 with its fixed points located at:

$$a = (0.07,\ 0.0),\ b = (5.1,\ 0.002), \text{ and } d = (0.0,\ 1.0)\ .$$

The flow has changed again and now the point in the bulk of the ordered region (point b) is an attractive point.

The method that we apply here, captures correctly the general features of the model's phase diagram and suggests some new features that are not found by standard mean field or mesoscopic Langevin treatments. Our approach relies upon computational determination of the cluster probability. For better quantitative accuracy, aditional simulations on larger lattices are needed. The sink for the ordered phase is located at approximately $(\gamma = 0.04, E = \infty)$ for the cases that we have checked. In all cases the point $(\gamma = 0.0,\ E = \infty)$ is a trivial fixed point of the flow.

Runs at a density of 0.95 on a 120×120 lattice, rescaled to a 60×60 lattice, show that the spiral topology around the fixed point e in Fig. 38 is still present. However, the location of the fixed point moves toward smaller values of E and γ. The position of the sink for the ordered phase, the point c on Fig. 38, stays at the same place within the error bars.

Suggested future work includes simulations on larger lattices and parameter estimation from different larger shapes, i.e. a triplet along the parallel direction. The simplicity of the model allows another approach to be tested, namely the maximum entropy method (Jaynes, 1957). One can work with the same shapes used here and express the righthand side of the master equation in terms of only one cluster. For

the shapes used in this chapter, that would be the cluster "Q" in Fig. 34. Then, the number of unkowns (81 for this shape) can be reduced greatly by the symmetries of the system. The rest of the unknowns are obtained from the maximization of the quantity $S(Q) = -\sum_{i=1}^{81} Q_i \log Q_i$ constrained by the symmetry relations between the Q_i's, the master equations and the normalization $\sum_{i=1}^{81} Q_i = 1$. Preliminary work whithin this approach shows that it is a promising direction to pursue.

CHAPTER 6

CONCLUSIONS AND SUGGESTIONS FOR FUTURE WORK

In this thesis, we have developed and tested new methods for the treatment of systems far from equilibrium. At the same time, we have explored the criticality of stochastic models for driven lattice gases using these methods. The models chosen provide intricate phase diagrams and, at the same time, are simple enough to be tractable. For one-dimensional systems, we have developed a position-space renormalization-group approach and applied it to the fully asymmetric exclusion process. The method yields the known critical fixed point and the first and second phase boundary locations exactly. Even with a length rescaling factor of only three, a good approximation for the correlation length exponent is obtained. These results show that for non-equilibrium systems, as in equilibrium statistical mechanics, renormalization-group ideas are very powerful for studying critical phenomena. The critical exponent results could possibly be improved by using a larger length rescaling factor, and the applicability of this approach to other models is certainly a fruitful direction for future work.

In the second part of this research, we have combined Monte Carlo renormalizaion-group and information theoretic approaches to study the criticality of two-dimensional driven lattice gases. Our study has specifically compared the behavior of two infinitely driven cases, one in which the field is always in the same direction and the other in which the direction switches randomly, but is always uniform throughout the lattice. Since these two models have different symmetries, one would expect them to be in different universality classes. Field theoretic treatments support this intuition,

predicting different critical exponents in the two cases. To our knowledge, our study is the first application of a Shannon entropy calculation to driven lattice gases and to anisotropic systems. Our experimentation with different cluster shapes leads to two possible interpretations of the correlation length exponents obtained. One is that there are two separate correlation length exponents, describing behaviors parallel and perpendicular to the field, and the shapes tend to find the average of the two. The perpendicular positioning of the shape is less reliable since it often crosses the phase interface. In the thermodynamic limit, the interface effect would become negligible. The second interpretation is that there is in fact only one correlation length exponent describing the system's behavior. Our value for the correlation length exponent is consistent with that obtained by a very different approach measuring correlations directly from a Monte Carlo simulation. The surprising result that a straight shape aligned parallel to the field and an angle-bended shape sampling both directions yield approximately the same value for the correlation length exponent can be explained by either of these two possiblities. Further exploration of anisotropic systems, especially those with known properties, will help clarify the interpretation of these results. Two additional areas for future study are finite size scaling in highly anisotropic systems and the optimization of block transformations in these cases.

The last part of this research shows how a length rescaling transformation can be developed from the system's master equations for small clusters. This approach, introduced for the three-state, two-dimensional driven lattice gas, shows an intricate flow topology as a function of density, field, and ease of particle-particle exchange. In addition to the usual fixed points appearing as sinks for each phase and phase boundary, a new "source" fixed point occurs within the ordered phase for some parameter values. Also, the ordered phase shows two distinct regions, one clearly more stable than the other. Future work will focus on determining the quantifiable differences between these two regions within the ordered phase and experimenting with

the efficiency of using different types of clusters in the construction of the master equations.

To summarize, this thesis explores the application of new statistical mechanical approaches to systems far from equilibrium. The methods that we have developed are inspired by effective strategies from equilibrium statistical mechanics and information theory: position-space renormalization group, Monte Carlo renormalization group, and calculation of the measure entropy from small clusters. Our applications of these methods provide additional insight into the ordering and criticality of one- and two-dimensional model systems and suggest that these methods can be applied more broadly to better understand systems that reach a steady state far from equilibrium.

REFERENCES

Albano, E. V. and Saracco, G. (2002). Dynamic Behavior of Anisotropic Nonequilibrium Driving Lattice gases. *Phys. Rev. Lett.*, 88:145701.

Allegrini, P., Benici, V., Grigolini, P., Hamilton, P., Ignaccolo, M., Menconi, G., Palatella, L., Raffaelli, G., Scafetta, N., Virgilio, M., and Yang, J. (2002). Compression and Diffusion: A Joint Approach to Detect Complexity. *arXiv:cond-mat/0202123*.

An, G. (1988). A Note on the Cluster Variation Method. *Journal of Statistical Physics*, 52:727–734.

Archahbar, A., Garrido, P. L., Marro, J., and Munoz, M. A. (2001). Is the Particle Current a Relevant Feature in Driven Lattice Gases. *Phys. Rev. Lett.*, 87:195702.

Bellac, M. L. (1991). *Quantum and Statictical Field Theory*. Oxford University Press.

Binney, J. J., Dowrick, N. J., Fisher, A. J., and Newman, M. E. J. (1992). *The Theory of Critical Phenomena*. Oxford University Press.

Burkhardt, T. W. and van Leeuwen, J. M. J. (1976). Renormalization theory for ising-like spin systems. In Domb, C. and Green, M. S., editors, *Phase Transitions and Critical Phenomena*. Academic Press.

Burkhardt, T. W. and van Leeuwen, J. M. J. (1982). *Real-Space Renormalization*. Springer-Verlag Berlin Heidelberg.

Burley, D. M. (1972). Closed form approximations for lattice systems. In Domb, C. and Green, M. S., editors, *Phase Transitions and Critical Phenomena*. Academic Press.

Cover, T. and Thomas, J. (1991). *Elements of Information Theory*. John Wiley & Sons, Inc.

Creswick, R. J., Farach, H. A., and Poole, C. P. (1992). *Introduction to Renormalization Group Methods in Physics*. John Wiley & Sons, Inc.

Crutchfield, J. P. and Feldman, D. P. (2003). Regularities Unseen, Randomness Observed: Levels of Entropy Convergence. *Chaos*, 13:25–54.

Derrida, B., Domany, E., and Mukamel, D. (1992). An Exact Solution of a One-Dimensional Asymmetric Exclusion Model with Open Boundaries. *Journal of Statistical Physics*, 69:667.

Derrida, B. and Evans, M. R. (1997). Nonequilibrium statistical mechanics in one dimension. In Privman, V., editor, *Nonequilibrium Statistical Mechanics in One Dimension*. Cambridge University Press.

Derrida, B., Evans, M. R., Hakim, V., and Pasquier, V. (1993). Exact solution of a 1D asymmetric exclusion model using a matrix formulation. *Journal of Physics A: Mathematical and General*, 26:1493–1517.

Dünweg, B. (1996). Simulation of phase transitions: critical phenomena. In Binder, K. and Ciccotti, G., editors, *Conference proceedings: Monte Carlo and Molecular Dynamics of Condensed Matter Systems*. Editrice Compositori.

Ellis, R. S. (1985). *Entropy, Large Deviations, and Statistical Mechanics*. Springer, New York.

Essler, F. H. L. and Rittenberg, V. (1996). Representations of the quadratic algebra and partially asymmetric diffusion with open boundaries. *Journal of Physics A: Mathematical and General*, 29:3375–3407.

Feldman, D. P. and Crutchfield, J. P. (2002). Structural Information in Two-Dimensional Patterns: Entropy Convergence and Excess Entropy. *arXiv:cond-mat/0212078*.

Garrido, P. L., Lebowitz, J. L., Maes, C., and Spohn, H. (1990). Long-range correlations for conservative dynamics. *Phys. Rev. A*, 42:1954–1968.

Garrido, P. L. and Marro, J. (2000). Critical properties of nonequilibrium anisotropic lattice gases. *Physica A*, 279:143–150.

Garrido, P. L., Munoz, M. A., and de los Santos, F. (2000). Universality classes of driven lattice gases. *Phys. Rev. E*, 61:R4683–R4686.

Georgiev, I. T. and McKay, S. R. (2003). Position-space renormalization-group approach for driven diffusive systems applied to the asymmetric exclusion model. *Phys. Rev. E*, 67:056103.

Goldstein, S., Kuik, R., and Schlijper, A. G. (1990). Entropy and Global Markov Properties. *Comunn. Math. Phys.*, 126:469–482.

Grynberg, M. D., Newman, T. J., and Stinchcombe, R. B. (1994). Exact solutions for stochastic adsorption-desorption models and catalytic surface processes. *Phys. Rev. E*, 50:957–971.

Grynberg, M. D. and Stinchcombe, R. B. (1995). Dynamic Correlation Functions of Adsorption Stochastic Systems with Diffusional Relaxation. *Phys. Rev. Lett.*, 74:1242–1245.

Hinrichsen, H. (2000). Non-equilibrium critical phenomena and phase transitions into absorbing states. *Advances in Physics*, 49:815–958.

Hooyberghs, J., Carlon, E., and Venderzande, C. (2001). Generalized contact process with n absorbing states. *Phys. Rev. E*, 64:036124.

Hooyberghs, J. and Vanderzande, C. (2000). Real-space renormalization for reaction-diffusion systems. *Journal of Physics A: Mathematical and General*, 33:907–919.

Janssen, H. K. and Schmittmann, B. (1986). Field Theroy of Critical Behaviour in Driven Diffusive Systems. *Z. Phys. B*, 64:503.

Jaynes, E. T. (1957). Information Theory and Statistical Mechanics. *Physical Review*, 106:620–630.

Katz, S., Lebowitz, J. L., and Spohn, H. (1984). Nonequilibrium Steady State of Stochastic Lattice Gas Model of Fast Ionic Conductors. *Journal of Statistical Physics*, 34:497.

Kenneway, D., McKay, S. R., and Feldman, D. P. (2003). An Information Theoretic Study of the Two-Dimensional Ising Spin Glass. *in preparation*.

Kikuchi, R. (1951). A Theory of Cooperative Phenomena. *Physical Review*, 81:988–1003.

Korniss, G. (1997). *Non-equilibrium Phase Transitions and Steady States in Biased Diffusion of Two Species*. PhD dissertation, Virginia Polytechnic Institute, Department of Physics.

Korniss, G., Schmittmann, B., and Zia, R. K. P. (1997). Non-Equilibrium Phase Transitions in a Simple Tree-State Lattice Gas. *JSP*, 86:721.

Krug, J. (1991). Boundary-induced phase transitions in driven diffusive systems. *Phys. Rev. Lett.*, 67:1882–1885.

Landau, D. P. and Binder, K. (2000). *A Guide to Monte Carlo Simulations in Statistical Physics*. Cambridge University Press, Inc.

Leung, K. and Cardy, J. L. (1986). Field Theory of Critical Behavior in a Driven Diffusive Systems. *Journal of Statistical Physics*, 44:567.

Lindgren, K. (1988). Microscopic and macroscopic entropy. *Phys. Rev. A*, 38:4794–4798.

Marro, J., Achahbar, A., Garrido, P. L., and Alonso, J. J. (1996). Phase transitions in driven lattice gases. *Phys. Rev. E*, 53:6038–6047.

Marro, J. and Dickman, R. (1999). *Nonequilibrium Phase Transitions in lattice Models*. Cambridge University Press.

Mierovitch, H. (1984). Computer simulation study of hysteresis and free energy in the fcc Ising feromagnet. *Phys. Rev. B*, 30:2866–2874.

Mierovitch, H. (1999). Simulation of a free energy upper bond, based on the anticorrelation between an approximate free energy functional and its fluctuations. *Journal of Chemical Physics*, 111:7215–7224.

Morán-López, J. L. and Sanchez, J. M. (1996). *Theory and Application of the Cluster Variation and Path Probability Methods*. Plenum Press.

Newman, M. E. J. and Barkema, G. T. (1999). *Monte Carlo Methods in Statistical Physics*. Oxford University Press, Inc.

Niemeijer, T. and van Leeuwen, M. J. M. (1973). Wilson theory for spin systems on triangular lattice. *Phys. Rev. Lett.*, 31:1411.

Ódor, G. (2002). Phase transition universality classes of classical, nonequilibrium systems. *arXiv:cond-mat/0205644*.

Oppenheim, I., Shuler, K. E., and Weiss, G. H. (1977). *Stochastic Processes in chemical physics: the master equation*. The MIT Press.

Patashinskii, A. Z. and Pokrovskii, V. L. (1979). *Fluctuation Theory of Phase Transitions*. Pergamon Press Ltd.

Powell, M. J. D. (1989). TOLMIN: A fortran package for linearly constrained optimizations calculations. *DAMTP Report NA2, University of Cambridge, England*.

Præstgaard, E. L., Schmittmann, B., and Zia, R. K. P. (2000). A lattice gas coupled to two thermal reservoirs: Monte Carlo and field theoretic studies. *The European Physical Journal B*, 18:675–695.

Privman, V. (1990). *Finite Size Scaling and Numerical Simulation of Statistical Systems*. World Scientific, Singapore.

Privman, V. (1997). *Nonequilibrium Statistical Mechanics in One Dimension*. Cambridge University Press.

Ruelle, D. (1978). *Thermodynamic Formalism*. Addison Wesley.

Sandow, S. (1994). Partially asymmetric exclusion process with open boundaries. *Phys. Rev. E*, 50:2660.

Santos, F. and Garrido, P. L. (1998). Continuum Field Description of Driven Lattice Gases. *Journal of Statistical Physics*, 96:303–324.

Schlijper, A. G. (1984). Exact Variational Methods and Cluster-Variation Approximations. *Journal of Statistical Physics*, 35:285–301.

Schlijper, A. G. (1985). On Some Variational Approximations in Two-Dimensional Classical Lattice Systems. *Journal of Statistical Physics*, 40:1–27.

Schlijper, A. G. and Smit, B. (1989). Two-Sided Bounds on the Free Energy from Local States in Monte Carlo Simulations. *Journal of Statistical Physics*, 56:247–260.

Schmittmann, B., Janssen, H. K., Tauber, U. C., Zia, R. K. P., Leung, K.-t., and Cardy, J. L. (2000). Viability of competing field theories for the driven lattice gas. *Phys. Rev. E*, 61:5977.

Schmittmann, B. and Zia, R. K. P. (1991). Critical Properties of a Randomly Driven Diffusive System. *Phys. Rev. Lett.*, 66:357.

Schmittmann, B. and Zia, R. K. P. (1995). Statistical mechanics of driven diffusive systems. In Domb, C. and Lebowitz, J. L., editors, *Phase Transitions and Critical Phenomena*. Academic Press.

Schütz, G. and Domany, E. (1993). Phase Transitions in an Exactly Soluble One-Dimensional Exclusion Process. *Journal of Statistical Physics*, 72:227.

Stinchcombe, R. B. and Hanney, T. (2002). Exact and scaling approaches to nonequilibrium models. *Physica D*, 168:313–317.

Swendsen, R. H. (1979). Monte Carlo Renormalization Group. *Phys. Rev. Lett.*, 42:859–861.

Swendsen, R. H. (1982). Monte carlo renormalization. In Burkhardt, T. W. and van Leeuwen, J. M. J., editors, *Real Space Renormalization*. Springer-Verlag Berlin Heidelberg New York.

Wilson, K. G. (1971). Renormalization group and critical phenomena. I. Renormalization group and Kadanoff scaling picture. *Phys. Rev. B*, 4:3174.

Wilson, K. G. (1975). The renormalization group: Critical phenomena and the Kondo problem. *Rev. Mod. Phys.*, 47:773–840.

Wilson, K. G. and Fisher, M. E. (1972). Critical exponents in 3.99 dimensions. *Phys. Rev. Lett.*, 28:240.

Zhang, M. Q., Wang, J. S., Lebowitz, J. L., and Vallés, J. L. (1988). Power Law Decay of Correlations in Stationary Nonequilibrium Lattice Gases with Conservative Dynamics. *Journal of Statistical Physics*, 52:1461.

Zhvonkin, A. K. and Levin, L. A. (1970). The Complexity of Finite Objects and the Development of the Concepts of Information and Randomness by Means of the Theory of Algorithms. *Russ. Math. Surveys*, 25:83.

APPENDIX A

RECURSION RELATION COMPUTATION

Here we show the details for obtaining Eq. (3.17). Using the algebraic rules:

$$
\begin{aligned}
C &\equiv D + E \\
DE &= D + E \\
D|V\rangle &= \frac{1}{\beta}|V\rangle \\
\langle W|E &= \frac{1}{\alpha}\langle W|.
\end{aligned}
\tag{A.1}
$$

and the obvious consequences of them:

$$
\begin{aligned}
D &= C - E \\
D^2 &= C^2 - EC - C \\
D^3 &= C^3 - 2C^2 - EC^2 + EC, \text{ etc ....}
\end{aligned}
\tag{A.2}
$$

one can calculate the expressions:

$$
\begin{aligned}
\langle DC^N\rangle &= \langle C^{N+1}\rangle - \frac{1}{\alpha}\langle C^N\rangle \\
\langle D^2 C^N\rangle &= \langle C^{N+2}\rangle - (1 + \frac{1}{\alpha})\langle C^{N+1}\rangle \\
\langle D^3 C^N\rangle &= \langle C^{N+3}\rangle - (2 + \frac{1}{\alpha})\langle C^{N+2}\rangle + \frac{1}{\alpha}\langle C^{N+1}\rangle
\end{aligned}
\tag{A.3}
$$

In an analogous way, one can derive the formulas involving E and β. For example, below we show how the calculation for the expression in the denominator in Eq. (3.13)

is done.

$$\langle 1 - S_1 \rangle_T = \langle 100 \rangle_\tau + \langle 010 \rangle_\tau + \langle 001 \rangle_\tau + \langle 000 \rangle_\tau$$

$$\langle 100 \rangle_\tau = \frac{\langle W|DE^2C^{N-3}|V \rangle_\tau}{\langle W|C^N|V \rangle_\tau}$$

$$\langle 010 \rangle_\tau = \frac{\langle W|EDEC^{N-3}|V \rangle_\tau}{\langle W|C^N|V \rangle_\tau}$$

$$\langle 001 \rangle_\tau = \frac{\langle W|E^2DC^{N-3}|V \rangle_\tau}{\langle W|C^N|V \rangle_\tau}$$

$$\langle 000 \rangle_\tau = \frac{\langle W|E^3C^{N-3}|V \rangle_\tau}{\langle W|C^N|V \rangle_\tau} \qquad (A.4)$$

In order to calculate the average in the numerator for $\langle 100 \rangle_\tau$ we rewrite DE^2C^{N-3} as:

$$DE^2C^{N-3} = CEC^{N-3} = (C + E^2)C^{N-3} = C^{N-2} - E^2C^{N-3} . \qquad (A.5)$$

Now the ratio can easily be calculated using Eqs. (A.3) to give:

$$\frac{\langle W|DE^2C^{N-3}|V \rangle_\tau}{\langle W|C^N|V \rangle_\tau} = \frac{\langle W|C^{N-2}|V \rangle_\tau}{\langle W|C^N|V \rangle_\tau} + \frac{\langle W|E^2C^{N-3}|V \rangle_\tau}{\langle W|C^N|V \rangle_\tau} = J^2 + \frac{1}{\alpha^2}J^3 . \qquad (A.6)$$

In the same way we obtain the rest of the averages:

$$\langle 010 \rangle_\tau = \frac{\langle W|EC^{N-2}|V \rangle_\tau}{\langle W|C^N|V \rangle_\tau} = \frac{1}{\alpha}J^2$$

$$\langle 001 \rangle_\tau = \frac{\langle W|E^2DC^{N-3}|V \rangle_\tau}{\langle W|C^N|V \rangle_\tau} = \frac{1}{\alpha^2}J^2 - \frac{1}{\alpha^3}J^3$$

$$\langle 000 \rangle_\tau = \frac{\langle W|E^3C^{N-3}|V \rangle_\tau}{\langle W|C^N|V \rangle_\tau} = \frac{1}{\alpha^3}J^3 . \qquad (A.7)$$

Combining these expressions leads to the result for $\langle 1 - S_1 \rangle_T = (1 + \frac{1}{\alpha} + \frac{1}{\alpha^2} + \frac{J}{\alpha^2})J^2$. The rest of the calculations are done using the same techniques. Here we show the results one can get after a substantial amout of algebra:

$$\langle T_1(1 - T_2) \rangle = \langle 110100 \rangle + \langle 110010 \rangle + \langle 110001 \rangle + \langle 110000 \rangle$$

$$+ \langle 101100 \rangle + \langle 101010 \rangle + \langle 101001 \rangle + \langle 101000 \rangle$$

$$+ \langle 011100 \rangle + \langle 011010 \rangle + \langle 011001 \rangle + \langle 011000 \rangle$$

$$+ \langle 111100 \rangle + \langle 111010 \rangle + \langle 111001 \rangle + \langle 111000 \rangle . \qquad (A.8)$$

and the correlations on the right-hand side equal:

$$\langle 110100 \rangle \;=\; J^3 + (1 - 1/\alpha)J^4 + (2 - 1/\alpha)J^5 + (2/\alpha^2 + 1/\alpha^3)J^6$$

$$\langle 110010 \rangle \;=\; J^3 + (1 - 1/\alpha)J^4 + (1/\alpha^2)J^5$$

$$\langle 110001 \rangle \;=\; J^3 + (1 - 1/\alpha)J^4 + (-3 + 1/\alpha + 2/\alpha^2 + 1/\alpha^3)J^5 - \frac{1}{\alpha^2}(3 + 2/\alpha + 1/\alpha^2)J^6$$

$$\langle 110000 \rangle \;=\; J^4 + (3 - 1/\alpha)J^5 + (3/\alpha^2 + 2/\alpha^3 + 1/\alpha^4)J^6$$

$$\langle 101100 \rangle \;=\; J^3 + (1 - 1/\alpha^2)J^5 + (1/\alpha^2 + 1/\alpha^3)J^6$$

$$\langle 101010 \rangle \;=\; J^3$$

$$\langle 101001 \rangle \;=\; J^3 + (-2 + 1/\alpha^2 + 1/\alpha^3)J^5 - (2/\alpha^2 + 2/\alpha^3 + 1/\alpha^4)J^6$$

$$\langle 101000 \rangle \;=\; J^4 + 2J^5 + (2/\alpha^2 + 2/\alpha^3 + 1/\alpha^4)J^6$$

$$\langle 011100 \rangle \;=\; (1/\alpha)J^3 - (1/\alpha^2)J^4 + \frac{1}{\alpha}(1 - 1/\alpha)J^5 + (1/\alpha^3)J^6$$

$$\langle 011010 \rangle \;=\; (1/\alpha)J^3 - (1/\alpha^2)J^4$$

$$\langle 011001 \rangle \;=\; (1/\alpha)J^3 - (1/\alpha^2)J^4 + (-2/\alpha + 1/\alpha^2 + 1/\alpha^3)J^5 - (2/\alpha^3 + 1/\alpha^4)J^6$$

$$\langle 011000 \rangle \;=\; (1/\alpha)J^4 + (2/\alpha - 1/\alpha^2)J^5 + (2/\alpha^3 + 1/\alpha^4)J^6$$

$$\langle 111100 \rangle \;=\; J^2 - (1 + 1/\alpha)J^3 + (1 - 1/\alpha)J^5 + (1/\alpha^2)J^6$$

$$\langle 111010 \rangle \;=\; J^2 - (1 + 1/\alpha)J^3$$

$$\langle 111001 \rangle \;=\; J^2 - (1 + 1/\alpha)J^3 + (-3 + 2/\alpha + 1/\alpha^2)J^5 - (3/\alpha^2 + 1/\alpha^3)J^6$$

$$\langle 111000 \rangle \;=\; J^3 + (1 - 1/\alpha)J^4 + (3 - 2/\alpha)J^5 + (3/\alpha^2 + 1/\alpha^3)J^6 \tag{A.9}$$

from wich one obtains the recursion relations for the rates α and β. Here, to simplify

the notation, we have used short-hand abbreviations, for example $\langle 000100 \rangle$ represents

$\langle W|E^3 D E^2 C^{N-6}|V\rangle / \langle W|C^N|V\rangle$. The case of $p \neq 1$ can be handled in the same

manner, with modified algebra for the operators:

$$C \equiv D + E$$

$$pDE = D + E$$

$$D|V\rangle = \frac{1}{\beta}|V\rangle$$

$$\langle W|E = \frac{1}{\alpha}\langle W|. \tag{A.10}$$

We can simplify our calculation a little bit by observing that $\langle 111000 \rangle + \langle 110000 \rangle = \langle DDCEEE \rangle$, etc. Then one needs to calculate only

$$\langle D^2CE^3 \rangle + \langle D^2CED \rangle = (1/p^2)J^2 + (1/p^3 - 1/\alpha p^2)J^3 + (3/p^4 - 2/\alpha p^3)J^4 +$$

$$(3/\alpha^2 p^3 + 1/\alpha^3 p^2)J^5;$$

$$\langle D^2CEDE \rangle = (1/p^2)J^2 - (1/\alpha p^2)J^3 + (1/p^4 - 1/\alpha p^3)J^4 + (1/\alpha^2 p^3)J^5;$$

$$\langle D^2CDE^2 \rangle = (1/p^2)J^2 - (1/\alpha p^2)J^3 + (1/p^4 - 1/\alpha p^3)J^4 +$$

$$(3/p^5 - 2/\alpha p^4)J^5 + (3/\alpha^2 p^4 + 1/\alpha^3 p^3)J^6;$$

$$\langle DEDE^2C \rangle = (1/p^3)J^3 + (1/p^4)J^4 + (1/\alpha^2 p^3 + 1/\alpha^3)J^5;$$

$$\langle DEDEDE \rangle = (1/p^3)J^3;$$

$$\langle DED^2E^2 \rangle = (1/p^3)J^3 + (1/p^5 - 1/\alpha^2 p^3)J^5 + (1/\alpha^2 p^4 + 1/\alpha^3 p^3)J^6;$$

$$\langle ED^2E^2C \rangle = (1/\alpha p^2)J^3 + (1/\alpha p^3 - 1/\alpha^2 p^2)J^4 + (1/\alpha^3 p^2)J^5;$$

$$\langle ED^2EDE \rangle = (1/\alpha p^2)J^3 - (1/\alpha^2 p^2)J^4;$$

$$\langle ED^3E^2 \rangle = (1/\alpha p^2)J^3 - (1/\alpha^2 p^2)J^4 + (1/\alpha p^4 - 1/\alpha^2 p^3)J^5 +$$

$$(1/\alpha^3 p^3)J^6, \tag{A.11}$$

in order to get Eq. (3.35).

APPENDIX B

CLUSTER-VARIATION METHOD

In this Appendix we explain more rigorously why, in thermodynamic limit, we can successfully approximate the measure entropy of the model by a combination of the entropy of small clusters. One of the methods is the cluster-variation method, which usually generates a lower bound approximation to the entropy density and the other, elaborating on the Markov property of the entropy, uses conditional entropy which generates an upper bound to the entropy density (discussed in the text).

The cluster variation method (CVM) is an approximate method often used in statistical mechanics for calculating the phase diagram of complex systems (Kikuchi, 1951; Burley, 1972; Morán-López and Sanchez, 1996). For systems in equilibrium, one can define the exact variational principle for the free energy density f for the infinite system (Ruelle, 1978). We will call a *macroscopic state* ρ for an infinite system on Z^2 a positive linear functional on $C(\Omega)$, where $\Omega = (\Omega_0)^{Z^2}$ and $\Omega_0 = \{0, 1\}$ (assuming we have a system for which the state of any site can be coded in one bit). It is normalized, i.e. $\rho(1) = 1$, and its restriction on $C(\Omega_A)$, A is finite, defines a probability measure. Also we will focus our attention on the set of translationally invariant states only that are induced by the natural translational symmetry on Z^2. This set is denoted by I.

The Hamiltonian for a finite subset $A \subset Z^2$ is:

$$H[A] = \sum_{X \subset A} \Phi[X] , \tag{B.1}$$

where $\Phi[X]$ is the potential energy of a cluster $X \subset A$. For the case of nearest neighbor interactions, the above sum is over clusters made of a site plus its, say, right

and upper neighbors. Then, the variational principle says that the free energy density is:

$$f = \min_{\rho \in I}[\rho(e) - s(\rho)] \,, \tag{B.2}$$

where

$$\rho(e) = \lim_{A \to Z^2} \rho\left[\frac{H[A]}{|A|}\right]$$
$$s(\rho) = \lim_{A \to Z^2} \rho\left[\frac{S_\rho[A]}{|A|}\right] \tag{B.3}$$

and

$$S_\rho[A] = -\rho(\ln \rho[A]) = - \sum_{\omega \in (\Omega_0)^A} \rho[A](\omega) \ln \rho[A](\omega) \,. \tag{B.4}$$

Therefore the equilibrium state is the one that minimizes the free energy functional above. After minimization, one obtains the well known Boltzmann factor. This formalism is exact and general for all equilibrium models.

Another variational method that still gives the exact result is obtained by finding the state that minimizes (Schlijper, 1984):

$$f_D = \min_{\rho \in I_D}[\rho(e) - b(\rho)] \,, \tag{B.5}$$

where

$$b(\rho) = \lim_{n \to \infty} \frac{S_\rho(D_n) - S_\rho(L_n)}{n} \,. \tag{B.6}$$

D is a rectangular infinite in one direction and extends as much as the interaction length between the particles in the other direction. For the case of nearest neighbor interactions, it is a infinite stripe with height of two lattice sites. D_n and L_n are respectively a double line and a line of n sites in one direction and two sites in the other, as illustrated below. I_D denotes the set of translation invariant functionals ρ on $C(\Omega_D)$. The advantage is that we reduce dimensionality by one having a cluster of sites that extends to infinity in only one of the directions. The problem in this case is to find the ρ that minimizes the above functional, which will be the exact solution.

Note that we have to modify the expression of the entropy term $b(\rho)$ in order to find the exact solution.

The CVM is based upon the idea of approximating the configurational entropy density of the system by the entropy contributions of finite clusters. There is a very elegant proof of the CVM using Möbius inversion (An, 1988). Along these lines, we can start approximating the exact functional $b(\rho)$ by

$$B_n(\rho) = \frac{S_\rho(D_n) - S_\rho(L_n)}{n} , \qquad (B.7)$$

or

$$C_n(\rho) = [S_\rho(D_n) - S_\rho(L_n)] - [S_\rho(D_{n-1}) - S_\rho(L_{n-1})] . \qquad (B.8)$$

The later expression converges faster and, therefore, is better suited for computer simulations. In the figure below we show some of the shapes mentioned here and in the text :
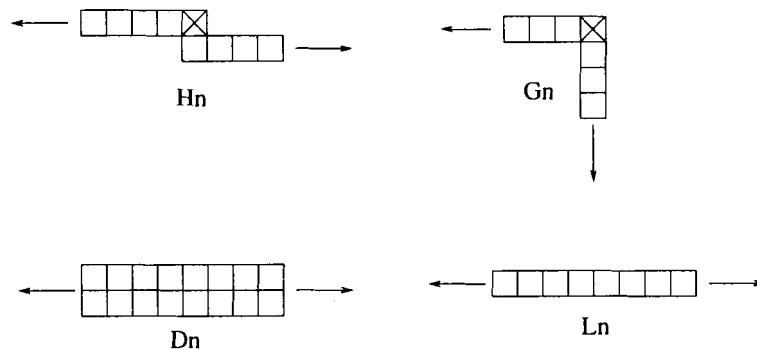

Figure B.1: Different shapes.

It is noteworthy that the nth approximation of the entropy density using H_n always overestimates the true entropy while the applications of the D and L shapes in Eq. (B.8) underestimate it. Thus, studies combining pairs of shapes can yield both upper and lower bonds on the entropy.

APPENDIX C

MULTI-SPIN CODING

We show here the code used for the simulations of DLG utilizing the whole machine word on a computer to produce a very fast and efficient algorithm, i.e. the so-called multi-spin coding technique. The basic idea is to use each bit of the computer word (our computers have 32-bit word) to represent the state of a single site on the lattice. Of course this can be used only if the state on a single lattice site can be coded by a single bit, like spin-up (spin-down) or particle(hole). We show below how to extend the algorithm when the state on a site cannot fit into one single bit, the case for the three-state model of a driven diffusive system.

Usually one uses this code

```
#define Lx 100
#define Ly 100
#define DIM (Lx*Ly)
unsigned long Data[DIM];
```

for a declaration of a lattice. Each element of the array **Data** will be used as a storage for the current value on some site of the lattice. In the case of spins (or a single kind of particles) we need only the values 0 and 1 to represent its current state and the rest $(2^{32} - 2)$ values of this **unsigned long** variable will not be used at all. It is an obvious waste of computer memory that one would generally like to avoid. Also, it is known that the computers do bit-wise operations much faster than anything else. These are the two reasons for trying to recode our algorithms into a bit-wise mode (for simple examples see Newman and Barkema (1999)).

The two-state model

The numbering of the sites in the cluster involved in one MCS is shown on this picture:
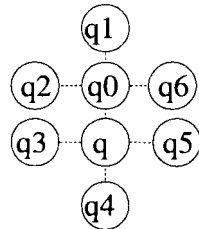

Figure C.1: Naming convention for the interaction cluster.

The code shown below simulates 32 lattices simultaneously at the same temperature. At each time step we pick a random **site** on the lattices. Then we pick a direction u for attempting a jump (1 is for a horizontal jump and 0 is for a vertical jump). Note that u is an **unsigned long** variable with each of its bits a random variable, so on the different lattices different attempts will be made.

```
#define ZERO 0x00000000

double JProb[4]; // lookup table
double T=1.6; // the temperature
double J = 1.0/(0.5673*T);// the interaction constant
JProb[1] = exp(-1.0*J);
JProb[2] = exp(-2.0*J);
JProb[3] = exp(-3.0*J);


/*****************************
// This function makes DIM = Lx*Ly attempts to update the
// lattice. The lattice is stored as one-dimensional array
// of unsigned integers with dimensions Lx and Ly.
// lrandom() is a random number generator for bits,
// i.e. it generates a machine word which bits are random.
/*****************************

void Step()
{
  static unsigned long Q0, Q1, Q2, Q3;
  static unsigned long q, q0, q1, q2, q3, q4, q5, q6, qH;
  static unsigned long site, X, Y;
```

```
static unsigned long i, u, r1, r2, r3;

for(i=0; i<DIM; i++) {
  site = DIM*drandom();
  X = site%Lx;
  Y = site/Lx;
  u = lrandom();

  if(drandom()< 2.0*JProb[1])  r1 = lrandom();
  else                         r1 = ZERO;
  if(drandom()< 2.0*JProb[2])  r2 = lrandom();
  else                         r2 = ZERO;
  if(drandom()< 2.0*JProb[3])  r3 = lrandom();
  else                         r3 = ZERO;

  q  = Data[site];
  qH = Data[Y*Lx + (X+1)%Lx];
  q0 = Data[((Y-1+Ly)%Ly)*Lx + X];
  q1 = Data[((Y-2+Ly)%Ly)*Lx + X];
  q2 = Data[((Y-1+Ly)%Ly)*Lx + (X-1+Lx)%Lx];
  q3 = Data[Y*Lx + (X-1+Lx)%Lx];
  q4 = Data[((Y+1)%Ly)*Lx + X];
  q5 = Data[Y*Lx + (X+1)%Lx];
  q6 = Data[((Y-1+Ly)%Ly)*Lx + (X+1)%Lx];

  Q1 = (q & q3 & ~q0 & ~q1 & ~q2 & ~q4 & ~q5 & ~q6) |
       (q & q4 & ~q0 & ~q1 & ~q2 & ~q3 & ~q5 & ~q6) |
       (q & q5 & ~q0 & ~q1 & ~q2 & ~q3 & ~q4 & ~q6) |
       (q & q3 & q4 & q1 & ~q0 & ~q2 & ~q5 & ~q6) |
       (q & q3 & q4 & q2 & ~q0 & ~q1 & ~q5 & ~q6) |
       (q & q3 & q4 & q6 & ~q0 & ~q1 & ~q2 & ~q5) |
       (q & q3 & q5 & q1 & ~q0 & ~q2 & ~q4 & ~q6) |
       (q & q3 & q5 & q2 & ~q0 & ~q1 & ~q4 & ~q6) |
       (q & q3 & q5 & q6 & ~q0 & ~q1 & ~q2 & ~q4) |
       (q & q4 & q5 & q1 & ~q0 & ~q2 & ~q3 & ~q6) |
       (q & q4 & q5 & q2 & ~q0 & ~q1 & ~q3 & ~q6) |
       (q & q4 & q5 & q6 & ~q0 & ~q1 & ~q2 & ~q3) |
       (q & q1 & q2 & q3 & q4 & q5 & ~q0 & ~q6) |
       (q & q1 & q6 & q3 & q4 & q5 & ~q0 & ~q2) |
       (q & q2 & q6 & q3 & q4 & q5 & ~q0 & ~q1) |
       (q0 & q1 & ~q & ~q2 & ~q3 & ~q4 & ~q5 & ~q6) |
       (q0 & q2 & ~q & ~q1 & ~q3 & ~q4 & ~q5 & ~q6) |
       (q0 & q6 & ~q & ~q1 & ~q2 & ~q3 & ~q4 & ~q5) |
       (q0 & q1 & q2 & q3 & ~q & ~q4 & ~q5 & ~q6) |
       (q0 & q1 & q2 & q4 & ~q & ~q3 & ~q5 & ~q6) |
```

```
      (q0 & q1 & q2 & q5 & ~q & ~q3 & ~q4 & ~q6) |
      (q0 & q1 & q6 & q3 & ~q & ~q2 & ~q4 & ~q5) |
      (q0 & q1 & q6 & q4 & ~q & ~q2 & ~q3 & ~q5) |
      (q0 & q1 & q6 & q5 & ~q & ~q2 & ~q3 & ~q4) |
      (q0 & q2 & q6 & q3 & ~q & ~q1 & ~q4 & ~q5) |
      (q0 & q2 & q6 & q4 & ~q & ~q1 & ~q3 & ~q5) |
      (q0 & q2 & q6 & q5 & ~q & ~q1 & ~q3 & ~q4) |
      (q0 & q1 & q2 & q3 & q4 & q6 & ~q & ~q5) |
      (q0 & q1 & q2 & q3 & q5 & q6 & ~q & ~q4) |
      (q0 & q1 & q2 & q4 & q5 & q6 & ~q & ~q3) ;


Q2 = (q & q1 & q3 & q4 & q5 & ~q0 & ~q2 & ~q6) |
     (q & q2 & q3 & q4 & q5 & ~q0 & ~q1 & ~q6) |
     (q & q3 & q4 & q5 & q6 & ~q0 & ~q1 & ~q2) |
     (q & q3 & q4 & ~q0 & ~q1 & ~q2 & ~q5 & ~q6) |
     (q & q3 & q5 & ~q0 & ~q1 & ~q2 & ~q4 & ~q6) |
     (q & q4 & q5 & ~q0 & ~q1 & ~q2 & ~q3 & ~q6) |
     (q0 & q1 & q2 & q3 & q6 & ~q & ~q4 & ~q5) |
     (q0 & q1 & q2 & q4 & q6 & ~q & ~q3 & ~q5) |
     (q0 & q1 & q2 & q5 & q6 & ~q & ~q3 & ~q4) |
     (q0 & q1 & q2 & ~q & ~q3 & ~q4 & ~q5 & ~q6) |
     (q0 & q1 & q6 & ~q & ~q2 & ~q3 & ~q4 & ~q5) |
     (q0 & q2 & q6 & ~q & ~q1 & ~q3 & ~q4 & ~q5);

Q3 = (q & ~q0 & q3 & q4 & q5 & ~q1 & ~q2 & ~q6) |
        (~q & q0 & q1 & q2 & q6 & ~q3 & ~q4 & ~q5) ;


Q0 = ~Q1 & ~Q2 & ~Q3 ;


Data[site] ^= (u & q & ~qH) | (~u & Q0 & (q ^ q0)) |
              (~u & Q1 & r1) | (~u & Q2 & r2) |
              (~u & Q3 & r3) ;


Data[Y*Lx + (X+1)%Lx] ^= ( u & q & ~qH ) ;


Data[((Y-1+Ly)%Ly)*Lx + X] ^= (~u & Q0 & (q ^ q0)) |
                              (~u & Q1 & r1) |
                              (~u & Q2 & r2) |
                              (~u & Q3 & r3) ;
      }
}
```

An obvious improvement would be to simplify the expresions for Q1, Q2, and Q3 by using Karnaugh's maps.

Three-state model

The multi spin code for the three-state model is little bit more complicated because now we have three possibilities for the occupation number at each site: a hole, a positive charge or a negative charge. We have used the convention that $(0,0)$ will represent a hole, $(0,1)$ is a positive particle and $(1,0)$ a negative particle. So we need 2 bits in order to code the state on a single lattice. The source code should change like this:

```
void Step()
{
  static unsigned long q1, qR1, qU1, q2, qR2, qU2, u;
  static unsigned site, siteR, siteU;
  static unsigned i, X, Y;
  static unsigned long r2, r3, r4;

  for(i=0 ; i<DIM ; i++) {
    site = DIM*drandom();
    X = site%Lx;
    Y = site/Lx;
    siteR = Y*Lx + (X+1)%Lx;
    siteU = ((Y-1+Ly)%Ly)*Lx + X;
    u = lrandom();

    if(Delta<0.5)
      if(drandom()< 2.0*Delta) r2 = lrandom();
      else r2 = ZERO;

    else if (Delta>0.5)
      if(drandom()< (2.0-2.0*Delta)) r2 = lrandom();
      else r2 = BIGONE;

    else r2 = lrandom();

    if(e_E<0.5)
      if(drandom()< 2.0*e_E) r3 = lrandom();
      else r3 = ZERO;

    else if (e_E>0.5)
      if(drandom()< (2.0-2.0*e_E)) r3 = lrandom();
      else r3 = BIGONE;
```

```
    else r3 = lrandom();

    if(Delta_2E<0.5)
      if(drandom()< 2.0*Delta_2E) r4 = lrandom();
      else r4 = ZERO;

    else if (Delta_2E>0.5)
      if(drandom()< (2.0-2.0*Delta_2E)) r4 = lrandom();
      else r4 = BIGONE;

    else r4 = lrandom();

    q1  = Data1[site];
    qR1 = Data1[siteR];
    qU1 = Data1[siteU];
    q2  = Data2[site];
    qR2 = Data2[siteR];
    qU2 = Data2[siteU];

    Data1[site] = (u & ~q1 & ~q2 & qU1 & ~qU2 ) |
    (u & ~q1 & q2 & qU1 & ~qU2 & r2) |
    (u & q1 & ~q2 & ~qU1 & qU2 & ~r2) |
    (u & q1 & ~q2 & qU1 & ~qU2) |
    (~u & q1 & ~q2 & ~qR1 & qR2 & ~r4 )|
    (~u & ~q1 & ~q2 & qR1 & ~qR2 ) |
    (~u & ~q1 & q2 & qR1 & ~qR2 & r2 ) |
    (~u & q1 & ~q2 & qR1 & ~qR2 ) |
    (~u & q1 & ~q2 & ~qR1 & ~qR2 & ~r3 );

    Data2[site] = (u & ~q1 & ~q2 & ~qU1 & qU2 )|
    (u & ~q1 & q2 & ~qU1 & qU2) |
    (u & ~q1 & q2 & qU1 & ~qU2 & ~r2) |
    (u & q1 & ~q2 & ~qU1 & qU2 & r2) |
    (~u & ~q1 & ~q2 & ~qR1 & qR2 & r3 )|
    (~u & ~q1 & q2 & ~qR1 & qR2) |
    (~u & q1 & ~q2 & ~qR1 & qR2 & r4 )|
    (~u & ~q1 & q2 & qR1 & ~qR2 & ~r2 );

    Data1[siteU] = (u & ~q1 & q2 & qU1 & ~qU2 & ~r2) |
    (u & q1 & ~q2 & ~qU1 & ~qU2 ) |
    (u & q1 & ~q2 & ~qU1 & qU2 & r2) |
    (u & q1 & ~q2 & qU1 & ~qU2 ) |
    (~u & qU1);

    Data2[siteU] = (u & ~q1 & q2 & ~qU1 & ~qU2) |
```

```
(u & ~q1 & q2 & ~qU1 & qU2) |
(u & ~q1 & q2 & qU1 & ~qU2 & r2) |
(u & q1 & ~q2 & ~qU1 & qU2 & ~r2 ) |
(~u & qU2);

Data1[siteR] = (~u & q1 & ~q2 & ~qR1 & qR2 & r4) |
(~u & q1 & ~q2 & qR1 & ~qR2) |
(~u & q1 & ~q2 & ~qR1 & ~qR2 & r3) |
(~u & ~q1 & q2 & qR1 & ~qR2 & ~r2) |
(u & qR1);

Data2[siteR] = (~u & ~q1 & ~q2 & ~qR1 & qR2 & ~r3 )|
(~u & ~q1 & q2 & ~qR1 & qR2) |
(~u & q1 & ~q2 & ~qR1 & qR2 & ~r4 )|
(~u & ~q1 & q2 & qR1 & ~qR2 & r2 )|
(~u & ~q1 & q2 & ~qR1 & ~qR2) |
(u & qR2);
```

The other difference is that the cluster involved in one single Monte Carlo exchange consists of only three sites: the site we randomly choose and its upper and right nearest neighbors.

APPENDIX D

MASTER EQUATIONS FOR PAIRS

Following the same notations as in Section 5.2, we write down explicitly the master equations for pairs along the driving field. The symbols with the tilde above are for the symmetrical cluster from the horizontal axis to the clusters shown in Fig. 34.

$$
\begin{aligned}
\frac{\mathrm{d}T_0}{\mathrm{d}t} =\ & \varphi(-E)\,P_3 + (L_3 + \tilde{L}_3)\,\delta + \varphi(E)\,P_6 + (L_6 + \tilde{L}_6)\,\delta \\
& + \varphi(E)\,P_3 + (N_1 + \tilde{N}_1)\,\delta + \varphi(-E)\,P_6 + (N_2 + \tilde{N}_2)\,\delta \\
& - \varphi(E)\,P_9 - (L_9 + \tilde{L}_9)\,\delta - \varphi(-E)\,P_{18} - (L_{18} + \tilde{L}_{18})\,\delta \\
& - \varphi(-E)\,P_1 - (N_9 + \tilde{N}_9)\,\delta - \varphi(E)\,P_2 - (N_{18} + \tilde{N}_{18})\,\delta
\end{aligned}
$$

$$
\begin{aligned}
\frac{\mathrm{d}T_1}{\mathrm{d}t} =\ & \varphi(-E)\,P_4 + (L_4 + \tilde{L}_4)\,\delta + \varphi(E)\,P_7 + (L_7 + \tilde{L}_7)\,\delta \\
& + \varphi(-E)\,P_1 + (N_9 + \tilde{N}_9)\,\delta + \gamma\varphi(-2E)\,P_7 + (N_{11} + \tilde{N}_{11})\,\gamma + \varphi(E)\,T_3 \\
& - \varphi(E)\,P_{10} - (L_{10} + \tilde{L}_{10})\,\delta - \varphi(-E)\,P_{19} - (L_{19} + \tilde{L}_{19})\,\delta \\
& - \varphi(E)\,P_3 - (N_1 + \tilde{N}_1)\,\delta - \gamma\varphi(2E)\,P_5 - (N_{19} + \tilde{N}_{19})\,\gamma - \varphi(-E)\,T_1
\end{aligned}
$$

$$
\begin{aligned}
\frac{\mathrm{d}T_2}{\mathrm{d}t} =\ & \varphi(-E)\,P_5 + (L_5 + \tilde{L}_5)\,\delta + \varphi(E)\,P_8 + (L_8 + \tilde{L}_8)\,\delta \\
& + \varphi(E)\,P_2 + (N_{18} + \tilde{N}_{18})\,\delta + \gamma\varphi(2E)\,P_5 + (N_{19} + \tilde{N}_{19})\,\gamma + \varphi(-E)\,T_6 \\
& - \varphi(E)\,P_{11} - (L_{11} + \tilde{L}_{11})\,\delta - \varphi(-E)\,P_{20} - (L_{20} + \tilde{L}_{20})\,\delta \\
& - \varphi(-E)\,P_6 - (N_2 + \tilde{N}_2)\,\delta - \gamma\varphi(-2E)\,P_7 - (N_{11} + \tilde{N}_{11})\,\gamma - \varphi(E)\,T_2
\end{aligned}
$$

$$\frac{\mathrm{d}T_3}{\mathrm{d}t} = \varphi(E)\,P_9 + (L_9 + \tilde{L}_9)\,\delta + \gamma\,\varphi(2E)\,P_{15} + (L_{15} + \tilde{L}_{15})\,\gamma$$
$$+ \varphi(E)\,P_{12} + (N_4 + \tilde{N}_4)\,\delta + \varphi(-E)\,P_{15} + (N_5 + \tilde{N}_5)\,\delta + \varphi(-E)\,T_1$$
$$- \varphi(-E)\,P_3 - (L_3 + \tilde{L}_3)\,\delta - \gamma\,\varphi(-2E)\,P_{21} - (L_{21} + \tilde{L}_{21})\,\gamma$$
$$- \varphi(-E)\,P_{10} - (N_{12} + \tilde{N}_{12})\,\delta - \varphi(E)\,P_{11} - (N_{12} + \tilde{N}_{12})\,\delta - \varphi(E)\,T_3$$

$$\frac{\mathrm{d}T_4}{\mathrm{d}t} = \varphi(E)\,P_{10} + (L_{10} + \tilde{L}_{10})\,\delta + \gamma\,\varphi(2E)\,P_{16} + (L_{16} + \tilde{L}_{16})\,\gamma$$
$$+ \varphi(-E)\,P_{10} + (N_{12} + \tilde{N}_{12})\,\delta + \gamma\,\varphi(-2E)\,P_{16} + (N_{14} + \tilde{N}_{14})\,\gamma$$
$$- \varphi(-E)\,P_4 - (L_4 + \tilde{L}_4)\,\delta - \gamma\,\varphi(-2E)\,P_{22} - (L_{22} + \tilde{L}_{22})\,\gamma$$
$$- \varphi(E)\,P_{12} - (N_4 + \tilde{N}_4)\,\delta - \gamma\,\varphi(2E)\,P_{14} - (N_{22} + \tilde{N}_{22})\,\gamma$$

$$\frac{\mathrm{d}T_5}{\mathrm{d}t} = \varphi(E)\,P_{11} + (L_{11} + \tilde{L}_{11})\,\delta + \gamma\,\varphi(2E)\,P_{17} + (L_{17} + \tilde{L}_{17})\,\gamma$$
$$+ \varphi(E)\,P_{11} + (N_{21} + \tilde{N}_{21})\,\delta + \gamma\,\varphi(2E)\,P_{14} + (N_{22} + \tilde{N}_{22})\,\gamma + \gamma\,\varphi(-2E)\,T_7$$
$$- \varphi(-E)\,P_5 - (L_5 + \tilde{L}_5)\,\delta - \gamma\,\varphi(-2E)\,P_{23} - (L_{23} + \tilde{L}_{23})\,\gamma$$
$$- \varphi(-E)\,P_{15} - (N_5 + \tilde{N}_5)\,\delta - \gamma\,\varphi(-2E)\,P_{16} - (N_{14} + \tilde{N}_{14})\,\gamma - \gamma\,\varphi(2E)\,T_5$$

$$\frac{\mathrm{d}T_6}{\mathrm{d}t} = \varphi(-E)\,P_{18} + (L_{18} + \tilde{L}_{18})\,\delta + \gamma\,\varphi(2E)\,P_{21} + (L_{21} + \tilde{L}_{21})\,\gamma$$
$$+ \varphi(E)\,P_{21} + (N_7 + \tilde{N}_7)\,\delta + \varphi(-E)\,P_{24} + (N_8 + \tilde{N}_8)\,\delta + \varphi(E)\,T_2$$
$$- \varphi(E)\,P_6 - (L_6 + \tilde{L}_6)\,\delta - \gamma\,\varphi(2E)\,P_{15} - (L_{15} + \tilde{L}_{15})\,\gamma$$
$$- \varphi(-E)\,P_{19} - (N_{15} + \tilde{N}_{15})\,\delta - \varphi(E)\,P_{20} - (N_{24} + \tilde{N}_{24})\,\delta - \varphi(-E)\,T_6$$

$$\frac{\mathrm{d}T_7}{\mathrm{d}t} = \varphi(-E)\,P_{19} + (L_{19} + \tilde{L}_{19})\,\delta + \gamma\,\varphi(-2E)\,P_{22} + (L_{22} + \tilde{L}_{22})\,\gamma$$
$$+ \varphi(E)\,P_{19} + (N_{15} + \tilde{N}_{15})\,\delta + \gamma\,\varphi(-2E)\,P_{25} + (N_{17} + \tilde{N}_{17})\,\gamma + \gamma\,\varphi(E)\,T_5$$
$$- \varphi(E)\,P_7 - (L_7 + \tilde{L}_7)\,\delta - \gamma\,\varphi(E)\,P_{16} - (L_{16} + \tilde{L}_{16})\,\gamma$$
$$- \varphi(E)\,P_{21} - (N_7 + \tilde{N}_7)\,\delta - \gamma\,\varphi(E)\,P_{23} - (N_{25} + \tilde{N}_{25})\,\gamma - \gamma\,\varphi(-2E)\,T_7$$

$$\frac{dT_8}{dt} = \varphi(-E)\ P_{20} + (L_{20} + \tilde{L}_{20})\ \delta + \gamma\ \varphi(-2E)\ P_{23} + (L_{23} + \tilde{L}_{23})\ \gamma$$

$$+\ \ \varphi(E)\ P_{20} + (N_{24} + \tilde{N}_{24})\ \delta + \gamma\ \varphi(2E)\ P_{23} + (N_{25} + \tilde{N}_{25})\ \gamma +$$

$$-\ \ \varphi(E)\ P_8 - (L_8 + \tilde{L}_8)\ \delta - \gamma\ \varphi(E)\ P_{17} - (L_{17} + \tilde{L}_{17})\ \gamma$$

$$-\ \ \varphi(-E)\ P_{24} - (N_8 + \tilde{N}_8)\ \delta - \gamma\ \varphi(-2E)\ P_{25} - (N_{17} + \tilde{N}_{17})\ \gamma$$

Similar equations can be writen for any shape. For the selected shape, one must include, for each state of the cluster, the appropriate states on the shapes contributing to its one-step time evolution.

BIOGRAPHY OF THE AUTHOR

Ivan Tsvetanov Georgiev was born in Vidin, Bulgaria on March 30, 1969. He graduated from Vidin Mathematics High School in 1987 with honors. He was a member of the Bulgarian team of the XVIII International Physics Olympics, held in Yena, Germany, where he received the third individual award. From 1987 till 1989, Ivan completed the mandatory service in the Bulgarian armed forces.

Ivan was accepted as a student at the Sofia State University "St. Kliment Ohridski". After two years of study, he left the school for four years to work as a computer animator in the first private TV station in Bulgaria. He continued his study again in 1996 and was accepted in 1998 as a graduate student of the Physics and Astronomy Department at the University of Maine.

Ivan is a candidate for the Doctor of Philosophy degree in Physics from The University of Maine in August, 2003.